

# **Simulation of Helium Jet Cooling for Spallation Targets**

*By*

**P. SELVARAJ**  
(ENGG02200904003)

**Indira Gandhi Centre for Atomic Research  
Kalpakkam**

**A thesis submitted to the  
Board of Studies in Engineering Sciences  
In partial fulfillment of requirements  
For the Degree of**

**DOCTOR OF PHILOSOPHY**

*of*

**Homi Bhabha National Institute**



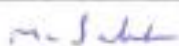
**August 2016**

# Homi Bhabha National Institute

## Recommendations of the Viva Voce Board

As members of the Viva Voce Board, we certify that we have read the dissertation prepared by **Mr. P. SELVARAJ** entitled “**Simulation of Helium Jet Cooling for Spallation Targets**” and recommend that it may be accepted as fulfilling the dissertation requirement for the Degree of Doctor of Philosophy.

Chairman – **Dr. M. Sai Baba**



Date: 13/9/2017

Guide / Convener – **Dr. T. Sundararajan**



Date: 13-9-17

Co-guide – **Dr. K. Velusamy**



Date: 13/9/2017

External Examiner – **Dr. B. V. S. S. Prasad**



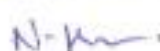
Date: 13-9-17

Member – **Dr. R. Baskaran**



Date: 13/9/17

Technology Advisor – **Shri N. Kasinathan**



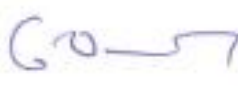
Date: 13/9/17

Final approval and acceptance of this dissertation is contingent upon the candidate's submission of the final copies of the dissertation to HBNI.

We hereby certify that we have read this dissertation prepared under our direction and recommend that it may be accepted as fulfilling the dissertation requirement.

Date: 13/9/2017

Place: Kalpakam



Dr. K. Velusamy

(Co-guide)

13/9/2017



Dr. T. Sundararajan

(Guide)

13/9/2017

## STATEMENT BY AUTHOR

---

This dissertation has been submitted in partial fulfillment of requirements for an advanced degree at Homi Bhabha National Institute (HBNI) and is deposited in the Library to be made available to borrowers under rules of the HBNI.

Brief quotations from this dissertation are allowable without special permission, provided that accurate acknowledgement of source is made. Requests for permission for extended quotation from or reproduction of this manuscript in whole or in part may be granted by the Competent Authority of HBNI when in his or her judgment the proposed use of the material is in the interests of scholarship. In all other instances, however, permission must be obtained from the author.



(P. Selvaraj)

## DECLARATION

---

I, hereby declare that the investigation presented in this thesis entitled “**Simulation of Helium Jet Cooling for Spallation Targets**” submitted to **Homi Bhabha National Institute (HBNI)**, Mumbai, India for the award of **Doctor of Philosophy in Engineering Sciences** is the record of work carried out by me under the guidance of **Prof. T. Sundararajan and Dr. K. Velusamy**. The work is original and has not been submitted earlier as a whole or in part for a degree /diploma at this or any other Institution/ University.



(P. Selvaraj)

*Dedicated to my parents,  
wife and daughters*

## ACKNOWLEDGEMENT

---

I wish to express my sincere gratitude to my guides **Prof. T. Sundararajan** and **Dr. K. Velusamy** for their invaluable guidance, keen interest, motivation, continuous support and valuable suggestions during my research work. Their patience, enthusiasm, and immense knowledge helped me throughout the time of my research and writing thesis. I am very much grateful to my mentors **Shri. S. C. Chetal**, **Dr. G. Vaidyanathan** and **Dr. T. Jayakumar** for motivation and encouragement. I would like to express my sincere thanks to my colleagues **Mr. K. Natesan**, **Dr. Anil Kumar Sharma**, **Mr. E. Hemanth Rao**, **Mr. Juby Abraham**, **Dr. K. G. Muraleedaran Nair**, **Shri. V. Baskaran**, **Dr. B. K. Nashine**, **Shri. G. Padmakumar**, **Dr. D Ponraju**, **Shri. V. Vinod**, **Shri. S. Kishore**, **Shri. Vijay Singh Sikarwar**, **Dr. B. Venkatraman**, **Smt. M. Menaka** for their kind help and wholehearted support. It is my great privilege to acknowledge members of the Doctoral committee: **Dr. R. Baskaran** and **Shri N. Kasinathan** for their critical review and valuable comments. I take this opportunity to sincerely acknowledge **Dr. M. Sai Baba**, Dean Student Affairs and **Dr. G. Sasikala**, Dean Engineering Sciences for their motivation and constant support to complete the research work.

Words would be inadequate to express my sincere gratitude to my wife **Smt. S. Revathi**, my daughters **S. Uma Maheswari & S. Swarna** and my mother **P. Saraswathi** and other family members for their love, affection, encouragement and support to complete the research work. I am thankful to **Smt. Shanthi Rajendran** and **Smt. Indra Ramdoss** for providing typing and printing support.

Finally, I thank one and all who have helped me during the research work.



**P. Selvaraj**

# CONTENTS

	<b>Page No.</b>
<b>Synopsis</b>	ii
<b>List of figures</b>	vi
<b>List of tables</b>	x
<b>Glossary</b>	xi
<b>List of symbols</b>	xii
 <b>CHAPTER 1</b>	 1
<b>INTRODUCTION</b>	2
<b>1.1 Jet impingement cooling</b>	5
<b>1.2 Applications of jet impingement cooling</b>	9
<b>1.3 Effects of various parameters on impingement heat transfer</b>	12
<b>1.4 Motivation for the Present Study</b>	14
<b>1.5 Research Objective</b>	14
<b>1.6 Organization of Thesis</b>	15
 <b>CHAPTER 2</b>	 17
<b>LITERATURE REVIEW</b>	18
<b>2.1 Cooling Systems for high heat flux applications</b>	18
2.1.1 Microchannels	18
2.1.2 Jet impingement cooling	20
2.1.3 Spray cooling with enhanced heat transfer area	21
2.1.4 Passive cooling	22
2.1.5 Jet impingement Vs micro channel cooling	22
2.1.6 Spray cooling using water based polymer additive	25
2.1.7 Transient boiling cooling	25
2.1.8 Wicks for high heat flux applications	27
2.1.9 High heat flux micro evaporator	27

2.1.10 Closure	28
<b>2.2 Experimental Studies on Jet Cooling</b>	<b>29</b>
2.2.1 Jet impingement cooling	29
2.2.2 Effects of jet plate size and plate spacing on the stagnation Nusselt number for a confined circular air jet impinging on a flat surface	29
2.2.3 Effect of Controlling Parameters on Heat Transfer during Jet Array Impingement Cooling of a Hot Steel Plate	30
2.2.4 Experimental study and theoretical analysis of local heat transfer distribution between smooth flat surface and impinging air jet from a circular straight pipe nozzle	31
2.2.5 Experimental study of heat transfer coefficient on hot steel plate during water Jet impingement cooling	32
2.2.6 Experimental Investigation of Jet Impingement Cooling On a Ribbed Surface with Holes	33
2.2.7 Heat and mass transfer between impinging gas jets and solid surface	34
2.2.8 Heat transfer behaviors of a confined slot jet impingement	37
2.2.9 Forced convective heat transfer with impinging rectangular jets	37
2.2.10 Cooling of a heated flat plate by an obliquely impinging slot jet	39
2.2.11 Effect of jet-jet spacing on convective heat transfer to confined, impinging arrays of axisymmetric air jets	39
2.2.12 Influence of the shape of the nozzle on local heat transfer distribution between smooth flat surface and impinging air jet	41
2.2.13 Effect of nozzle geometry on heat transfer characteristics from a single circular air jet	42
2.2.14 Optimum jet-to-jet spacing of heat transfer for staggered arrays of impinging air jets	43
2.2.15 Closure	44
<b>2.3 Computational Simulation of Jet Cooling</b>	<b>45</b>
2.3.1 Large Eddy Simulation	46



2.3.2 Direct Numerical Simulation	48
2.3.3 Reynolds-Averaged Navier-Stokes Equation Modeling	51
2.3.4 Closure	54
<b>CHAPTER 3</b>	<b>55</b>
<b>EXPERIMENTAL STUDIES WITH SINGLE JET</b>	<b>56</b>
<b>3.0 Introduction</b>	<b>56</b>
<b>3.1 Description of Experiment</b>	<b>56</b>
<b>3.2 Cooling by circular air jets</b>	<b>61</b>
<b>3.3 Empirical Correlations</b>	<b>68</b>
<b>3.4 Cooling by slot air jets</b>	<b>70</b>
<b>3.5 Cooling by inclined slot air jets</b>	<b>78</b>
<b>3.6 Comparison</b>	<b>78</b>
<b>3.7 Closure</b>	<b>79</b>
<b>CHAPTER 4</b>	<b>81</b>
<b>COMPUTATIONAL SIMULATION OF SINGLE JET EXPERIMENTS</b>	<b>82</b>
<b>4.0 Introduction</b>	<b>82</b>
<b>4.1 Modelling Details</b>	<b>82</b>
<b>4.2 Prediction by various turbulence models</b>	<b>85</b>
4.2.1 k- $\epsilon$ Model	85
4.2.2 k- $\epsilon$ RNG Model	86
4.2.3 Reynolds Stress Model	86
4.2.4 Comparison of Predictions	87
<b>4.3 Parametric study on distance between jet and target</b>	<b>91</b>
<b>4.4 Impingement of two inclined jets</b>	<b>96</b>
<b>4.5 Effect of compressibility</b>	<b>100</b>
<b>4.6 Closure</b>	<b>100</b>

<b>CHAPTER 5</b>	<b>102</b>
<b>SPALLATION TARGET COOLING SYSTEM</b>	<b>103</b>
<b>5.0 Introduction</b>	<b>103</b>
<b>5.1 Spallation target helium cooling system</b>	<b>103</b>
<b>5.2 CFD simulation for estimation of heat removal capacity</b>	<b>109</b>
<b>5.3 CFD simulation for estimation of temperature difference</b>	<b>112</b>
<b>5.4 Closure</b>	<b>113</b>
<b>CHAPTER 6</b>	<b>117</b>
<b>EXPERIMENTAL STUDIES WITH MULTIPLE AIR JETS</b>	<b>118</b>
<b>6.0 Introduction</b>	<b>118</b>
<b>6.1 Thermal imaging</b>	<b>118</b>
<b>6.2 Experiments with four and two air jets</b>	<b>122</b>
<b>6.3 Closure</b>	<b>124</b>
<b>CHAPTER 7</b>	<b>126</b>
<b>CONCLUSIONS AND SCOPE FOR FUTURE WORK</b>	<b>127</b>
<b>REFERENCES</b>	<b>130</b>
<b>Appendix - A: Experimental uncertainty</b>	<b>142</b>
<b>Appendix - B: Model Calculation for circular air jet (at 90° with horizontal)</b>	<b>144</b>
<b>Appendix – C Comparison of heat transfer characteristics between helium and air system</b>	<b>150</b>
<b>PUBLICATIONS BASED ON THE THESIS</b>	<b>152</b>

## Synopsis

A high intensity proton beam from the cyclotron provides a unique facility for radiation damage studies on nuclear structural materials, as energetic charged particles are useful for simulating the bulk damage induced by neutrons. For example, 20 MeV protons with 350  $\mu\text{A}$  current can produce a damage rate of  $2 \times 10^{-5} \text{ dpa/s}$  over a stainless steel sample of thickness 0.7 mm. This is an order higher than the damage rate produced in fast reactors ( $\sim 10^{-6} \text{ dpa/s}$ ). Due to the availability of high energy protons, thick samples of the order of 0.5 to 1 mm can be irradiated. The main interest is in studying the irradiation effects on structural materials like zirconium based alloys, D9, D9I and ferritic steels used in thermal and fast breeder reactors.

The irradiation by high intensity proton beam also generates large amount of heat in thin metal specimens. This heat needs to be removed continuously to prevent the sample from melting as well as to keep the sample at a particular temperature. Highest cooling rates of specimens for mechanical experiments are achieved by immersing the specimens in liquid metals or by contacting them to a cooling block by a liquid metal film. Both techniques have been attempted to simulation experiments. But, they suffer from poor temperature control and production of radioactivity. Another method is the use of helium gas to cool the specimen. The amount of heat removal in this case is limited compared to the cooling by liquid metals. But, helium is non-radioactive, it is compatible with structural materials and it can be raised to very high temperatures. Helium cooling system will be simple compared to liquid metal or water cooling system. Even though helium is used for spallation target cooling, experimental or numerical studies regarding heat removal and the temperature difference within the sample are not available in literature. In this thesis, the main focus is on the helium cooling system wherein, various parametric studies are carried out to maximize the heat removal. Both numerical as well as experimental studies are carried out. Experimental studies are carried out

with air as cooling medium. In the air jet cooling studies, most of the studies carried out are with vertical impingement jet at the center of the target plate. This cannot be adapted here because it will interfere with the proton beam. The jets have to be necessarily inclined and also away from the target plate such that they will not interfere with the proton beam. Hence it is planned to carry out jet cooling experiments with air as coolant, validate the available empirical correlation from the literature using the experiments as well as computational fluid dynamics simulation.

The objective of the present research work is (i) to carry out impingement jet cooling experiments with air to understand the heat transfer characteristics, (ii) to identify the parameters which can give the maximum possible heat transfer coefficient by varying the parameters in the air jet cooling experiments, (iii) comparison of experimental results with empirical correlations available in the literature, (iv) numerical predictions of helium jet cooling heat transfer characteristics with various cooling arrangements and (v) conceptual design of helium cooling circuit for cooling irradiation target specimen.

**Experimental studies with single jet:** Compressed air from compressors is sent to a buffer tank from where it is sent to a nozzle. The flow rate is measured using a rotameter. The stainless steel sample of 20 mm x 20 mm x 0.5 mm is held by Teflon rods and heated by electric current. An array of circular/slot nozzles is used to produce the air jets. The air jet is perpendicular to the sample and is focused towards the center of the sample so that the air splits in all directions. The air flow rate is varied from 5 -15 m<sup>3</sup> / h. Three different nozzle diameters/widths and three nozzle to target distances are used in the experiments. The sample temperature is measured using K-type thermocouples. In these experiments, the interest is to estimate the average Nusselt number for the whole sample. Therefore, one thermocouple is attached at the center of each quadrant and the average temperature of the four quadrants is used for the estimation of average Nusselt number. With no cooling it is found that when the

sample temperature goes beyond 380°C oxidation of the sample takes place. Hence, it was decided to keep the sample temperature below 300 °C during the experiments. Depending on the electric current and coolant flow rate, the sample temperature varies between 23-210 °C during the experiments.

Experiments were performed with circular air jets, with jet Reynolds number varying from  $10^4$  to  $4 \times 10^4$ . Simultaneously, the value of  $H/S$  (where  $H$  is the distance between nozzle and the target and  $S$  is the characteristic length equal to jet diameter) was also varied from 4.7 to 24. The Nusselt number attains a maximum at  $H/S = 4.7$ . This matches well with the reported literature optimum value of 5 for  $H/S$ . Generally the current experimental data were found to be 50 – 70% more than the correlation reported in the literature. It is further seen that for identical Reynolds number, the Nusselt number is higher if the jet diameter is higher. This is due to the fact that the mass flow rate is higher for large jet diameter even if the Reynolds number is same. Experiments were also performed with slot air jets and inclined slot jets. The results show that for similar conditions circular jets give higher average heat transfer coefficient compared to slot jet. In the present experiments, the Nusselt number shows an increasing trend with the Reynolds number. Hence there is possibility to enhance the heat removal by increasing the air flow rate.

**Computational Fluid Dynamics simulation of single jet experiments:** Numerical simulation of the phenomenon has been carried out using general purpose CFD code and the predictions are compared against empirical correlations and experimental results. The length of the jet is large compared to its width (1 to 2 mm). Hence, the flow pattern would be similar along the length of the jet. Therefore, two dimensional section of the jet along the length direction is considered for the analysis. The prediction capability of various turbulence models has been assessed. It is found that the predictions of RNG  $k-\varepsilon$  model are closer to that

of LES model. Considering the computational time, the former is adapted in the present research.

**CFD simulation for spallation target cooling system:** The proposed scheme for spallation target cooling adopts helium jets impinging on target plates from either side. CFD results show that there is large variation in temperature of the order of 200 °C in the target plate. Temperature variation of this order is not acceptable for metallographic investigations. The interaction between the jets injected from one side of the target plate could be the reason for the large temperature variation of the target plate. In order to eliminate the interaction between the jets, analysis has been carried out on a configuration with only two jets (one jet on either side of the plate). For this case the plate temperature is nearly uniform except at the tip of the plate with a maximum variation of 20 °C only. Therefore, this configuration has been selected for the target plate cooling in the cyclotron. Due to the elimination of interaction between jets, there is ~ 10 % improvement in the heat removal capacity.

To confirm the numerical results for multiple jets, experiments were carried out with four and two air jets. The temperature fields on the specimen were obtained using thermal imaging. Results show that the maximum as well as the average temperature of the specimen for two jets cooling arrangement is lower than the four jets for given flow rate and test conditions. Based on the current and voltage measured the heat transfer coefficient for the case with four jets is 275 W/m<sup>2</sup>K and for two jets the value is 407 W/m<sup>2</sup>K. This is 48% higher compared to the four jets case. This confirms the numerical prediction. Hence two jet configuration is recommended for the spallation target cooling.

## List of Figures

<b>Fig. No.</b>	<b>Caption</b>	<b>Page No.</b>
Fig.1.1	Types of Impingement Jets	6
Fig.1.2	Characteristics of Impingement Jet	7
Fig.1.3	Flow Field of a free submerged jet	8
Fig.2.1	Schematic of a typical jet impingement arrangement and microchannel cooling system	24
Fig.2.2	Schematic of Target Plate	33
Fig.2.3	Comparison of DNS prediction by Chung and Luo against experimental data	50
Fig.2.4	Prediction of secondary flow and recirculation flow by DNS	50
Fig.3.1a	Schematic of the experimental set up	58
Fig.3.1b	Experimental Set up	58
Fig.3.1c	Arrangement of specimen	59
Fig. 3.2a	Array of circular jet nozzles	59
Fig.3.2b	Slot jet nozzles	60
Fig.3.3	Schematic showing alignment of jet with the sample	60
Fig.3.4	Experimental results for diameter = 1 mm and nozzle to target distance = 14 mm	62
Fig.3.5	Experimental results for diameter = 1 mm and nozzle to target distance = 19 mm	62
Fig.3.6	Experimental results for diameter = 1 mm and nozzle to target distance = 24 mm	63
Fig.3.7	Experimental results for diameter = 2 mm and nozzle to target distance = 14 mm	63
Fig.3.8	Experimental results for diameter = 2 mm and nozzle to target distance = 19 mm	64
Fig.3.9	Experimental results for diameter = 2 mm and nozzle to target distance = 24 mm	64
Fig.3.10	Experimental results for diameter = 3 mm and nozzle to target distance = 14 mm	65

Fig.3.11	Experimental results for diameter = 3 mm and nozzle to target distance = 19 mm	65
Fig.3.12	Experimental results for diameter = 3 mm and nozzle to target distance = 24 mm	66
Fig. 3.13	Nu Vs Re for different H/D ratios	66
Fig. 3.14	Nu Vs H/D ratio for Re = 12280	68
Fig.3.15	Experimental results for slot width = 1 mm and jet to nozzle distance = 14 mm	71
Fig.3.16	Experimental results for slot width = 1 mm and jet to nozzle distance = 19 mm	71
Fig.3.17	Experimental results for slot width = 1 mm and jet to nozzle distance = 24 mm	72
Fig.3.18	Experimental results for slot width = 2 mm and jet to nozzle distance = 14 mm	72
Fig.3.19	Experimental results for slot width = 2 mm and jet to nozzle distance = 19 mm	73
Fig.3.20	Experimental results for slot width = 2 mm and jet to nozzle distance = 24 mm	73
Fig.3.21	Experimental results for slot width = 3 mm and jet to nozzle distance = 14 mm	74
Fig.3.22	Experimental results for slot width = 3 mm and jet to nozzle distance = 19 mm	74
Fig.3.23	Experimental results for slot width = 3 mm and jet to nozzle distance = 24 mm	75
Fig.3.24	Nu Vs Re for different H/D ratios	75
Fig. 3.25	Nu Vs H/D ratio	76
Fig.4.1	Schematic of geometry and boundary conditions (BC)	83
Fig.4.2	Coarse and fine mesh patterns considered for the analysis	84
Fig.4.3	Predicted velocity distribution of 15 m <sup>3</sup> /h flow rate using k- $\epsilon$ RNG model	88
Fig.4.4	Predicted temperature distribution of 15 m <sup>3</sup> /h flow rate using k- $\epsilon$ RNG model	88
Fig.4.5	Temperature distribution along the length of plate (jet flow rate =	89



15 m<sup>3</sup>/h and prediction by k- $\epsilon$  RNG model)

Fig.4.6	Axial velocity distribution at different locations from the jet	89
Fig.4.7	Average heat transfer coefficient predicted by various turbulence models	90
Fig.4.8	Evolution of average temperature of plate predicted by LES model	90
Fig.4.9a	Velocity distribution for nozzle to target distance = 14 mm	92
Fig.4.9b	Temperature distribution for nozzle to target distance = 14 mm	92
Fig.4.10a	Velocity distribution for nozzle to target distance = 19 mm	93
Fig.4.10b	Temperature distribution for nozzle to target distance = 19 mm	93
Fig.4.11a	Velocity distribution for nozzle to target distance = 24 mm	94
Fig.4.11b	Temperature distribution for nozzle to target distance = 24 mm	94
Fig.4.12	Predicted heat transfer coefficient against distance between jet and target	95
Fig.4.13a	Predicted velocity distribution with two inclined jets (45°)	97
Fig.4.13b	Predicted temperature distribution with two inclined jets (45°)	97
Fig.4.14a	Predicted velocity distribution with two inclined jets (52°)	98
Fig.4.14b	Predicted temperature distribution with two inclined jets (52°)	98
Fig.4.15a	Predicted velocity distribution with two inclined jets (60°)	99
Fig.4.15b	Predicted temperature distribution with two inclined jets (60°)	99
Fig.4.16	Heat transfer coefficient variation against angle of inclination of two jets	100
Fig.5.1	Schematic of the target chamber for irradiation of specimen	104
Fig.5.2	Schematic of helium cooling circuit for spallation target cooling	105
Fig.5.3a	Envisaged cooling arrangement for the specimen	106
Fig. 5.3b	Envisaged cooling arrangement for the specimen	106
Fig.5.4	Heat removal capacity of jet cooling arrangement with helium	107
Fig.5.5	Evolution of specimen temperature in case of loss of cooling	107
Fig.5.6	Schematic of the CFD model for analysis of target cooling	110

Fig.5.7	Velocity pattern with 45° inclined jets and jet velocity of 200 m/s	110
Fig.5.8	Temperature distribution with 45° inclined jets and jet velocity of 200 m/s	111
Fig.5.9	CFD prediction of heat removal capacity of inclined slot jet cooling system	111
Fig.5.10	Predicted temperature distribution along the length of plate	114
Fig.5.11	Predicted velocity distribution with two jets inclined at 30° and other two at 45°	114
Fig.5.12	Predicted velocity distribution with two jets inclined at 45°	115
Fig.5.13	Predicted heat removal capacity for different configurations of jets	115
Fig.6.1	Spectral radiation intensity of a black body for different temperatures	120
Fig.6.2	Surface temperature of the sample with four air jets	123
Fig.6.3	Surface temperature of the sample with two air jets	123
Fig.6.4	Average temperature of the specimen	124

## List of Tables

Table No.	Caption	Page No.
Table 4.1	Estimated values of heat transfer coefficient based on average plate temperature by various turbulence models	91
Table 4.2	Heat transfer prediction as a function of distance between jet and target	95

# Glossary

BNCT	Boron Neutron Capture Therapy
CFD	Computational Fluid Dynamic
CHF	Critical Heat Flux
DNS	Direct numerical simulation
LES	Large eddy simulation
RANS	Reynolds- Averaged Navier-Stokes equation
RNG	Renormalization Group
SGS	Subgrid-scle
URANS	Unsteady Reynolds- Averaged Navier-Stokes equation
WALE	Wall-adapting local eddy-viscosity model

### List of Symbols

a	area of the nozzle
A	surface area of the specimen
B	width of the slot jet
D, d	diameter of the nozzle
f	Relative nozzle area – ratio of the nozzle exit cross section to the area of the square attached to it.
H	nozzle to target distance
h	heat transfer coefficient due to jet impingement
I	applied current
k	thermal conductivity of air
n	number of holes in the circular array of nozzles
Nu	Nusselt number ( $=h S / k$ )
Pr	Prandtl number
P	heat transfer from the sample
Q	air flow rate
Re	Reynolds number
S	Hydraulic diameter ( $= d$ for circular jet) ( $=2 B$ for slot jet)
Sc	Schmidt number
T	average temperature
v	velocity of air
V	voltage drop across the sample
x	specimen length / 2

## **Greek Symbols**

$\varepsilon$	emissivity of the sample
$\sigma$	Stefan - Boltzmann constant, $5.67 \times 10^{-8} \text{ W / m}^2 \text{ K}^4$
$\nu$	kinematic viscosity of air

## **Subscripts**

j	jet
t	total
r	radiation
a	ambient
avg	average

\* \* \*

# Chapter-1

## Introduction

In accelerator high heat flux removal is one of the main requirements. This is also the case for a number of engineering systems, such as computer chips, laser diodes and nuclear fusion and fission reactors. To realize fusion power, cooling requirements are very high. High heat flux technology development is one of the major requirements for diverter. Other such systems which require high-flux thermal management are advance defense devices found in radars, directed-energy laser and microwave weapon systems and avionics. Heat fluxes from defense devices are now projected to exceed  $10 \text{ MW/m}^2$  [1]. This level of heat dissipation exceeds the capabilities of today's most advanced dielectric liquid cooling systems, single-phase or two-phase, which points to an urgent need to develop new powerful cooling solutions. Micro channels, mini-channels, jet impingement cooling, spray cooling and cooling by transient boiling are some of the methods adapted to remove high heat fluxes. In these methods to further augment the heat removal capacity enhanced surface areas, different cooling mediums and use of phase changes are adapted.

Microchannel and jet impingement are the two methods adopted for high heat flux removal. Small hydraulic diameter increases the convective heat transfer coefficient in micro channels. Micro channel heat sinks also feature small size and weight, and require minimal coolant inventory. The two main disadvantages of the micro channel method are high pressure drop and large temperature gradients. Jet impingement gives large heat transfer coefficients at the impingement location with less pressure drop compared to micro channels. But away from the impingement location the heat transfer coefficient reduces. Moreover, it doesn't give uniform temperature field. Hence multiple jets are employed for high-flux heat removal. In this case care has to be taken to avoid interference between the impingement jet and the spent coolant flow. Both micro channel and jet impingement are good for high-flux heat removal, but there are practical challenges to overcome.



The high intensity proton beam from cyclotrons provides a unique facility for radiation damage studies on nuclear structural materials, as energetic charged particles are useful for simulating the bulk damage induced by neutrons. For example, 20 MeV protons with 350  $\mu\text{A}$  current will produce in stainless steel a damage rate of  $2 \times 10^{-5}$  dpa/s over a sample thickness of 0.7 mm [2]. This is an order higher than the damage rate produced in fast reactors ( $\sim 10^{-6}$  dpa/s). Due to the availability of high energy protons thick samples of the order of 0.5 to 1 mm can be irradiated. This facilitates the post irradiation investigation of the samples by a variety of bulk techniques like X-ray diffraction, positron lifetime, mechanical property measurements etc. feasible. The main interest will be in studying the irradiation effects on structural materials of thermal and fast breeder reactors like zirconium based alloys, D9, D9I and ferritic steels.

The nuclear structural material targets will be mainly coupons with typical dimension of 20 mm x 20 mm. The thickness of the sample can vary between 0.5 mm to 2 mm. The samples will be subjected to various doses. The geometric size of the target is very small and the heat flux very high. The target cooling facility for the irradiation sample should be designed in such a way that during irradiation, the heat deposited on the sample is carried away effectively by the cooling medium such that irradiation can be carried out at a desired temperature with good control. Based on the technical specification of proton beam produced in the cyclotron, the heat generated in the sample during irradiation can be as high as 6 kW. Designing a cooling arrangement for such a large heat flux of the order of  $15 \text{ MW/m}^2$  is a great challenge. The cooling medium should be such that it has good heat transfer properties, negligible proton activation and is easy to handle. One technique based on jet-impingement has been shown to be able to deal with fluxes up to  $400 \text{ MW/m}^2$ , over an area of a few square millimeters, with water as coolant [3]. Blackburn et al. [4] used this technique to develop a high power target for production of neutrons in an accelerator. Lienhard [5] provided a

detailed review of the research work done on this technique. Mitsutake and Monde [6] and Zhen-Hua et al. [7] also studied the heat fluxes removable by water jets. With water as coolant, very high jet velocities more than 100 m/s are needed for heat fluxes of  $400 \text{ MW/m}^2$ . An ultra high critical heat flux was attempted using a highly sub cooled liquid jet impinging on a small rectangular heated surface of length 5 ~10 mm and width 4 mm [6]. Experiments were carried out at jet velocities of 5 ~ 60 m/s, a jet temperature of  $20^\circ\text{C}$  and system pressures of 0.1 ~1.3 MPa. The maximum critical heat flux achieved in these experiments was  $211.9 \text{ MW/m}^2$ , recorded at system pressure of 0.7 MPa, jet velocity of 35 m/s and jet sub cooling of 151 K. A possible improvement might be achieved by using a liquid metal (such as gallium or gallium-based alloy), which significantly improves the heat transfer efficiency of the jet [5, 8]. Blackburn and Yanch [9, 10] used this technique to improve the performance of their accelerator target for BNCT (Boron Neutron Capture Therapy). Miner and Ghoshal [11] presented results for a miniature gallium jet impingement system for cooling high-power microelectronic devices.

High cooling rates of spallation targets are achieved by immersing the specimens in liquid metals or by contacting them to a cooling block by a liquid metal film. Both techniques have been applied to simulation experiments but suffer from poor temperature control and the production of radioactivity or from a small available temperature range [12, 13]. Thosen et al. [14] proposed, the criteria and procedural steps for choosing coolants for target plate in neutron source at high power densities. They also highlighted the experience with water cooling at moderate power densities and a brief overview at several existing and planned neutron (spallation) sources approaches. Jurns et al. [15] carried out preliminary design of the target moderator to provide the cooling for hydrogen cryogenic moderator system for the European Spallation Source used in neutron science facility funded by a collaboration of 17 European countries. The heat deposited into the hydrogen was suggested to be removed via a

heat exchanger in a hydrogen circulation cold box that transfers the heat from the hydrogen circuit to a gaseous helium circuit operating between 15 K and 20 K. Another method is the use of helium gas to cool the specimen. The amount of heat removal in this case is limited compared to the cooling by liquid metals but helium is non-radioactive, it is compatible with structural materials and it can be raised to very high temperatures. Helium cooling system will be simple compared to liquid metal or water cooling system. Even though helium is used for spallation target cooling [12, 13], experimental or numerical studies regarding heat removal and the temperature difference within the sample are not available in literature. In this project the main focus is on the helium cooling system and various parametric studies are carried out to maximize the heat removal. Both numerical as well as experimental studies are carried out. Experimental studies are carried out with air as cooling medium. Empirical correlation from the literature is used for evaluating the heat removal rate from the samples. The empirical correlation is compared against Computational Fluid Dynamic (CFD) simulations and experiments.

## **1.1 Jet impingement cooling**

An impingement cooling system is an array of jets of high velocity fluid which is made to strike a target surface. Such impinging flow devices allow for short flow paths and relatively high rates of cooling from comparatively small surface area. Various industrial processes involving high heat transfer rates use impinging jets due to effective and flexible way to transfer energy or mass. Few industrial processes which employ impinging jets are drying of food products, textiles, films and papers, processing of some metals and glass, cooling of gas turbine blades and outer wall of the combustion chamber, cooling of electronic equipments, etc.

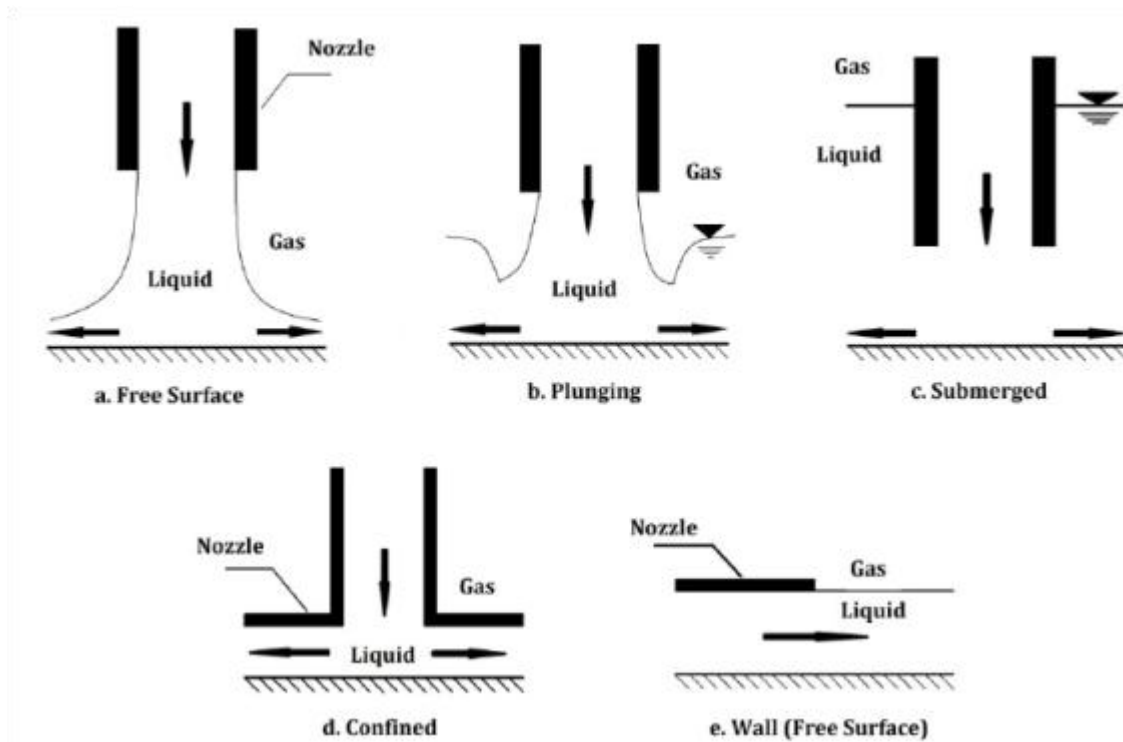


**Fig. 1.1 Types of impingement jets**

Impinging jets can be classified as either free surface or submerged [16]. If the fluid issuing from the jet is of the same density and nature as that of the surrounding fluid then the jet is called the submerged. If the fluid issuing from the nozzle is of a different density and nature than that of the surrounding fluid then the jet is called free. Further classification between jets can be made for confined and un-confined jets. In the case of confined, the jet remains bounded between two surfaces during its flow. There is less entrainment of air from the atmosphere. Un-confined jets are free to expand after they impinge on the target surface. Types of impingement jets are shown in Fig. 1.1.

Submerged jets exude into a space containing the same liquid at rest and can be configured as confined or unconfined, depending on the jet-to-target distance. In a submerged configuration, the interaction of the issuing jet and the stagnant fluid leads to entrainment in the shear zone and the development of a potential core near the jet centerline [17].

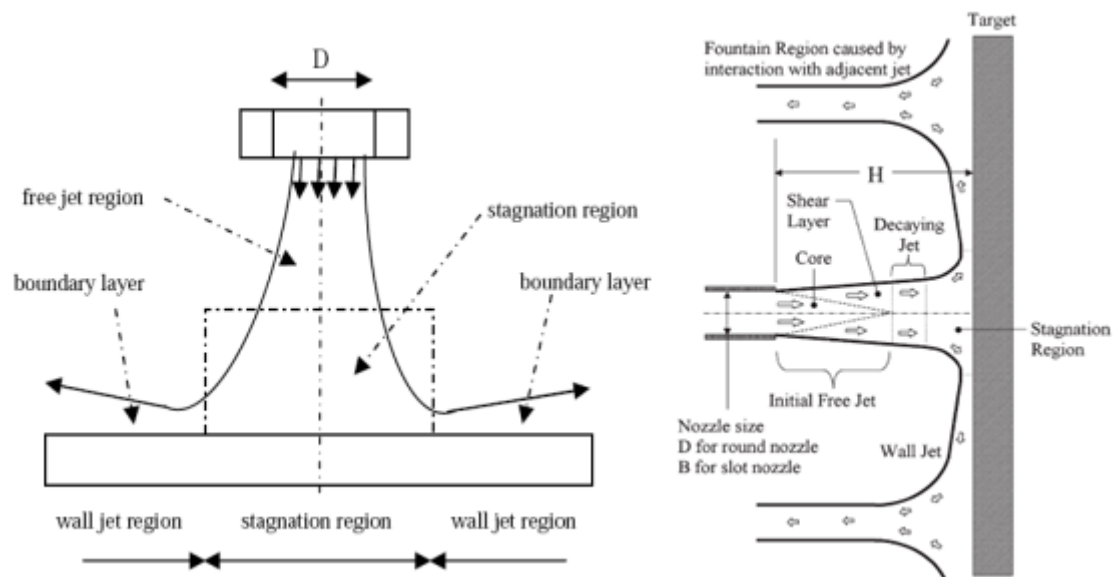


**Fig 1.2 Characteristics of impingement jet**

Flow field of a submerged impinging jet is characterized by a jet zone, a stagnation zone and a wall jet zone [18] as indicated in Fig. 1.2. The jet emerges from a nozzle or opening with a velocity and temperature profile and turbulence characteristics dependent upon the upstream flow. For a pipe-shaped nozzle, also called a tube nozzle or cylindrical nozzle, the flow develops into the parabolic velocity profile common to pipe flow plus a moderate amount of turbulence developed upstream. In contrast, a flow delivered by application of differential pressure across a thin, flat orifice will create an initial flow with a fairly flat velocity profile, less turbulence, and a downstream flow contraction.

The potential core is the region in which the velocity of the jet remains largely unaffected by the spreading of the jet due to entrainment. In the confined case, the fluid heated by the target plate can, in some instances, get re-circulated and be entrained back into the impinging jet. This causes the formation of a re-circulation zone in the outflow region. In an unconfined configuration, such as the case when jets are issuing from long tubes, the jet interacts with the ambient and otherwise quiescent surroundings and has associated with it higher heat transfer coefficients because the heated fluid is not entrained back into the jet, as

is sometimes the case for confined jets. The point at which jets differentiate between fully confined and fully unconfined will likely depend on many factors, including but not limited to  $Re$ ,  $H/d$  and surface topology.

In a free-surface jet configuration, the fluid is discharged from the nozzle into an ambient gas, typically air, before impinging upon the target surface. Therefore, entrainment of the surrounding fluid can be considered to be negligible so that a potential core is not relevant in this case. Due to the intensive trend of component miniaturization, the available space for the cooling device will likely be very restricted.

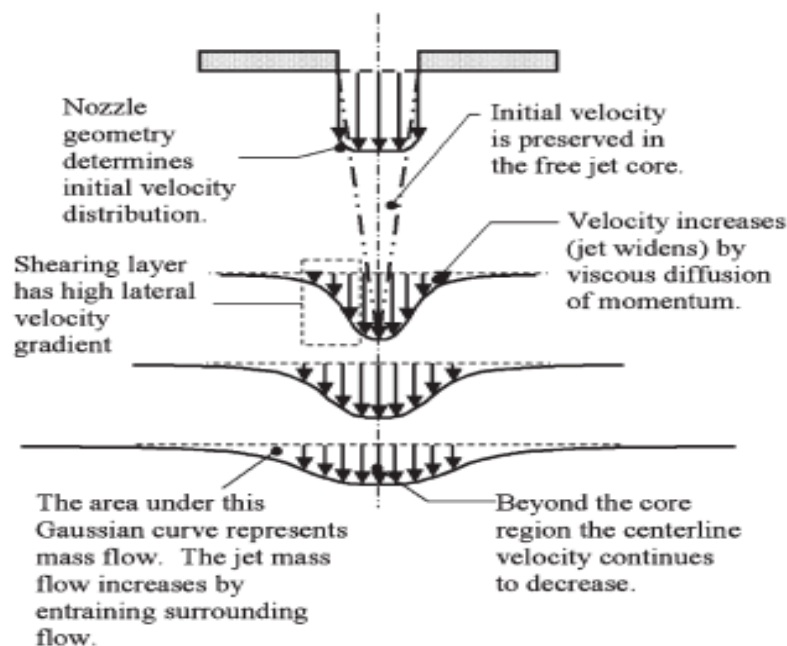


**Fig. 1.3 Flow field of a free submerged jet**

Typical jet nozzle designs use either a round jet with an axi-symmetric flow profile or a slot jet, a long, thin jet with a two-dimensional flow profile. After it exits the nozzle, the emerging jet may pass through a region where it is sufficiently far from the impingement surface to behave as a free submerged jet. Here, the velocity gradients in the jet create a

shearing at the edges of the jet which transfers momentum laterally outward, pulling additional fluid along with the jet and raising the jet mass flow, as shown in Fig. 1.3. In the process, the jet loses energy and the velocity profile is widened in spatial extent and decreased in magnitude along the sides of the jet. Flow interior to the progressively widening shearing layer remains unaffected by this momentum transfer and forms a core region with a higher total pressure, though it may experience a drop in velocity and pressure decay resulting from velocity gradients present at the nozzle exit. A free jet region may not exist if the nozzle lies within a distance of two diameters ( $2D$ ) from the target. In such cases, the nozzle is close enough to the elevated static pressure in the stagnation region for this pressure to influence the flow immediately at the nozzle exit.

## **1.2 Applications of Jet Impingement**

Jet impingement heat transfer cooling systems plays a significant role in many industrial applications. This is due to the fact, that the impinged jet provides higher rate of heat and mass transfer. A directed liquid or gaseous flow released against a surface can efficiently transfer large amounts of thermal energy or mass between the surface and the fluid. Heat transfer applications include cooling of stock material during material forming processes, to quench products after rolling and heat treatment [19], cooling of electronic components, heating of optical surfaces for defogging, cooling of turbine components, cooling of critical machinery structures, and many other industrial processes. Typical mass transfer applications include drying and removal of small surface particulates. In gas turbine engines, impinging jets are applied for cooling of turbine blades/vanes. In laser/plasma cutting processes, with jet impingement cooling, thermal deformation of products can be reduced. Besides the above applications, impinging jets are also adopted to enhance electronic cooling.

In the example of turbine cooling applications, impinging jet flows may be used to cool several different sections of the engine such as the combustor case, turbine case/liner, and the critical high temperature turbine blades. The gas turbine compressor offers a steady flow of pressurized air at temperatures lower than those of the turbine and of the hot gases flowing around it. The blades are cooled using pressurized bleed flow, typically available at 600 °C. The bleed air must cool a turbine immersed in gas of 1400 °C total temperatures [20], which requires heat transfer coefficients in the range of 1000–3000 W/m<sup>2</sup> K. This equates to a heat flux on the order of 1 MW/m<sup>2</sup>. The ability to cool these components in high-temperature regions allows higher cycle temperature ratios and higher efficiency, improving fuel economy, and raising turbine power output per unit weight. Modern turbines have gas temperatures in the main turbine flow in excess of the temperature limits of the materials used for the blades, meaning that the structural strength and component life are dependent upon effective cooling flow. Compressor bleed flow is commonly used to cool the turbine blades by routing it through internal passages to keep the blades at an acceptably low temperature. The same air can be routed to a perforated internal wall to form impinging jets directed at the blade exterior wall. Upon exiting the blade, the air may combine with the turbine core airflow. Variations on this design may combine the impinging jet device with internal fins, smooth or roughened cooling passages, and effusion holes for film cooling.

Compared to other heat or mass transfer arrangements that do not employ phase change, the jet impingement device offers efficient use of the fluid, and high transfer rates. For example, compared with conventional convection cooling by confined flow parallel to (under) the cooled surface, jet impingement produces heat transfer coefficients that are up to three times higher at a given maximum flow speed, because the impingement boundary layers are much thinner, and often the spent flow after the impingement serves to further enhance the turbulence in the surrounding fluid. Given a required heat transfer coefficient, the flow



required from an impinging jet device may be two orders of magnitude smaller than that required for a cooling approach using a free wall-parallel flow. For more uniform coverage over larger surfaces multiple jets may be used. The impingement cooling approach also offers a compact hardware arrangement.

Some disadvantages of impingement cooling devices are:

- (1) For moving targets with very uneven surfaces, the jet nozzles may have to be located too far from the surface. For jets starting at a large height above the target (over 20 jet nozzle diameters) the decay in kinetic energy of the jet as it travels to the surface may reduce average  $Nu$  by 20% or more.
- (2) The hardware changes necessary for implementing an impinging jet device may degrade structural strength (one reason why impinging jet cooling is more easily applied to turbine stator blades than to rotor blades).
- (3) In static applications where very uniform surface heat or mass transfer is required, the resulting high density of the jet array and corresponding small jet height may be impractical to construct and implement, and at small spacings jet-to-jet interaction may degrade efficiency.

Heat transfer rates in case of impinging jets are influenced by various parameters like Reynolds number, jet-to-plate spacing, radial distance from stagnation point, Prandtl number, target plate inclination, confinement of the jet, nozzle geometry, curvature of target plate, roughness of the target plate and turbulence intensity at the nozzle exit. Prior to the design of an impinging jet device, the heat transfer at the target surface is typically characterized by a Nusselt number ( $Nu$ ), and the mass transfer from the surface with a Schmidt number ( $Sc$ ). For design efficiency studies and device performance assessment, these values are tracked vs.

jet flow per unit area ( $G$ ) or vs. the power required to supply the flow (incremental compressor power).

### 1.3 Effects of various parameters on impinging heat transfer

Considerable research has been done on jet impingement heat transfer and enhancement by various methods. Jambunathan et al. [21] did a detailed survey on jet impingement cooling. They concluded that the simplest correlation for local heat transfer coefficient is a function of jet Reynolds number ( $Re$ ), jet height-to-jet diameter ratio ( $H/d$ ), radial distance-to-jet diameter ratio ( $r/d$ ) and Prandtl number ( $Pr$ ). Goldstein et al. [22] investigated the effect of entrainment on the heat transfer to a circular air jet impinging on a flat plate. They found that both the Nusselt number and heat transfer effectiveness would not be affected by the temperature difference between the ambient air and jet. Bouchez et al. [23] investigated the impingement cooling of a circular jet with/without a cross flow. The result shows that, for a moderate jet-to-cross flow mass flux ratio, the jet was deflected by the cross flow. Sparrow et al. [24] also investigated the heat transfer of a confined jet impingement with a cross flow. It was found that the convective heat transfer coefficient for case with jet impingement could be tenfold that without jet impingement. Goldstein et al. [25] performed an experiment on a confined circular jet with/without a cross flow. They concluded that, at large plate spacing, the cross flow diminishes the heat transfer coefficient; at small plate spacing, the cross flow would increase the peak heat transfer coefficient. Sparrow et al. [26] developed an analogy technique, by measuring the amount of sublimation of naphthalene on a jet impingement surface, for evaluation of the convective heat transfer coefficient. It was found that the dimensionless mass transfer coefficient varies with the 0.8 power of the jet Reynolds number. An optical technique developed by Goldstein and Timmers [27] and Goldstein and Franchett [28] was used in measuring the heat transfer of an impinging jet with

different inclined angles. The isothermal lines on the impingement plate were clearly observed. Huang and EL-Genk [29] investigated the heat transfer of an unconfined jet with low jet Reynolds numbers and small jet height-to-jet diameter ratios. The average Nusselt number was found proportional to  $Re^{0.76}$ . Lytle and Webb [30] performed a heat transfer measurement for an impinging jet with jet height-to-jet diameter ratios less than 1.0. The result indicates that the stagnation Nusselt number is proportional to the 0.53 power of the jet Reynolds number and -0.191 power of the jet height-to-jet diameter ratio. Li and Garimella [31] investigated the stagnation and area-averaged Nusselt numbers for a confined jet impinging on a small and discrete heat-source area. The stagnation Nusselt number was found proportional to the 0.444 power of the Prandtl number and 0.483 power of the jet Reynolds number. Garimella and Rice [32] and Fitzgerald and Garimella [33] performed experiments to examine the flow field of a confined jet impingement. A toroidal recirculation-flow pattern in the downstream was clearly shown. Angibletti et al. [34] investigated the flow field and heat transfer for a jet impinging on a flat plate. The flow structure was used to interpret the heat transfer characteristics of the jet impingement. Narayanan et al. [35] investigated the flow and heat transfer characteristics of a slot jet impinging on a flat plate. The result indicates that, for transitional jet impingement, the heat transfer coefficient monotonically decays in the flow direction; for potential-core jet impingement, a secondary peak in heat transfer appears at 3.2 times the hydraulic diameter from the jet centerline. Zhou and Lee [36] performed an experiment on the heat transfer of an impinging jet with a mesh screen installed in front of jet nozzle. The result shows that, with the mesh screen, the heat transfer can be slightly upgraded.

Huber and Viskanta [37] investigated the effect of jet-to-jet spacing on the heat transfer for a confined impinging jet array. It was found that, for large plate spacing, jet

interference causes a significant degradation of the heat transfer. San and Lai [38] had also investigated the effect of jet interference on the heat transfer for staggered arrays of impinging jets. An optimum jet-to-jet spacing of heat transfer was found. Dano et al. [39] investigated the effect of nozzle geometry on the heat transfer for an in-lined array of impinging jets. The heat transfer performance of the cusped ellipse nozzle appears to be superior to that of the circular nozzle. From the results indicated in the literature, besides nozzle geometry and jet Reynolds number, the heat transfer characteristics of a confined jet are also dependent on geometry of jet plate and that of impingement plate.

#### **1.4 Motivation for the present study**

Even though helium is used for spallation target cooling, experimental or numerical studies regarding heat removal, ways for enhancing the heat removal, temperature difference within the sample and the ways to reduce the temperature difference are not available in literature. In the air jet cooling studies, most of the studies are with vertical impingement jet at the center of the target plate. This cannot be adapted here because it will interfere with the proton beam. The jets have to be necessarily inclined and also away from the target plate such that they will not interfere with the proton beam. For this case the heat removal and temperature distribution of the sample are different compared to the case where jet is impinging at the center. Hence it is planned to carry out jet cooling experiments with air as coolant. Compare the available empirical correlation from the literature using the experiments as well as computational fluid dynamics simulation. The above studies will be used for designing the spallation target cooling system.

#### **1.5 Research objective**

The objective of the present research work is:

- Impingement jet cooling experiments with air to understand the heat transfer characteristics.
- To identify the parameters which can give the maximum possible heat transfer coefficient by varying the parameters in the air jet cooling experiments.
- Comparison of experimental results with empirical correlations available in the literature.
- Comparison of experimental results and empirical correlation with numerical predictions.
- Numerical predictions of helium jet cooling heat transfer characteristics with various cooling arrangements.
- Conceptual design of helium cooling circuit for cooling irradiation target specimen.

## **1.6 Organization of Thesis**

A review of various methods of removing high heat fluxes from the literature is given in Chapter 2. Details regarding experimental and numerical studies carried out for jet impinging heat transfer and also empirical correlations available in literature are explained in this chapter. Chapter 3 contains details regarding the experimental setup and single air jet experimental studies. For comparison with empirical correlations initially experimental studies are carried out using single vertical jet. Experiments have been carried out with both single array of circular jets and slot jet. Parametric studies are carried out by varying the nozzle diameter and nozzle to target distance. The experimental results are compared with empirical correlations. Numerical simulation of the jet cooling phenomenon, including modeling details, comparison of various turbulence models, selection of appropriate model and comparison of numerical and experimental results are presented in Chapter 4. In chapter 5, the CFD results for the proposed scheme for spallation target cooling are given. Helium

jets are placed two on each side. Geometry and boundary conditions of the model used are explained. The objective of the first part of the study is to estimate the heat removal capacity for various values of jet velocity. The second part of the study is to optimize the jet angle for minimizing temperature variation in the target. The complete helium cooling system is explained in this chapter. In Chapter 6, details of the multiple air jet experiments carried out to confirm the final configuration selected based on the numerical studies for the cooling of target specimen is given. Chapter 7 includes an overview of the studies carried out and final conclusions arrived from the studies. Areas of possible future R&D both experimental and numerical are also presented here.

\* \* \*

# Chapter-2

## **Literature Review**

### **2.1 Cooling systems for high heat flux applications**

High heat flux removal with minimum pressure drop and minimum manufacturing cost is a major requirement in the design of a number of systems, such as high-performance computer chips, laser diodes, accelerator systems and nuclear fusion and fission reactors. As engineering design progress towards the realization of commercial energy from nuclear fusion, solutions are being sought which address the extreme thermal management and cooling requirements. The divertor in particular is an area which requires development of high heat flux technology for it to be viable as the reactor power exhaust. High-flux thermal management is also a primary design concern for advanced defense devices found in radars, directed-energy laser and microwave weapon systems and avionics. While these devices follow the trend of escalating power density of commercial electronics, heat fluxes from defense devices are now projected to exceed  $10 \text{ MW/m}^2$ . This level of heat dissipation exceeds the capabilities of today's most advanced dielectric liquid cooling systems, single-phase or two-phase, which points to an urgent need to develop new powerful cooling solutions. Microchannels, minichannels, jet impingement cooling, spray cooling and cooling by transient boiling are some of the methods adapted to remove high heat fluxes. In these methods to further augment the heat removal capacity enhanced surface areas, different cooling mediums and use of phase changes are adapted. Details of some of these studies from the literature are given in this report.

#### **2.1.1 Microchannels**

Microchannels and minichannels are naturally well suited for this task, as they provide a large heat transfer surface area per unit fluid flow volume. They provided an



efficient way to remove heat from a surface but pose challenges in bringing fresh coolant to the heated surface and returning it to the cooling system before the coolant reaches the stringent temperature rise limits. The problem is interlinked with the performance issues of the cooled systems, which dictate a lowering of the surface temperature to increase reliability, speed of the processor units, or other overall system considerations.

Micro channels were first proposed for electronics cooling applications by Tuckerman and Pease [40], who employed the direct circulation of water in micro channels fabricated in silicon chips. The micro channel heat sink was able to dissipate  $7.9 \text{ MW/m}^2$  with a maximum temperature difference of  $71^\circ\text{C}$ . However, the pressure drop was quite large at 200 kPa with plain micro channels and 380 kPa with pin fin-enhanced micro channels. Another major milestone was achieved by Phillips [41], who analyzed the heat transfer and fluid flow processes in micro channels and provided detailed equations for designing micro channel geometries. The use of enhanced micro channels was suggested by Tuckerman and Pease [40], Phillips [41], Steinke and Kandlikar [42], and Kandlikar and Grande [43], among others. Colgan et al. [44] provided the results of a practical implementation of enhanced micro channels with strip-fin geometry. Kandlikar and Upadhye [45] presented a detailed set of equations and the results of an optimization procedure for selecting micro channel flow geometries under a given pressure drop constraint. The implementation of micro channel heat sinks in a notebook computer was discussed by Pokharna et al. [46]. They considered the operational issues of a micro channel two-phase loop and also discussed the manufacturing and cost issues associated with mass producing such systems. The developments on incorporating flow boiling in micro channels have been somewhat limited because of the issues associated with the stable operation of flow boiling systems and critical heat flux limitations.

**Cooling Medium:** Another issue that is becoming apparent is the requirement of low operating surface temperatures that cannot be easily accomplished with water as the phase change fluid unless the cooling system is operated at sub atmospheric pressures. Experimental data with refrigerants is not yet available to guide a designer in the selection of a proper working fluid to meet the desired high heat transfer coefficient requirement as well. Among the most demanding areas of the reactor design are the high heat flux systems, which will receive continuous power densities in the order of  $10\text{MW/m}^2$  [47]. To address such requirements, attention must be focused on coolant specification in combination with heat exchanger design. The candidate reactor coolants being considered are chiefly helium, water,  $\text{CO}_2$ , molten salts, or dual-cooling using a liquid metal. In developing power plant concepts much attention has been given to helium, including as coolant for the divertor [47], but recently interest has increased in water as it is simpler to implement, makes use of existing power generation technology and has a high power handling capability. The disadvantages of water are a limited power conversion efficiency, high pumping power and power handling limited by the critical heat flux (CHF), the departure from nucleate boiling with sudden reduction in heat transfer efficiency. However, these limitations could all be mitigated by the use of nanofluids, which are suspensions of 0.001-10% nanoparticles of  $<100\text{ nm}$  size [48]. Water-based nanofluids have the potential to deliver much improved high heat flux cooling [49] while retaining all the advantages of water.

### 2.1.2 Jet impingement cooling

Heat fluxes from defense devices are now projected to exceed  $10\text{ MW/m}^2$  [1]. In pursuing such cooling solutions, it is useful to examine the attributes of today's most effective cooling schemes. Those schemes are based mostly on two types of coolant flows, micro channel and jet impingement. Small hydraulic diameter greatly increases the

convective heat transfer coefficient in micro channels. Micro channel heat sinks also feature small size and weight, and require minimal coolant inventory. Two key drawbacks of micro channel heat sinks are high pressure drop and large temperature gradients along the direction of coolant flow. Jet impingement produces enormous heat transfer coefficients in the impingement zone and generally require smaller pressure drop than micro channels. However, they also produce large surface temperature gradients away from the impingement zone. To diffuse this concentrated cooling effect, multiple jets are preferred for high-flux heat removal, especially from large surface areas. However, this greatly increases the coolant's flow rate and complicates the routing of spent coolant within the cooling module. Clearly, both micro channel flow and jet impingement are good candidates for high-flux heat removal, but they also pose practical challenges.

### **2.1.3 Spray cooling with enhanced heat transfer area**

Many critical applications today, in electronics, optics and aerospace fields, among others, demand advanced thermal management solutions as described above for the acquisition of high heat loads they generate in order to operate reliably and efficiently. Current competing technologies for this challenging task include several single and two phase cooling options. When these cooling schemes are compared based on the high heat flux removal ( $1 - 10 \text{ MW/m}^2$ ) and isothermal operation aspects, as well as system mass, volume and power consumption, spray cooling appears to be the best choice. Bostanci [50] carried out extensive work on high heat flux spray cooling with ammonia on enhanced surfaces. He found that the ammonia possesses important advantages such as low saturation temperature, and high heat absorbing capability compared to some other commonly used coolants. Moreover, enhanced surfaces offer potential to greatly improve heat transfer performance. The main objectives of the study were to investigate the effect of surface enhancement on

spray cooling performance, and contribute to the current understanding of spray cooling heat transfer mechanisms. These objectives were pursued through a two stage experimental study. While the first stage investigated enhanced surfaces for the highest heat transfer coefficient at heat fluxes of up to  $5 \text{ MW/m}^2$ , the second stage investigated the optimized enhanced surfaces for critical heat flux.

#### **2.1.4 Passive cooling**

Mitsuo Hashimoto [51] developed a two-phase heat spreader for cooling high heat flux sources in high-power lasers, high-intensity light emitting diodes, and semiconductor power devices. The heat spreader targets the passive cooling of heat sources with fluxes greater than  $5 \text{ MW/m}^2$  without requiring any active power consumption for the thermal solution.

#### **2.1.5 Jet impingement Vs microchannel cooling**

The high heat flux treatment has also become a crucial technology for the cooling of plasma facing components in fusion reactors [52] and the cooling of high power optical components in synchrotrons and power beaming applications [53]. While both jet impingement and micro channel cooling technologies are known to provide very high heat transfer performance, it is desirable to understand which is preferable for a given high heat flux application. In the jet impingement scheme, thin hydrodynamic and thermal boundary layers forming in the impingement region result in high heat transfer coefficients. On the other hand, micro channels provide a large area of contact between the solid and coolant as well as a huge temperature gradient in the coolant near the channel wall due to the extremely small channel width. The prominent features of each technology concerned with the high heat transfer capabilities have allowed a variety of applications, while the main fields of

applications have been distinguished from each other. The jet impingement has been widely used in industrial transport processes while, the micro channel cooling has been mainly employed in the cooling of microelectronic devices. The increasing applications required for high heat flux treatments have drawn substantial improvement of each technology and expanded each field covering ground previously reserved for either one of these technologies. The use of jet impingement for the cooling of electronic components is an example of such infringement of the two competing technologies [54]. The competition between the two technologies has become unavoidable, thus requiring a systematic and objective comparison of the two technologies. The manufacturing cost, compactness and economic maintenance are also of importance in addition to the heat transfer characteristics. In some applications such as fusion reactors and synchrotrons, the heat transfer characteristics, however, are the most critical factor among all other considerations. In such cases, it is important to determine which technology provides a higher heat transfer capability. To this end the thermal aspect serves as the primary one towards a comprehensive comparison. With this in mind Lee and Vafai [55] carried out a detailed study aimed at providing criteria in selecting one technology over another in maximizing the heat transfer process. They characterized the flow field into three separate regions of impinging jet, each with its distinct characteristics: the free jet region, the impingement region and the radial flow region as shown in Fig. 2.1 along with and micro channel cooling system.

The flow in the free jet region is mainly in the axial direction and is not much affected by the presence of the impingement surface. Within this free jet region are two sub regions, the potential core with velocity equal to the jet exit velocity and the lower velocity shear layer, which results from the entrainment of the surrounding fluid. Downstream of the nozzle, the shear layer progressively grows and displaces the potential core, eventually

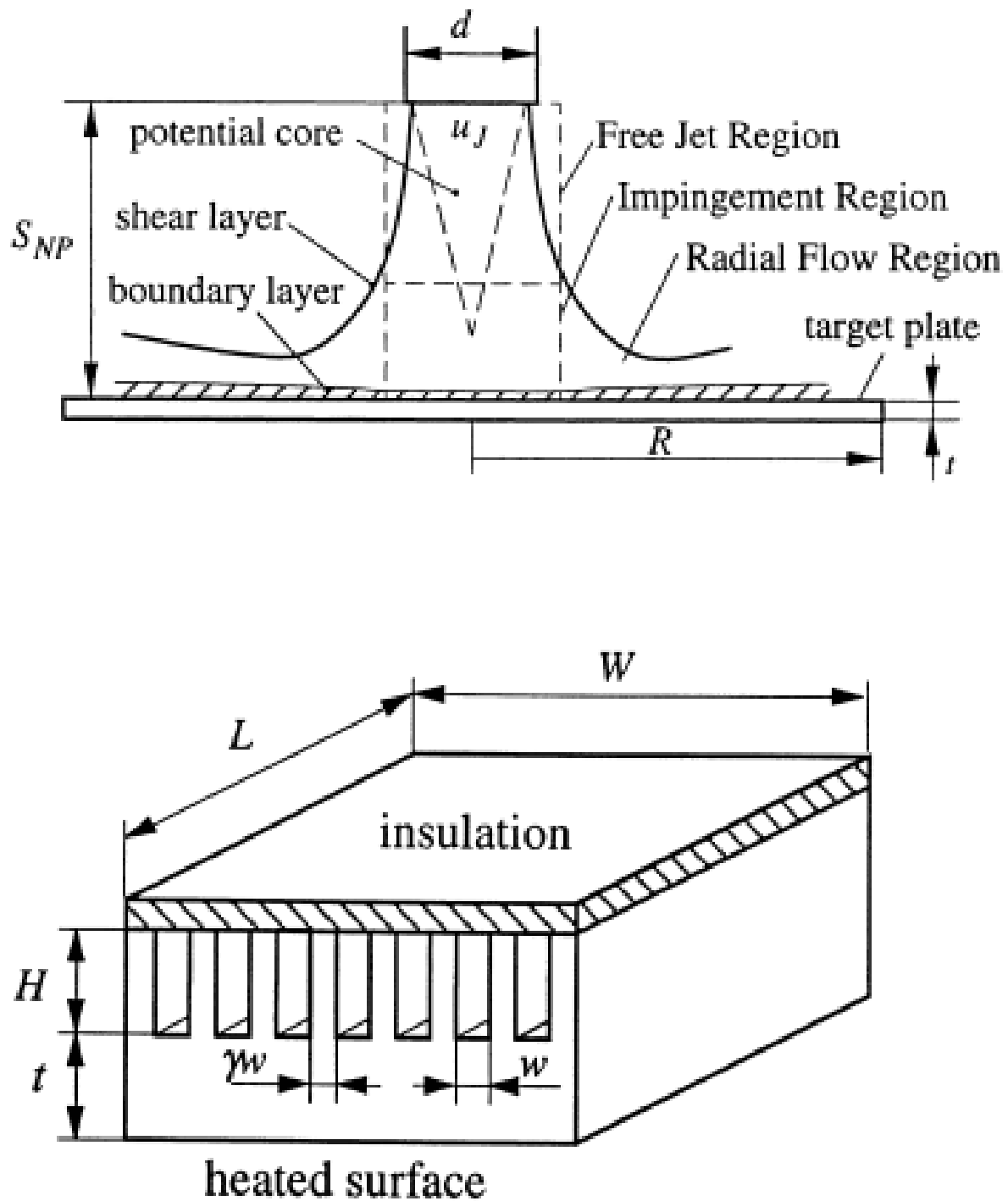


**Fig. 2.1 Schematic of a typical jet impingement arrangement and microchannel cooling system**

reaching the jet centerline. Based on the optimization procedures the maximum heat flux attainable by each technology was evaluated within practical operation constraints. The thermal performance of each technology evaluated at the respective optimal condition is

compared to each other with the target dimension as a main parameter. Heat removal by micro channel cooling decreases significantly due to even a small increase in the plate thickness. It is seen that the thermal performance of the jet impingement without any treatment of spent flow is substantially lower than that by the micro channel cooling regardless of the target plate dimension. With proper treatment of spent flow, however, the jet impingement is quite comparable to the micro channel cooling.

### **2.1.6 Spray cooling using water based polymer additive**

The experimental investigation of using water based polymer additive to enhance the spray cooling performance of hot steel plate, has been carried out by Ravikumar [57]. The ultra-high heat flux cooling system has been developed using an air-atomized spray, containing dissolved polyvinyl pyrrolidone in water at different concentration ranges between 10 and 150 ppm and compared with the cooling performance of pure water. The results explain that the polymer solution has a significant effect on the enhancement of surface heat flux, critical heat flux, as well as the cooling rate of the test plate. It was observed that an increase in the polymer concentration increases the heat transfer rate up to an optimal concentration; after which it results in a reduction in the rate. A maximum cooling rate of 253 °C / s was obtained with a critical heat flux of 4.212 MW/m<sup>2</sup>, which can be termed as the higher range of an ‘Ultrafast cooling’ process.

### **2.1.7 Transient boiling cooling**

Warrier et al. [58] proposed and analyzed a novel two-phase micro channel cooling device that incorporates perforated side walls for potential use as an embedded thermal management solution for high heat flux semiconductor devices. A dense array of perforated side walls separate alternating liquid and vapor microchannels, allowing the vapor generated

through evaporation of liquid supplied through micro-perforations to flow only in the dedicated vapor channels. By separating the liquid and vapor flows, these “perspiring” side walls enable us to circumvent flow instabilities and other challenges associated with conventional two-phase microchannel cooling while at the same time effectively take advantage of the large extended surface areas available in high-aspect-ratio microchannels. They demonstrated the potential of their proposed device for handling high heat flux electronic and optoelectronic semiconductor devices.

Filipovic et al. [59] performed transient boiling experiments using a large preheated test specimen exposed to a water wall jet on its top surface. They reported that during much of the quenching process, conditions on the test surface were characterized by propagation of a quench front in the direction of flow along the surface. Heat transfer occurred by nucleate boiling or single-phase convection upstream of the front, while film boiling existed in a precursory region downstream of the front. The front itself was at the leading edge of a transition-boiling zone, which was approximately coincident with location of maximum heat flux. They also found that the location of the maximum heat flux on the surface moved downstream with increasing time and its value decreased with time. Kumagai and Suzuki [60] also conducted a transient cooling experiment of a hot metal slab but with an impinging plane jet. They observed that local surface temperature fell rapidly when the temperature at that point reached the temperature corresponding to the high heat flux region of transition boiling. Hall et al. [61] performed an experimental study of boiling heat transfer during quenching of a cylindrical copper disk by a subcooled, circular, free-surface water jet. Their study reveals that quenching measurements encompass three distinct boiling regimes; nucleate boiling in the impingement zone, the upper limit of nucleate boiling (maximum heat flux for the entire surface) and transition boiling which is characterized by minimum film



boiling heat flux and the temperatures for the radial flow region. They correlated the radial distributions of maximum heat flux data with relations developed by others researchers from steady-state experiments for radial flow region.

### **2.1.8 Wicks for high heat flux applications**

Experimental study of biporous wicks for high heat flux applications was carried out by Semenik and Catton [62]. Biporous wicks are wicks with two distinguished characteristic pore sizes while monoporou wicks are wicks with a single characteristic pore size. The best monoporou wick tested had CHF at  $3 \text{ MW/m}^2$  ( $21^\circ\text{C}$  superheat), the best thin biporous wick tested had CHF at  $5.2 \text{ MW/m}^2$  ( $50^\circ\text{C}$  superheat), and the best thick biporous wick tested had CHF at  $9.9 \text{ MW/m}^2$  ( $147^\circ\text{C}$  superheat). Thick biporous wicks can be used for  $6 - 10 \text{ MW/m}^2$  applications where high superheats and heat spreading into the wick are acceptable. For applications below  $6 \text{ MW/m}^2$  are recommended thin biporous wicks and for applications below  $3 \text{ MW/m}^2$  are recommended monoporou wicks.

### **2.1.9 High heat flux micro-evaporator**

Takashihiro Tsukamoto and Ryoji Imai [63] designed a high heat flux micro-evaporator that can remove more than  $1 \text{ MW/m}^2$ . For achieving heat flux a thin liquid film is evaporated. The liquid film is stabilized in micro-channels by capillary forces. The micro-channels are fabricated by chemical etching on silicon to reduce thermal resistance. For the experiments, the channel plate is heated by a thin film heater deposited on the opposite side of the channel plate. Influence of heat flux, coolant flow rate, and inlet temperature on the temperature of the heater element are investigated. Water is used as working fluid. A maximal heat flux of  $1.25 \text{ MW/m}^2$  could be achieved for water inlet temperature of  $90^\circ\text{C}$  and flow rate of 1.0

ml/min. The temperature of the heater element is kept constant at about 120 °C with fluctuations within 8 °C. The measured pressure drop is less than 1000 Pa.

#### 2.1.10 Closure

A review of various methods of removing high heat fluxes from the literature is reported in this chapter. Microchannels, minichannels, jet impingement cooling, spray cooling and cooling by transient boiling are some of the methods adapted to remove high heat fluxes. In these methods, to further augment the heat removal capacity, enhanced surface areas, different cooling mediums and use of phase changes are adapted. High-heat-flux removal can be achieved by either single-phase flow or two-phase flow boiling heat transfer. Microchannels and mini microchannels are used in electronic cooling applications. The heat dissipation rate is of the order of 7.9 MW/m<sup>2</sup>. With the current single-phase enhanced micro channel technology, a heat dissipation rate as high as 10 MW/m<sup>2</sup> seems possible. Another important method for high heat flux removal is by jet impingement. Jet-impingement has been shown to be able to deal with fluxes up to 400 MW/m<sup>2</sup>, over an area of a few square millimeters, with water as coolant [3]. Blackburn et al. [4] used this technique to develop a high power target for production of neutrons in an accelerator. Lienhard [5] provided a detailed review of the research work done on this technique. Both microchannel flow and jet impingement are good candidates for high-flux heat removal, but they also pose practical challenges. Two key drawbacks of microchannel heat sinks are high pressure drop and large temperature gradients along the direction of coolant flow. Jet impingement produces enormous heat transfer coefficients in the impingement zone and generally requires smaller pressure drop than microchannels. However, it also produces large surface temperature gradients away from the impingement zone. To diffuse this concentrated cooling effect, multiple jets are preferred for high-flux heat removal, especially from large surface areas.

## **2.2 Experimental Studies on Jet Cooling**

### **2.2.1 Jet impingement cooling**

Colin Glynn et al. [64] have conducted experiments for both air and water jets. Three orifice plates are used in the current study, containing single nozzles of 0.5 mm, 1 mm and 1.5 mm in diameter respectively. The orifice plates are of 5 mm constant thickness and all nozzles are sharp-edged. A single jet issues from the orifice plate and impinges normally onto an electrically heated stainless steel foil. The foil is electrically heated by clamping at each end to one of the large sides of two opposite copper bus bar electrodes. Each clamp is between the bus bar and a copper plate minimizing contact resistance. The electrical supply is from a DC Genesys 6V, 200A power source. Either the voltage or the current can be varied with such a power source. The thermal boundary condition on the impingement surface was that of a uniform heat flux. From this study, it has been shown that the area averaged heat transfer increases with decreasing jet diameter and this is attributed to the higher jet velocities when smaller nozzles are used. For the air jets, secondary peaks were present at low jet-to-target spacings and high Reynolds numbers. The peaks became more pronounced with decreasing  $H/d$  and increasing Reynolds number. The water jets also exhibit secondary peaks, however these have only been observed at a low Reynolds number of  $\sim 10000$  and a low  $H/d$  of 1.

### **2.2.2 Effects of jet plate size and plate spacing on the stagnation Nusselt number for a confined circular air jet impinging on a flat surface**

Jung-Yang San et al. [65] investigated the stagnation Nusselt number of a confined circular air jet vertically impinging on a flat plate. Jet Reynolds number ( $Re$ ), jet plate width-to-jet diameter ratio ( $W/d$ ), jet plate length-to-jet diameter ratio ( $L/d$ ) and plate spacing-to-jet diameter ratio ( $H/d$ ) were treated as variables. The main objective of this work was to

correlate the effects of plate spacing, jet plate width and length on the jet-impingement heat transfer viz., the measured stagnation Nusselt number could be correlated into a simple function using the above parameters for application of impinging jet for electronic cooling. The setup consists of a jet plate, which can move in the x and y directions individually by adjusting two screws and impingement plate assembly with stainless steel heating foils backed up by fiberglass insulation sandwiched between two Bakelite plates. During the experiment, high-pressure air is passed through the jet orifice and directly impinged on the middle heating foil. An electric current, supplied by DC power supply, was arranged to flow through the heating foils to generate a uniform surface heat flux. Many thermocouples were orderly embedded below the middle heating foil. Many experiments were conducted by varying the jet plate, air volumetric flow rate and heated-surface width. From the experimental data, the stagnation Nusselt number was successfully correlated into a simple equation i.e., as a function of the 0.638 power of the Re. The H/d, W/d and L/d were verified to be the other three parameters affecting the stagnation Nusselt number. The result shows that the stagnation Nusselt number is proportional to the -0.3 power of the H/d and proportional to an exponential function with exponent of  $[-0.044(W/d) - 0.011(L/d)]$ .

### **2.2.3 Effect of Controlling Parameters on Heat Transfer during Jet Array Impingement Cooling of a Hot Steel Plate**

Mishra et al. [66] have experimentally investigated the effect of various controlling parameters such as water pressure, mass impingement density, mass flow rate and shower exit to surface distance on impingement cooling of a hot steel plate by an array of jets. Electrical coil heater of 2.5 KW, bounded over asbestos plate was used to heat up the selected test piece. For generating jet arrays, a commercially available shower was used and the flow rate was regulated by changing the water discharge pressure. The test piece was a square

plate of side 120mm and 4mm thickness. It was embedded by four K – type thermocouples at suitable locations to record the temperature of the steel plate. The bed was designed in such a manner that the distance between the test plate and the shower can be varied by means of a hand wheel. A mechanical patternator, which consists of an array of small collecting tubes, arranged parallel to the main jet axis was used to measure the impingement density. The main purpose of the experiment is to investigate the heat transfer characteristics of jet cooling and characterize the showers to achieve the optimum cooling effect. The initial temperature of the steel plate was varied between 750 °C to 950 °C and the jet to surface distance and mass flow rate were also varied. The major findings from the study indicate that the cooling rate is uniform over the entire surface of the steel plate. The cooling rate was observed to be increased gradually with increase in mass impingement, water pressure and flow rate.

#### **2.2.4 Experimental study and theoretical analysis of local heat transfer distribution between smooth flat surface and impinging air jet from a circular straight pipe nozzle**

Katti et al. [67] experimentally investigated the local distribution of heat transfer coefficients between the orthogonally impinging jet from square edged long pipe circular nozzle and flat plate. Reynolds number based on the nozzle exit condition is varied between 12,000 and 28,000 and jet-to-plate spacing from 0.5 to 8.0 nozzle diameters. Experiments are conducted to measure the wall static pressure distributions at different jet-to-plate spacing. A theoretical analysis is performed to derive semi empirical correlations for the local distribution of heat transfer coefficients between impinging axisymmetric circular jet and a flat plate. The flow rate is controlled by two needle valves, one on each side of the orifice flow meter. The nozzle is an aluminum pipe with length to diameter ratio sufficient to release for fully developed flow over the Reynolds number range investigated. The target plate is

clamped tightly and stretched between two copper bus bars. Thermal images are obtained from IR camera positioned on the side of the heater opposite the impinging nozzle. The back surface of heater element is painted black using a thin coat of 'Matt finish Asian' paint which provides high emissivity (0.99) surface. Infrared radiometry technique is used to measure local temperature.

From this study they identified three regions on the impingement surface based on flow characteristics of impinging jet. They are stagnation region ( $0 < r/d < 1$ ), transition region ( $1.0 < r/d < 2.5$ ) and wall jet region ( $r/d > 2.5$ ). Increase in Reynolds number increases the heat transfer at all the radial locations for a given  $H/d$ . For a given Reynolds number, Nusselt number at stagnation point increases with increase in  $H/d$  from 1.0 till around  $H/d = 6.0$ . This may be due to increase in near wall turbulence intensities with increase in jet-to-plate spacing. Stagnation point Nusselt numbers increase with decrease in  $H/d$  below 1.0. This may be due to flow accelerations under the jet at lower  $H/d$ . Analytical solution based on wall static pressure data in the vicinity of stagnation point confirms these trends.

### **2.2.5 Experimental study of heat transfer coefficient on hot steel plate during water jet impingement cooling**

Hemu Wang et al. [68] performed experiments under transient conditions, to investigate the heat transfer phenomena of stationary hot steel plate under multiple top circular jets on run-out table. Based on inverse heat conduction model, a two-dimensional finite difference program was developed to calculate the local surface convective heat transfer coefficients and corresponding temperatures. Effect of cooling water jet flow rate on convective heat transfer coefficient and surface temperature was analyzed. The water jet flow rate of the planar jet is controlled by electronic valves. The test plate was heated to the test

temperature in a 37 kW electrical furnace which can heat up to 1350 °C. The test steel plate was heated to desired temperature in electrical heating furnace, then withdrew from the furnace and positioned under the cooling water jets. The transient temperatures of steel plate at important locations were measured by Chromel-alumel thermocouples. The results show that heat transfer coefficients are nonlinear functions of surface temperature. The cooling flow rate has no effect on heat transfer coefficient and surface temperature at stagnation point. The study indicated that the surface temperature has a significant effect on heat transfer coefficient during water jet impingement cooling.

### 2.2.6 Experimental Investigation of Jet Impingement Cooling On a Ribbed Surface with Holes

Kartik Jujare et al. [69] have studied the effect of holes on the air flow patterns and heat transfer characteristics in an enclosure, which is having triangular ribs in parallel orientation with holes drilled between the ribs as shown in Fig. 2.2. The impinging air jet was issued through a nozzle, designed as a convergent type with smooth curve so as to allow rapid acceleration of fluid without flow separation and to obtain uniform velocity profile.

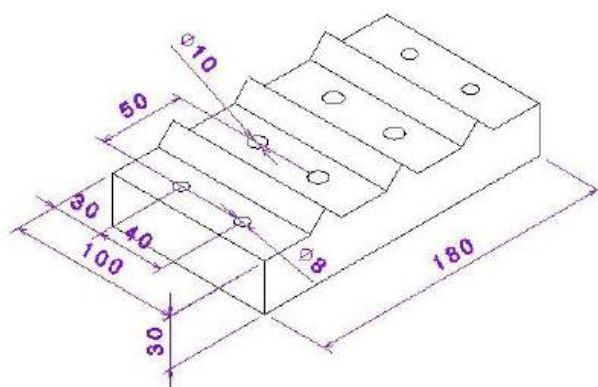


**Fig. 2.2 Schematic of Target Plate**

The target plate consists of triangular rib elements and holes which act as the sole exit route for the spent air and houses a heater pad, an asbestos insulation and another steel plate fastened to the target plate. Temperature is measured at inlet, exit hole, rib surface, heater assembly and ambient. Experiments were conducted for varying conditions of heat flux, H/d ratio, and Reynolds number. Results indicated an increase in the heat transfer with decrease in H/d ratio. The heat transfer rate was also observed to increase with Reynolds number for constant heat flux and H/d ratio.

### 2.2.7 Heat and mass transfer between impinging gas jets and solid surface

An extensive review of available convection coefficient data for impinging jets had been performed by Martin [70].

$$Nu = \frac{h D_h}{K} \quad D_h = \frac{4A}{P}$$

Where  $A$  = Area of slot

$P$  = Perimeter of slot

For large nozzle to plate separations, the distribution is characterized by a bell shaped curve for which  $Nu$  monotonically decays from a maximum value at the *stagnation point*. For small separations ( $H/D \sim 5$ ), the distribution is characterized by a second maximum, whose value increases with increasing jet Reynolds number and may exceed that of the first maximum. Appearance of secondary maximum is attributed to sharp rise in the turbulence level which accompanies the transition from an accelerating stagnation region flow to a decelerating wall jet. Average Nusselt numbers may be obtained by integrating local results over the appropriate surface area.



For single nozzles, the corresponding heat transfer correlations are expected to be of the form

$$Nu = f(Re, Pr, r/D_h, H/D_h)$$

$$\text{where} \quad Nu = \frac{h D_h}{K} \quad D_h = \frac{4A}{P}$$

$$Re = \frac{V D_h}{\nu}$$

$$D_h = 2W \text{ (Slot Nozzle)} \quad D_h = D \text{ (round nozzle)}$$

Martin recommends the following correlation for a *single slot nozzle*,

$$\frac{Nu}{Pr^{0.42}} = \frac{3.06}{x/W + H/W + 2.78} Re^m$$

$$\text{where, } m = 0.695 - \left[ \left( \frac{x}{2W} \right) + \left( \frac{H}{2W} \right)^{1.33} + 3.06 \right]^{-1}$$

$$\left[ \begin{array}{l} 3000 \leq Re \leq 90,000 \\ 2 \leq \frac{H}{W} \leq 10 \\ 4 \leq \frac{x}{W} \leq 20 \end{array} \right]$$

The correlation for *single round nozzle*,

$$\frac{Nu}{Pr^{0.42}} = G \left( \frac{r}{D}, \frac{H}{D} \right) F_1(Re)$$

where,  $F_1 = 2Re^{1/2}(1 + 0.005Re^{0.55})^{1/2}$  and

$$G = \frac{D}{r} \frac{1 - 1.1D/r}{1 + 0.2(H/D - 6)D/r}$$

or replacing  $D/r$  by  $2A_r^{1/2}$

$$G = A_r^{1/2} \frac{1 - 2.2A_r^{1/2}}{1 + 0.2(H/D - 6)A_r^{1/2}}$$

$$\left[ \begin{array}{c} 2000 \leq Re \leq 400000 \\ 2 \leq \frac{H}{D} \leq 12 \\ 2.5 \leq r/D \leq 7.5 \\ \text{or} \\ 0.04 \geq A_r \geq 0.004 \end{array} \right]$$

For an array of round nozzles,

$$\frac{Nu}{Pr^{0.42}} = K \left( A_r, \frac{H}{D} \right) G \left( A_r, \frac{H}{D} \right) F_2(Re)$$

$$\text{where, } K = \left[ 1 + \left( \frac{H/D}{0.6/A_r^{1/2}} \right)^6 \right]^{-0.05}$$

$$F_2 = 0.5Re^{2/3}$$

$$\left[ \begin{array}{c} 2000 \leq Re \leq 100000 \\ 2 \leq \frac{H}{D} \leq 12 \\ 0.04 \geq A_r \geq 0.004 \end{array} \right]$$

### 2.2.8 Heat transfer behaviors of a confined slot jet impingement [71]

For stagnation heat transfer numerical correlation is given by,

$$Nu_s = 5.574Re_D^{0.5}(H/W)^{-0.17} \quad (\text{It is over predicted})$$

When  $H/W$  is insignificant,

$$Nu = 4.315Re_D^{0.5}$$

This was carried out because of deviations in the experimental and numerical results.

Local Nusselt number ( $Nu_x$ ): Local Nu increases with increasing Reynolds number.

Average Nusselt number:  $\overline{Nu}$  increases with increasing Reynolds number,

$$\overline{Nu} = 3.755Re_D^{0.5}$$

If Prandtl number is taken into consideration

$$\frac{\overline{Nu}}{Pr^{1/3}} = 4.229Re_D^{0.5}$$

### 2.2.9 Forced convective heat transfer with impinging rectangular jets [72]

The experimental results show that the jet Reynolds numbers, the nozzle to plate spacing and the turbulence intensity have important influence on the heat transfer of impinging rectangular jets.

#### **Turbulence intensity**

Turbulence intensity at the center of impingement region increases till  $H/W=6.0$  and then decreases gradually. Turbulence intensity in the lateral distance decreases.

### **Heat transfer characteristics**

Higher heat transfer rates and stagnation Nusselt number for small nozzle to plate spacing till  $H/W=6.0$ .

Correlation for stagnation heat transfer rate,

$$Nu_{sg} = C_1 Re^{m_1} Pr^{n_1},$$

where,  $n_1 = 2/5$

$C_1 \& m_1$  = from least squares method.

The local Nusselt number has two peaks and second peak increases with jet Reynolds number and nozzle to plate spacing,

$$Nu = 0.138 Re^{0.609} (H/W)^{0.182}$$

### **Average Nusselt number**

Average Nusselt number increases with jet Reynolds number and decreases with nozzle to plate spacing. The average heat transfer rate in lateral direction,

$$\overline{Nu} = C_2 Re^{m_2} Pr^{n_2},$$

Where,  $n_2 = 2/5$

$C_2 \& m_2$  = from least squares method.

Correlation between average Nusselt number and the turbulence intensity of the impinging jet,

$$\frac{\overline{Nu}}{Re^{1/2}} = 0.014 \overline{Tu} Re^{1/2} + 0.472$$

The study provided better understanding on the fluid flow and heat transfer characteristics of

impinging air jets.

### 2.2.10 Cooling of a heated flat plate by an obliquely impinging slot jet [73]

Angle ( $\theta$ ) =  $90^\circ$ ,  $60^\circ$ ,  $45^\circ$  &  $30^\circ$

Reynolds number = 5860, 8879 & 11606

The nozzle to plate distance ( $H/D$ ) = 8 kept constant. The experiment was conducted in a closed field, a wind tunnel. In the range of parameters taken in this investigation, the region of maximum cooling shifts from the geometrical point towards the compression side of the plate. The point of maximum cooling is displaced from the geometrical point of the jet with the extent of displacement increasing as the inclination increases. Conventional type jet shows a symmetric position ( $\theta = 90^\circ$ ) as it is thought, but the distribution of temperatures on inclined surface shows a non-axisymmetric pattern. It is apparent that future work of surface pressure, velocity field and heat transfer for the same oblique impinging jet configuration is needed to resolve the issue of the relation between the point of maximum pressure, point of maximum heat transfer and the stagnation point for an obliquely impinging jet. For a constant Reynolds number, decrease in angle of inclination effects poor cooling.

### 2.2.11 Effect of jet-jet spacing on convective heat transfer to confined, impinging arrays of axisymmetric air jets [37]

The experiment included confined air jets.

Reynolds number,  $Re$ : 3500-20400

Nozzle to plate spacing,  $H/D$  = 0.25, 1.0 & 6.0

For an array jet at  $H/D$  = 6.0, adjacent jet interference before impingement causes significant degradation of the convective coefficient when compared to a single jet. However as the separation distance is decreased to one jet diameter, the adjacent jet interference before

impingement is minimized and the Nusselt numbers for the array jet and single jet were similar.

### Local Nusselt number

Also, at small separation distances ( $H/D < 1.0$ ) secondary maxima occur at the local convective coefficient for a jet in an array similar to a single jet. These secondary maxima enhance the average convective coefficients.

### Effect of jet-jet spacing

The  $S/D=4$  spacing resulted in the highest average Nusselt number for a given separation distance as well as the most uniform distribution over the impingement surface. However on a flux basis, the  $S/D=8$  array was found to be the most efficient.

### Effect of spent air exits

Spent air exits located between the jet orifices resulted in heat transfer enhancement minimizing adjacent jet interference in the wall jet region and cross flow degradation of the convective coefficient. As the jet–jet spacing is decreased, the effect of the spent air exits on the Nusselt number increases.

The average Nusselt number for  $H/D = 0.25, 1.0$  &  $6.0$  with spent air exits were correlated for the array with Reynolds number,  $H/D$ ,  $S/D$  as the independent variables.

$$\overline{Nu_D} = 0.285 Re_D^{0.710} Pr^{0.33} (H/D)^{-0.123} (S/D)^{-0.725}$$

$$\left\{ \begin{array}{l} 3400 \leq Re \leq 20500 \\ 4 \leq S/D \leq 8 \\ 0.0123 \leq A_r \leq 0.0491 \\ 0.25 \leq H/D \leq 6.0 \end{array} \right\}$$

### 2.2.12 Influence of the shape of the nozzle on local heat transfer distribution between smooth flat surface and impinging air jet [74]

Nozzle shapes

Type of nozzle	Breadth (mm)	Height (mm)	Hydraulic Diameter (mm)
circular	20	20	20
square	17	17	17
rectangular	26.8	12	16.6

$$H/D = 0.5 - 12.0$$

$$\text{Reynolds number} = 5000-15000$$

- The effect of Reynolds number on the performance of non-circular jets is similar to that for the circular jet. With increase of Reynolds number, the heat transfer rate increases. The heat transfer characteristics of square and circular jets show much similarity.
- There is a distinct difference between distribution of Nusselt numbers along the major and minor axis for rectangular jet.
- It was observed that, up to  $z/d$  of 6, the Nusselt number distribution along the horizontal axis for rectangular jet is higher in the stagnation region than those of circular and square jets.

#### **Average Nusselt number**

- The average Nusselt number for a Reynolds number at a particular  $H/D$  has same values for all 3 configurations.

- Average Nusselt number increases with increase in Reynolds number for all the nozzle configurations.
- Average Nusselt number decreases with increase in  $H/D$  for all Reynolds number.

**Pressure loss coefficient ( $K = DP / 0.5\rho \cdot V^2$ )**

$DP$  - Pressure drop across nozzle (Pa)

$\rho$  - Density of air corresponding to supply pressure ( $\text{kg/m}^3$ )

$V$  - Average velocity at the exit of the nozzle (m/s)

$K$  for circular jet is lower & for rectangular jet is higher. Therefore the maximum pumping power is required for rectangular jet & least for circular jet.  $K$  is almost insensitive to  $H/D$  for all the 3 nozzles.

**2.2.13 Effect of nozzle geometry on heat transfer characteristics from a single circular air jet [75]**

Nozzles-square edge nozzle

-chamfered edge nozzle

Reynolds number,  $Re = 6000$  to  $40000$

$H/D = 1$  to  $6$

- The chamfered edge has no effect of local Nusselt number distribution along the stream-wise direction.
- For a range  $H/D$  from 1 to 4, the stagnation Nusselt number values are nearly constant, and it is higher than at separation distance  $H/D = 6$  for all nozzle configurations tested.
- The local Nusselt number distribution around  $R/d=2$ , has a second peak for all nozzles inlet was formed particularly at higher Reynolds number values.



- The square edge nozzle yielded a higher average Nusselt number when compared with the other nozzles configurations.

Correlation of average Nusselt number in terms of  $Re$ ,  $H/D$ , and  $L_c/d$ ,

$$Nu = 0.047 * Re^{0.75} * (H/D)^{-0.016} \quad \text{for square edge nozzle}$$

$$Nu = 0.036 * Re^{0.76} * (H/D)^{-0.015} (L_c/D)^{-0.01} \quad \text{for chamfered edge nozzles}$$

For square edge nozzle, the average Nusselt number dependence is Reynolds number as

$$Nu \propto Re^{0.75}$$

However, the value of average Nusselt number for square edge nozzle has highest value than for other nozzles.

#### 2.2.14 Optimum jet-to-jet spacing of heat transfer for staggered arrays of impinging air jets [38]

Five confined circular jets in equilaterally staggered arrays were considered. The jet diameter, 3 mm, Reynolds number,  $Re=10000$ ,  $20000$  &  $30000$  were considered. Jet interference and jet fountain are two factors affecting the heat transfer characteristics of the staggered jet arrays. The former causes deterioration of the overall heat transfer. The latter causes a flow recirculation between the fountain and center jet. Two relative maxima of the stagnation Nusselt number coexist for some of the considered jet arrays with a large Reynolds number and a large  $H/D$ . The first relative maximum occurs at a smaller  $S/D$  and the second at a larger  $S/D$ .

Optimum  $S/D=16.0$  for  $H/D=2.0$

Optimum  $S/D=12.0$  for  $H/D=3.0$

Optimum  $S/D=12.0, 6.0, 6.1$  for  $H/d=4.0$  at Reynolds number =  $30000, 20000, 10000$  resp.

Optimum  $S/D=6.0$  for  $H/D=5.0$ .

The stagnation Nusselt number is correlated as a function of Reynolds number,  $S/D$  &  $H/D$ .

$$Nu_{sg} = (S/D) e^{\alpha_1 + \alpha_2 (S/D)} Re^\alpha$$

Where,  $\alpha_1 = \sum_{i=0}^2 \beta_i (H/D)^i$  &  $\alpha_2 = \sum_{i=0}^2 \gamma_i (H/D)^i$

Another correlation of higher order polynomial with  $Re$ ,  $S/D$  &  $H/D$  as variables were shown.

$$Nu_{sg} = \sum_{i=0}^2 \sum_{j=0}^5 c_{ij} (H/D)^i (S/D)^j$$

Where,  $c_{ij} = \sum_{k=0}^2 a_{ijk} Re^k$

$$\left\{ \begin{array}{l} 10000 \leq Re \leq 3000 \\ 4 \leq S/D \leq 16 \\ 2 \leq H/D \leq 5 \end{array} \right\}$$

### 2.2.15 Closure

Considerable research has been done on jet impingement heat transfer and enhancement by various methods. An extensive review of available convection coefficient data for impinging jets had been performed by Martin [70]. Jambunathan [21] also performed a detailed survey on jet impingement cooling. A compilation of empirical correlations is given by Zuckerman [17]. In this chapter some of the experiments from literature carried out for jet impingement cooling are described. The empirical correlations for different applications of jet impingement cooling are given along with the range of applicability.

### 2.3 Computational simulation of jet cooling

Jet impingement heat transfer has very wide industrial application. Because of the complex fluid mechanics involved in this process, it is also important from fundamental characteristics. Major benefit of this arrangement is that it has the maximum heat transfer rate among the single-phase heat transfer configurations. This property has led to increasing use of jet cooling in industry for cooling, heating, and drying of surfaces. Some typical industrial applications of jet impingement include cooling of electronic equipment, cooling of turbine blades, drying of paper, gas quenching of steel rings, and baking, freezing, and drying of various food items. The presence of complex fluid flow regimes namely, a free-shear region, a stagnation region, and a wall jet region within an impinging jet flow make it an excellent benchmark case for the development and assessment of Reynolds averaged Navier–Stokes (RANS) equations based turbulence models. Complex physical phenomena are difficult to realize in an experiment. Numerical simulations produce detailed information on simultaneous velocity and temperature fields, effects of different inlet forcing, etc. Several studies on impinging jet flows have been under taken over the last five decades. Initially, studies were focused on experimental simulations for fundamental understanding and parametric investigations of flow and heat transfer mechanisms. Rapid advancements of computational resources and numerical algorithms have paved the way for growing interest in the computational investigation of the impinging flows. Computations of impinging flows are performed to complement experiments in fundamental understanding of important flow and heat transfer phenomena, e.g., evolution of vortices, control of these vortices to gain heat transfer, etc. Computations are also performed for parametric investigations for designing impinging systems.

For fundamental investigation of impinging flows, three dimensional instantaneous

flow fields are required. Therefore, a high-resolution direct numerical simulation (DNS) is the obvious choice. However, reliability in large eddy simulation (LES) in recent times has led to its use in fundamental investigations at higher Reynolds numbers, which are unreachable in a DNS. Design of impinging systems mainly requires knowledge of the averaged flow fields, which are widely computed using RANS-based turbulence models due to their relatively small computational cost. Polat et al. [76] reviewed the available numerical techniques to predict laminar and turbulent impingement heat transfer on a flat surface. Zuckerman and Lior [17] reviewed the comparative accuracy of different turbulence models for predicting impinging flows from the perspective of design of impingement systems. From their study, it can be seen that the conventional RANS based turbulence models lack generality in predicting impinging flows.

Except some electronic cooling applications at low Reynolds numbers, most practical impinging flows are turbulent in nature. In contrast to laminar flows, turbulent flow consists of a large spectrum of scales, which leads to difficulty in computation. Therefore, the present discussion is concerned only with the computation of turbulent impinging jets.

### **2.3.1 Large Eddy Simulation [77-88]**

LES is a preferred technique for the simulation of impinging flows due to its capability to resolve turbulence due to large eddies in a manner similar to DNS and the effect of smaller eddies in a manner similar to eddy viscosity models. This method is preferred over DNS due to the lesser computational effort involved. Over years, the application of LES for impinging jet flows have increased in terms of complexity. This is mainly due to the development of computational technology which has enabled this technique to be applied to highly turbulent flows with Reynolds number in the range of 70,000. LES is a popular

technique for simulating turbulent flows. An implication of Kolmogorov's theory [77] of self similarity is that the large eddies of the flow are dependent on the geometry while the smaller scales more universal. This feature allows one to explicitly solve for the large eddies in a calculation and implicitly account for the small eddies by using a subgrid-scale model.

**Experience on the Application of LES Models on Impinging Jet Flows:** LES of a forced semi confined circular impinging jet were carried out by Olsson and Fuchs [85]. The Reynolds number was  $10^4$  and the inflow was forced at a Strouhal number of 0.27. The separation between the jet inlet and the opposing wall was four jet inlet diameters. Two simulations were performed without any explicit sub-grid-scale (SGS) model using  $128^3$  and  $96^3$  grid points, respectively. Two simulations were performed with two different SGS-models using  $96^3$  grid points; one with a dynamic Smagorinsky based model and one with a stress-similarity model. The existence of separation vortices in the wall jet region was confirmed. These secondary vortices were found to be related to the radially deflected primary vortices generated by the circular shear layer of the jet. It was also shown that the primary vortex structures that reach the wall were helical and not axisymmetric. A quantitative gain was found in the simulations with SGS-models. The stress-similarity model simulation correlated slightly better with the higher resolution simulation than the other coarse grid simulations. The variations in the results predicted by the different simulations were larger for the turbulence statistics than for the mean velocity. However, the variation among the different simulations in terms of the turbulence intensity was less than 10%. Wall-jet interaction was studied with LES in which a mixed-similarity sub grid scale closure was combined with the wall-adapting local eddy-viscosity (WALE) model for the eddy-viscosity term [86]. LES prediction capabilities were assessed by comparing flow statistical properties against experiment of an unconfined impinging round jet at Reynolds numbers of 23000 and

70000. They found that their new model (a mixed similarity with a WALE) performs quite well near the wall, especially in the stagnation region while, other two models (standard WALE and the Lagrangian dynamic Smagorinsky model) overestimated the stream wise turbulent fluctuations in this region. They attributed the accuracy of this new model to accurate representation of the backscatter of energy.

### **2.3.2 Direct Numerical Simulation [89-96]**

A direct numerical simulation DNS [89] is a simulation in computational fluid dynamics in which the Navier–Stokes equations are numerically solved without any turbulence model. This means that the whole range of spatial and temporal scales of the turbulence must be resolved. Numerical methods for the direct simulation of turbulence are required to accurately reproduce its evolution over a wide range of length and time scales. The range of scales that need to be accurately represented in a computation is dictated by the physics. The grid determines the scales that are represented, while the accuracy with which these scales are represented is determined by the numerical method. The computational cost of DNS is very high, even at low Reynolds numbers. For the Reynolds numbers encountered in most industrial applications, the computational resources required by a DNS would exceed the capacity of the most powerful computers currently available. However, direct numerical simulation is a useful tool in fundamental research in turbulence. Using DNS it is possible to perform "numerical experiments", and extract from them information difficult or impossible to obtain in the laboratory, allowing a better understanding of the physics of turbulence. Also, direct numerical simulations are useful in the development of turbulence models for practical applications, such as sub-grid scale models for Large eddy simulation (LES) and models for methods that solve the Reynolds-averaged Navier–Stokes equations (RANS).

**Experience on the Application of DNS on Impinging Jet Flows:** Unsteady heat transfer caused by a confined impinging jet was studied by Chung and Luo [92] using direct numerical simulation (DNS) in two dimensional frame. The time-dependent compressible Navier-Stokes equations were solved using high-order numerical schemes together with high fidelity numerical boundary conditions. A sixth-order compact finite difference scheme was employed for spatial discretization while a third-order explicit Runge-Kutta method was adopted for temporal integration. Number of grids used were in the order of  $384^2$  and the time step was selected to respect the stability criterion. The simulations cover several Reynolds numbers and two nozzle-to-plate distances. Comparison of predictions against experimental results of Sparrow and Wong [93] is shown in Fig. 2.3. The instantaneous flow fields and heat transfer distributions were found to be highly unsteady and oscillatory in nature, even at relatively low Reynolds numbers. The fluctuation of the stagnation or impingement Nusselt number was as high as 20 percent of the time-mean value. More chaotic and non-linear fluctuations are observed with increasing Reynolds numbers. The Nusselt number distribution away from the impingement point, on the other hand, was influenced by the secondary vortices which arise due to the interaction between the primary vortices and the wall jets.

Hattori and Nagano [94] used DNS to study the effect of nozzle to plate spacing on the heat transfer of a plane confined jet impingement. The prediction of secondary flow and recirculation flow is shown in Fig. 2.4. Range of Reynolds number considered in these studies is up to 10000. Three-dimensional eddy structures arising in plane and round impinging jets excited at the nozzle inlet were investigated numerically by Tsubokura et al [95] through direct numerical simulation and large eddy simulation. Special attention is focused on how spanwise or azimuthal disturbances imposed at the inlet velocity affect the

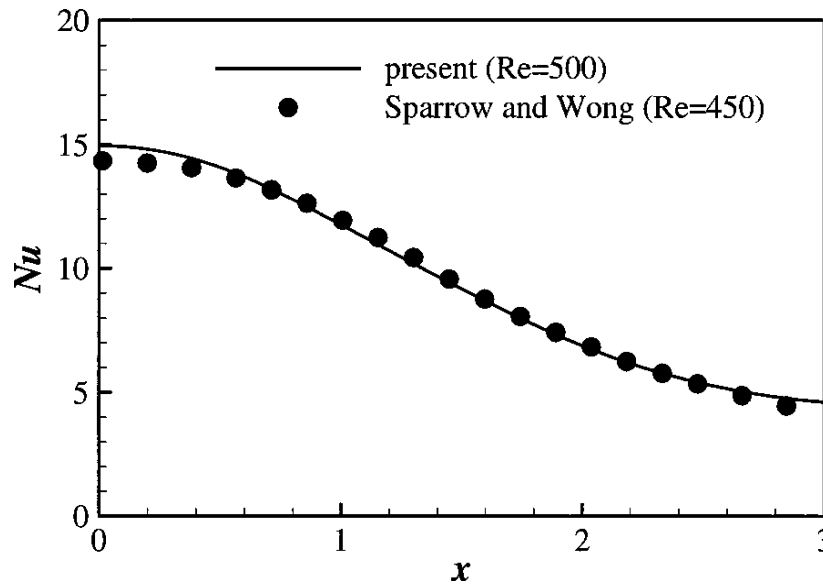


**Fig. 2.3 Comparison of DNS prediction by Chung and Luo against experimental data**

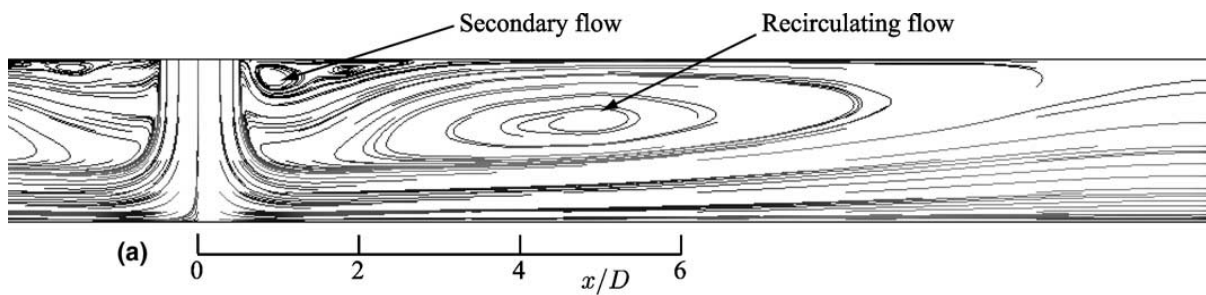


**Fig. 2.4 Prediction of secondary flow and recirculation flow by DNS**

eddy structures in the transition process. DNS simulation was carried out for  $Re=2000$  and LES simulation was carried out for  $Re=6000$ . The knowledge obtained in this study definitely indicates the possibility of controlling heat and mass transfer rates near the stagnation region of the plane jet by regulating the inlet forcing conditions. Satake and Kunugi [96] obtained mean velocity, turbulence profiles, pressure distribution, and turbulence kinetic energy budgets at various radial locations for a round jet impingement using DNS. Although these DNS studies are limited to low Reynolds number, detailed results provided by them, e.g.,



budgets of different turbulent quantities, would be very useful to construct a new turbulence model.

### 2.3.3 Reynolds-Averaged Navier–Stokes (RANS) Equation Modeling

Complete numerical simulation of turbulence requires direct numerical simulation in a fine grid model by performing a transient simulation with a time step capable of capturing the behavior of small scale eddies. Such studies are highly computational-intensive and are practically very difficult to perform. Therefore, usual approach adopted is the turbulence model wherein thermal hydraulic effects of turbulence on momentum and heat transport are simulated through appropriate models. Reynolds-averaged Navier-Stokes (RANS) equations are the oldest approach to turbulence modeling. In this, an ensemble version of governing equations is solved. RANS models can be divided into two broad approaches. The first approach involves using an algebraic equation for Reynolds stresses which includes determination of turbulent viscosity. Depending on the level of sophistication of the model, transport equations for turbulent kinetic energy ( $k$ ) and its dissipation rate ( $\epsilon$ ) are also solved in some of these models. These models include the  $k$ - $\epsilon$  model proposed by Launder and Spalding [97], mixing length model proposed by Prandtl [98] and Zero Equation model proposed by Smith and Cebeci [99]. The second approach solves transport equations for Reynolds stresses. This means introduction of transport equations for all the Reynolds stresses and hence this approach is much more costly in CPU effort.

**Prediction of Impinging Jet Thermal Hydraulics using RANS models:** Zuckerman and Lior [17] reviewed a large number of turbulence models. Several studies have been carried out using  $k$ - $\epsilon$  model and it has been concluded that the even the best  $k$ - $\epsilon$  models and associated wall treatments will yield Nusselt number profiles with local errors in the range of 15–30%, and the standard  $k$ - $\epsilon$  model is not recommended for use in the impinging jet

problem. These shortcomings are attributed to the assumption of isotropic turbulence and the use of wall functions that poorly approximate near-wall velocity fluctuation and associated transport properties.

Heck et al., [100] showed the RNG model provided a close match of  $Nu$  in the wall-jet region but an error up to 10% in the stagnation region. This is in part due to the RNG model's tendency to predict jet-spreading rates that are as high as twice that found in experiment. This flaw on the upstream end of the model leads one to question how the downstream results did not stay as far from measured values. It offers some improved performance over the standard  $k-\epsilon$  at a slightly higher computational cost and is recommended when only moderate accuracy is required.

The  $k-\omega$  model typically produces  $Nu$  profiles with a local error of up to 30% of the experimental  $Nu$  value. It can produce better predictions of the turbulent length scale than the  $k-\epsilon$  model. The  $k-\omega$  model can generate good predictions of flow properties in the wall jet, both in the sublayer and logarithmic region, without the need for damping functions. For a flow near a wall the boundary conditions are known – turbulent viscosity and the turbulent time scale are set to 0. The value of  $\omega$  at or near the wall cell may be set proportional to  $\nu/y^2$ , meaning the user can fully specify the turbulence conditions at the wall, unlike in the  $k-\epsilon$  model. Unfortunately, the  $k-\omega$  model is sensitive to far-field boundary conditions, much more so than the  $k-\epsilon$  model. The addition of cross-diffusion terms in various  $k-\omega$  models have succeeded in reducing its sensitivity to far-field  $\omega$  boundary conditions, a problem known to arise during use of the  $k-\omega$  model for unconfined or partially confined flows.

RSM modeling of impinging jets by Demuren [101] showed velocity predictions ranging from -40 to +40% of the experimentally measured velocities, and Reynolds stress errors of over 100%, which was attributed to a need for an extremely dense grid. Craft et al . [102] presented computed centerline wall-normal r.m.s. turbulent velocity levels, which matched within 25% of experiment at  $H/D=2$ , but had errors as large as 80–100% for  $H/D=6$ . The RSM can predict the occurrence of a secondary peak in  $Nu$ , but not necessarily at the correct location. This shows that although the various RSM implementations preserve all the Reynolds stress terms, they still use approximation equations based on a number of assumptions. That is, they eliminate the isotropy assumptions which yield the two-equation models but still rely upon other empirically generated equations to predict the stresses and do not give a ‘perfect’ solution. Given the high computational cost compared to the eddy-viscosity models, these results are disappointing and the RSM is not recommended as an alternative.

An important reason for the poor performance of the RANS-based models is the way time averaging is performed. It is based on the assumption that the flow is statistically stationary. However, recent studies show that quasi-periodic impingement of large scale coherent structures makes the flow and heat transfer in the impingement plate highly unsteady. Le Song and Prud’homme [103] used unsteady RANS (URANS) equations with steady boundary conditions to predict the coherent structures in jet impinging flows. An unsteady time averaging of the Navier–Stokes equations with a RANS model is called URANS. Because of the unsteady averaging, URANS can resolve vortices in the flow at lesser computational cost in comparison to LES and DNS. The Reynolds number of the study was 6000. The results showed that this method accurately reproduces coherent structures of the impinging flow.

### 2.3.4 Closure

Impinging jet flow has complex flow features due to the nature of turbulence and the kind of vortex structures involved. Experimental studies have limitations in deriving complete information about all these complex flow features. Direct numerical simulation is the best theoretical tool for numerically extracting this information. This information is essential for the development of simplified models for analyzing of geometrically complex situations. Application of DNS is limited due to the large computational resources involved. Large eddy simulation is a better compromise in this regard where in the flow features of large eddies are simulated in complete form and the effect of smaller eddies are treated through subgrid models. Depending on the nature of the smaller eddies and their effects different subgrid models have been developed and WALE model has been found to be the best for impinging jet flow due to the accurate representation of the backscatter of energy.

A few studies have been reported with hybrid RANS/LES for impinging flows and found its superior performance compared to RANS-based models. However, simple RANS models produce erroneous results; therefore, either a state-of the-art RANS model or some other means of near-wall modeling has to be considered. Although the number of LES studies has been found to increase in recent times, RANS-based models are still the most widely used for the prediction of industrial impinging flows due to the computational comfort and the high level of turbulence involved under practical conditions. An unsteady time averaging of the Navier–Stokes equations with a RANS model is called URANS. Because of the unsteady averaging, URANS can resolve vortices in the flow at lesser computational cost in comparison to LES and DNS. The results showed that this method accurately reproduces coherent structures of the impinging flow and has a promising potential for application.

\* \* \*

# Chapter-3

## **Experimental studies with single air jet**

### **3.0 Introduction**

First some basic experiments to understand the jet cooling phenomena are carried out with air as the cooling medium. Here the main objective is to identify the conditions for which the heat transfer coefficient attains the maximum value. Two types of nozzles are studied, viz., circular and slot. In each case, the effects of following parameters are studied: nozzle diameter / width, nozzle to target distance and angle of inclination. The above studies are carried out for three different air flow rates and two different current values. Only one slot nozzle or one array of circular nozzles is considered. The experimental results are compared against Martin's empirical correlations obtained from the literature. Details of the above studies are presented in this chapter.

### **3.1 Description of experiment**

The experimental set up is shown in Figs. 3.1a, 3.1b and 3.1c. Compressed air at 0.7 MPa from two air compressors are sent to a buffer tank of 1 m<sup>3</sup> capacity. The air from the buffer tank is sent to the nozzle. The flow rate is measured using a rotameter. An external power supply ranging from 0 - 30 V and 0 - 100 A was connected to the sample (20 mm x 20 mm x 0.5 mm) for externally heating the sample. The connection to the sample was made through copper plates which directly holds the sample, and is supported by the Teflon rods. The experimental readings were noted for current values of 80 A & 90 A and the corresponding voltages were noted. It was found that there was voltage drop in experimental arrangement of the sample and hence a multimeter was used to measure the actual voltage reading across the sample. Circular /slot nozzle is used to produce the air jet (Fig. 3.2). The air jet is perpendicular to the sample and is focused towards the center of the sample so that the air splits in the two directions (Fig. 3.3). The air flow rate is also varied from 5 m<sup>3</sup>/h to 15

m<sup>3</sup>/h. Three different nozzle diameters 1mm, 2mm and 3mm and three nozzle to target distances are used in the experiment. The sample temperature is measured using four K-type thermocouples. One thermocouple is attached at the centre of each quadrant. The average temperature of the four quadrants is used for the estimation of average Nusselt number. The radiation heat loss from the sample is subtracted for the estimation of heat removal by jet cooling.

$$P_t = P_j + P_r$$

Where  $P_t$  - Total heat transferred

$P_j$  - Heat transferred by jet cooling

$P_r$  - Heat transferred by radiation

$$P_t = V \times I$$

Where  $V$  - applied voltage

$I$  - Current through the sample

$$T_{avg} = (T_1 + T_2 + T_3 + T_4)/4$$

Where  $T_{avg}$  - Average temperature of the sample

$T_1, T_2, T_3$  &  $T_4$  - Measured temperature at the centre of each quadrant

$$P_r = 2 A \epsilon \sigma \{T_{avg}^4 - T_a^4\}$$

Where  $A$  - Area of the sample

$\epsilon$  - Emissivity of the sample

$\sigma$  - Stephen- Boltzmann constant

$T_a$  - Ambient temperature

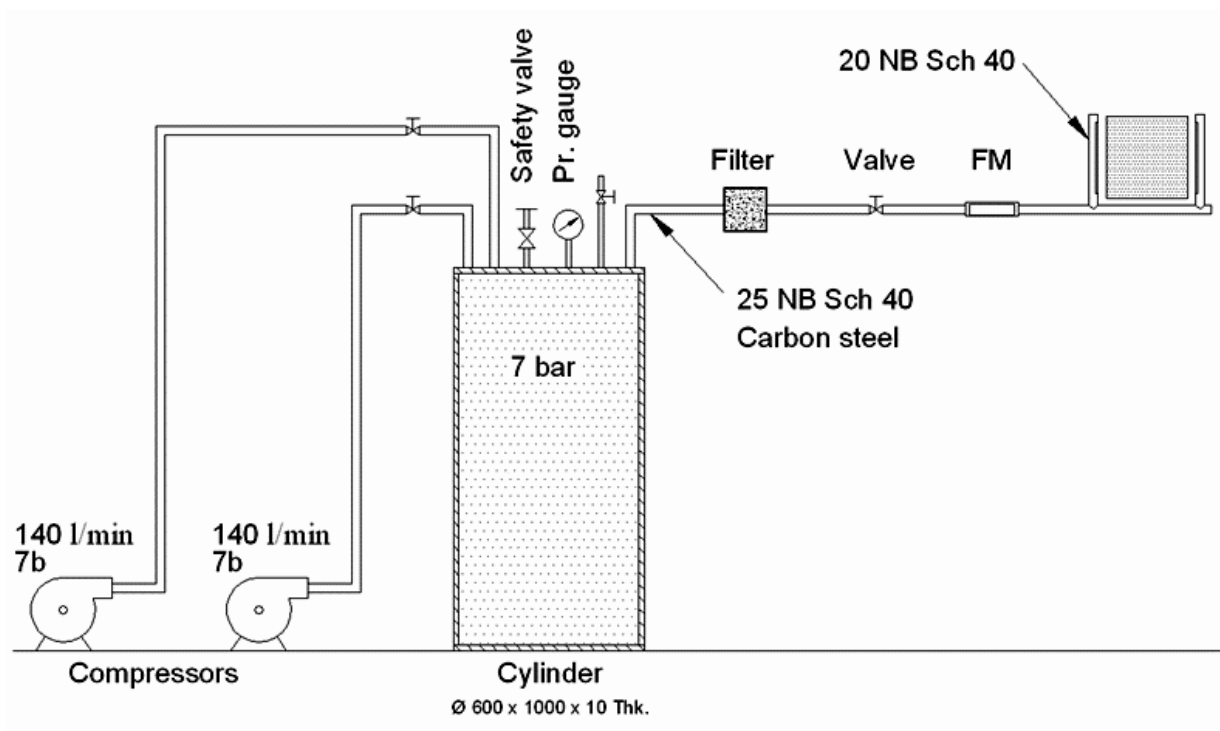


**Fig.3.1a Schematic of the experimental set up.**

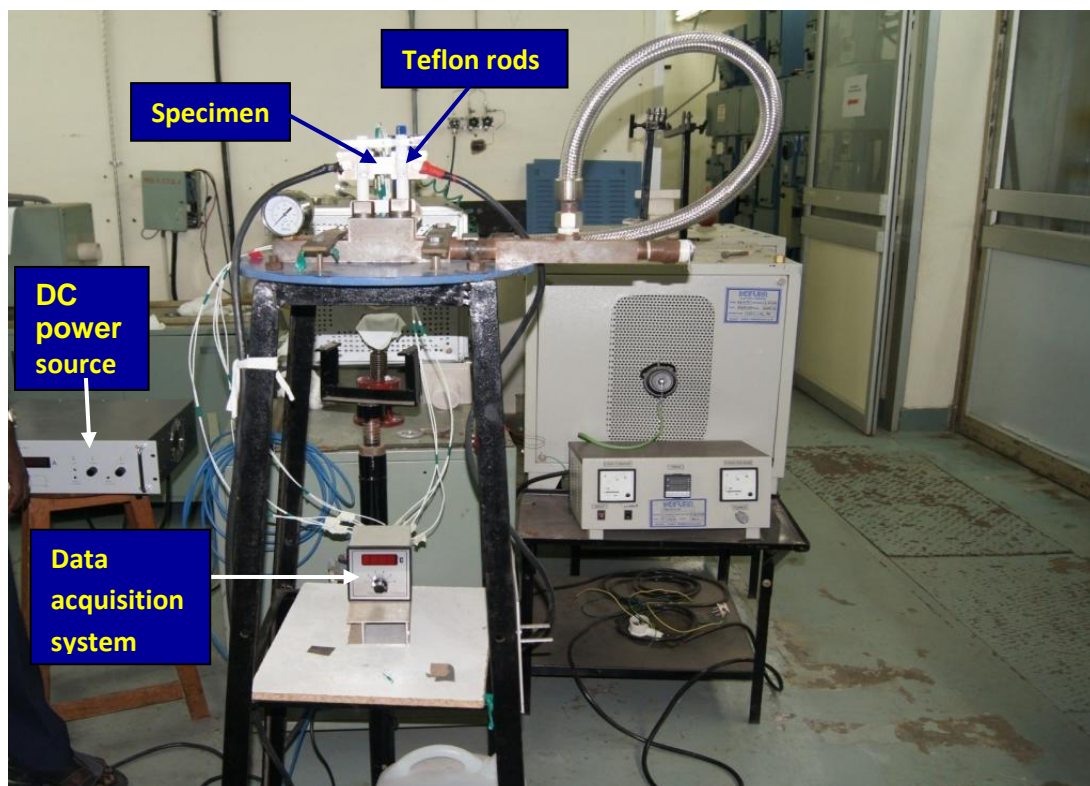


**Fig. 3.1b Experimental Set up**



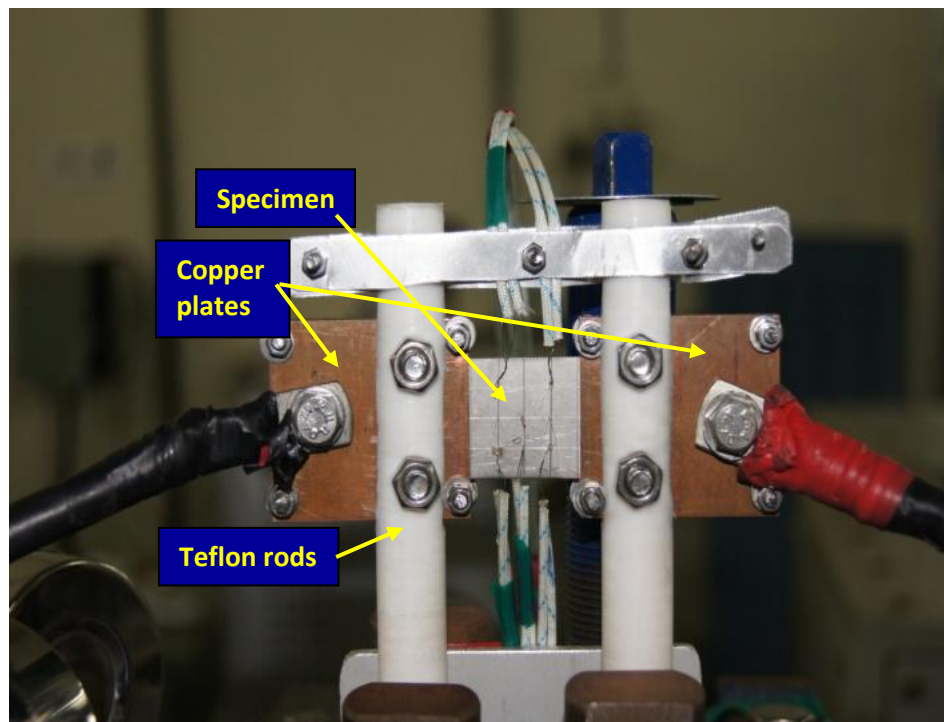


**Fig. 3.1c Arrangement of specimen**

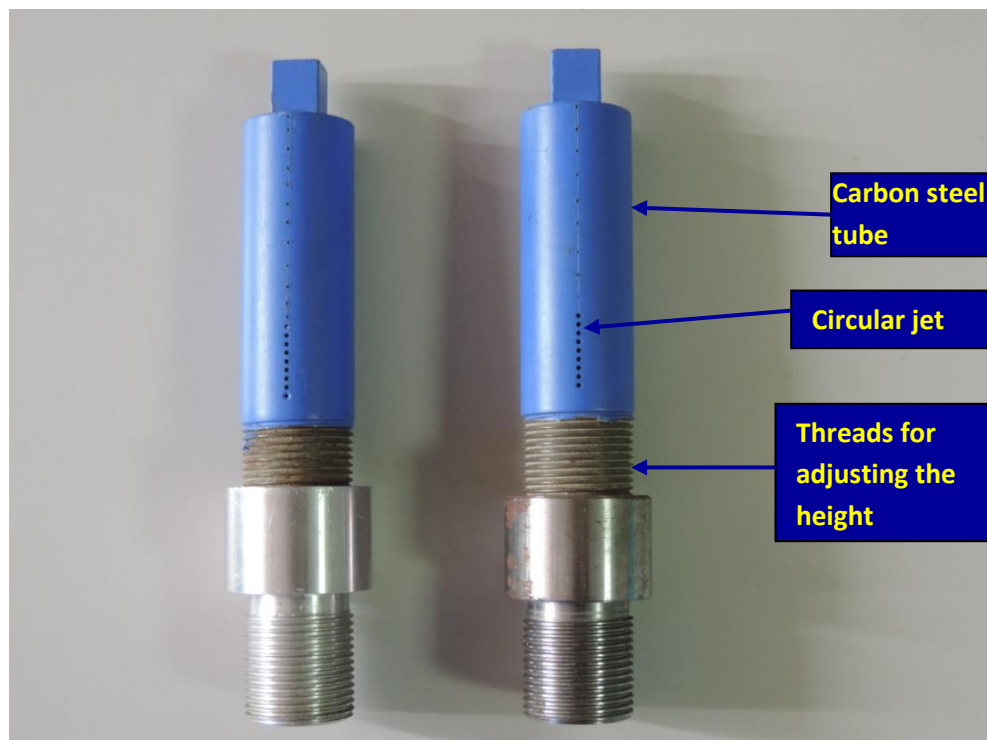


**Fig. 3.2a Array of circular jet nozzles**

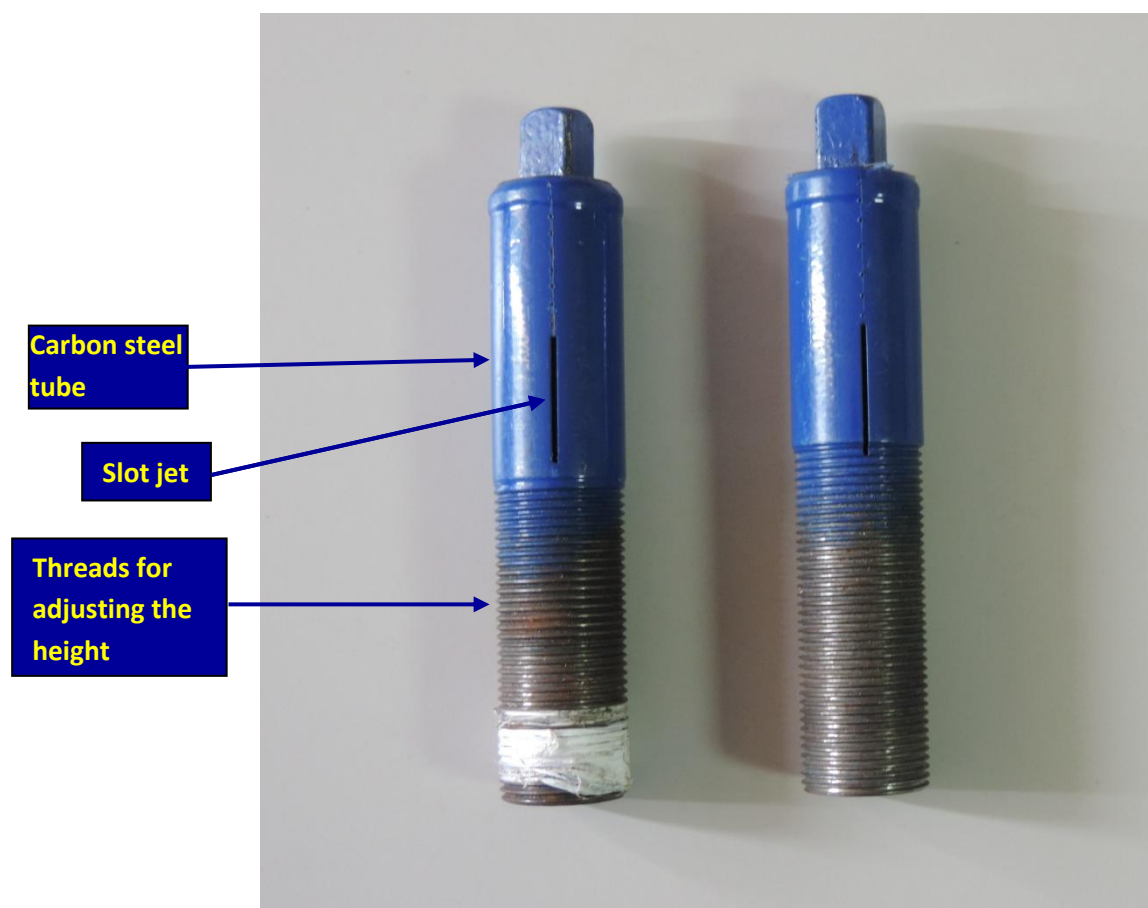


**Fig. 3.2b Slot jet nozzles**

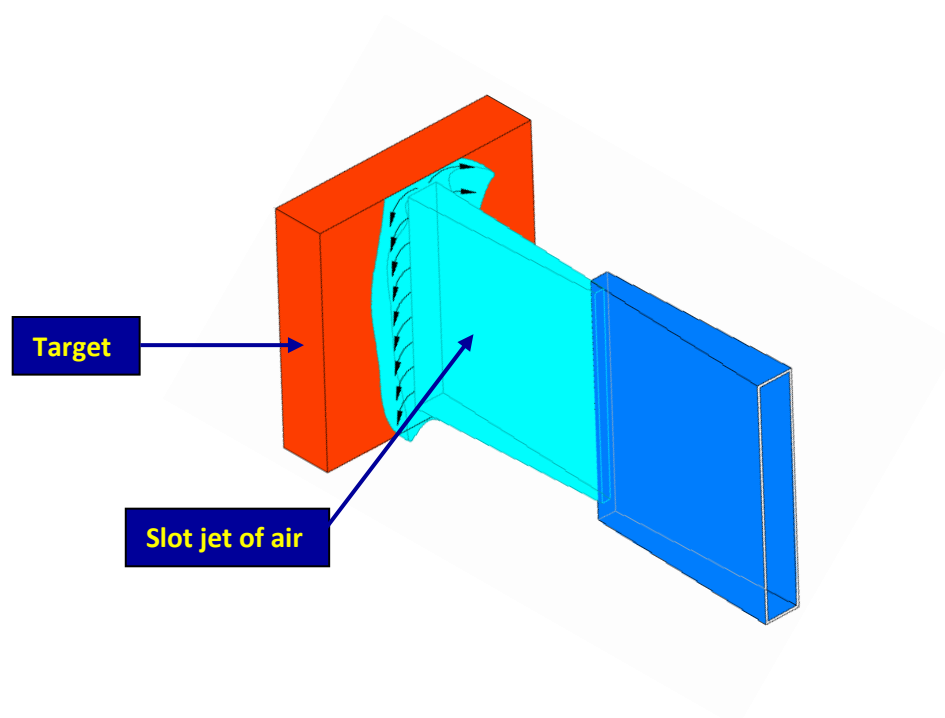


**Fig. 3.3 Schematic showing alignment of jet with the sample**

$$Q_j = h A \{T_{avg} - T_a\}$$

Where  $h$  - Heat transfer coefficient due to jet cooling

The margin of error for Type K thermocouple used is  $\pm 0.75\%$  or  $2.2\text{ }^{\circ}\text{C}$ , whichever is greater. The uncertainty in electric power measurement is  $\pm 1.5\%$ . The rotameter used for the air flow measurement has an accuracy of  $\pm 5\%$ . Hence the error in the Reynolds number calculated from the measured air flow will be  $\pm 5\%$ . These leads to an error of  $\pm 15\%$  in the Nusselt number calculated from the measured temperature and flow values. Details of uncertainty calculation in the Nusselt number is given in Appendix – A.

### 3.2 Cooling by circular air jets

Fig. 3.4 shows the variation of average Nusselt number with respect to Reynolds number, for circular nozzle diameter equal to 1 mm and target to nozzle distance of 14 mm for two current values 80 A & 90 A. The Nusselt number shows an increasing trend with Reynolds number. The curves for 80 A and 90 A almost coincide with each other. A sample of measured temperatures, the averaging process, radiation heat loss estimation and Nusselt number calculation are presented in Appendix B. Fig. 3.5 gives the variation of Nusselt number with respect to Reynolds number for the same nozzle diameter but with increased nozzle to target distance of 19 mm. In this case also the curves for 80 A and 90 A almost coincide with each other. For the case of increased target distance of 19 mm, the average Nusselt numbers are higher. The maximum Nusselt number for this case is 80 compared to the previous value of 58. Fig. 3.6 gives the average Nusselt number variation with respect to Reynolds number for the same nozzle diameter but with further increased nozzle to target distance of 24 mm. For the case of increased target distance of 24 mm, the average Nusselt

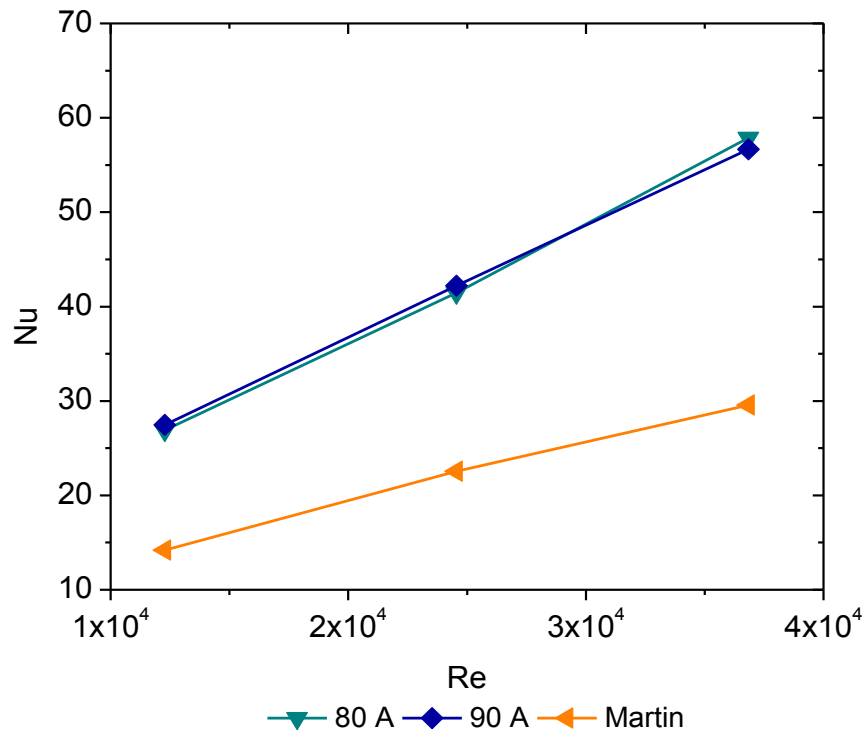


**Fig. 3.4 Experimental results for diameter = 1mm and nozzle to target distance = 14 mm**

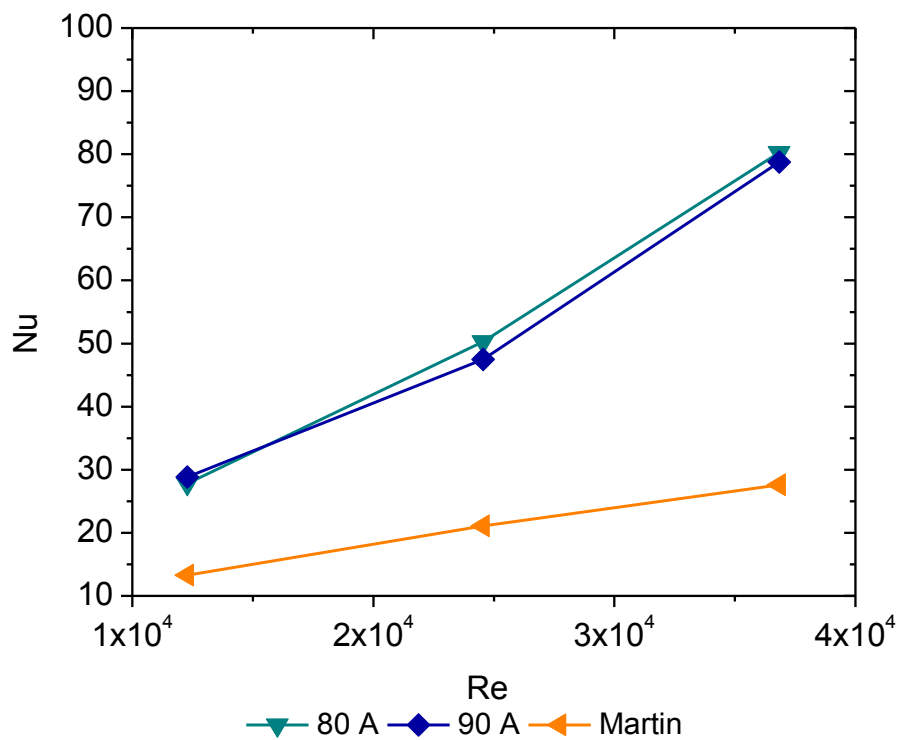


**Fig. 3.5 Experimental results for diameter = 1mm and nozzle to target distance = 19 mm**

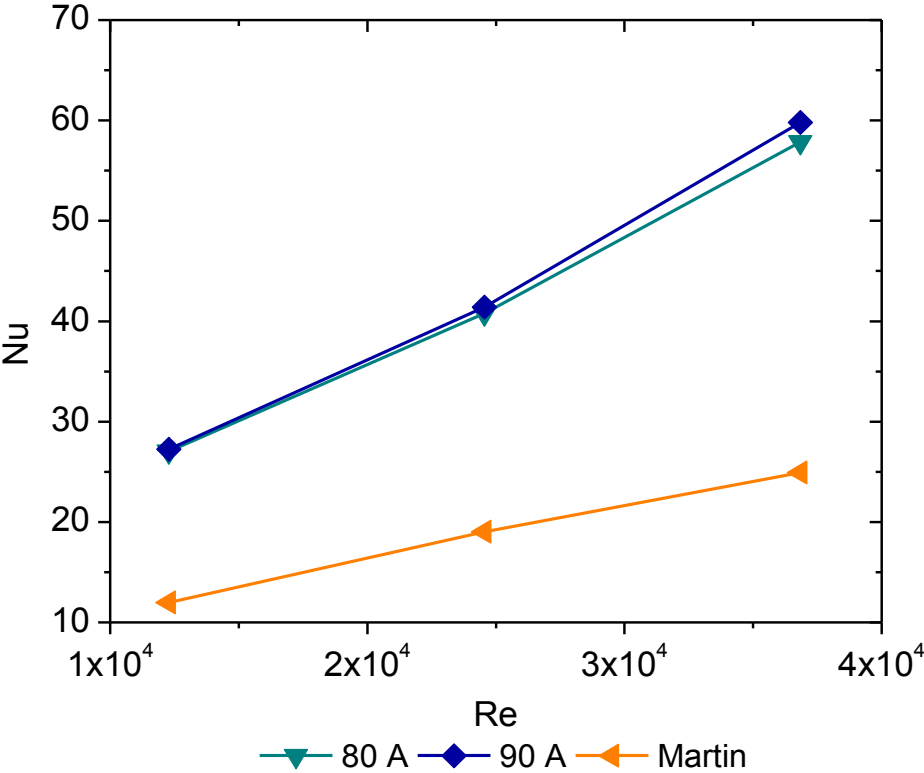


Fig. 3.6 Experimental results for diameter = 1mm and nozzle to target distance = 24 mm

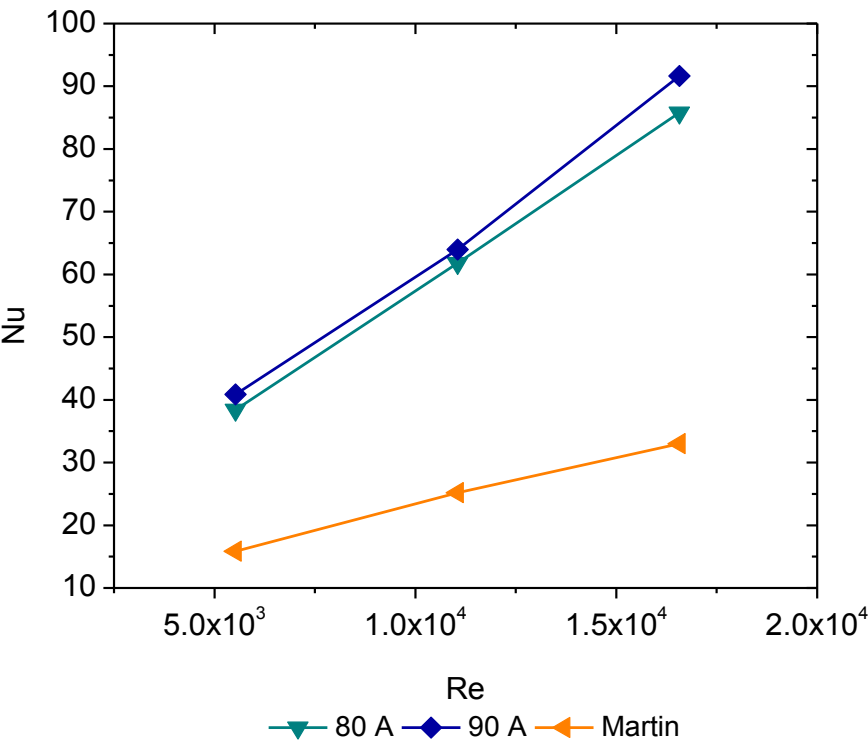
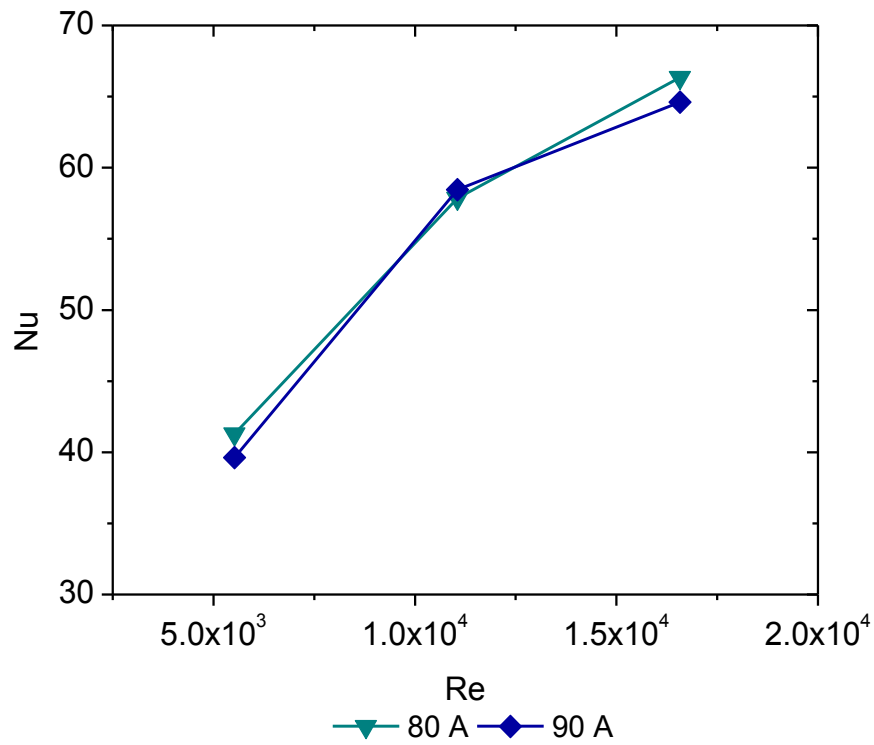
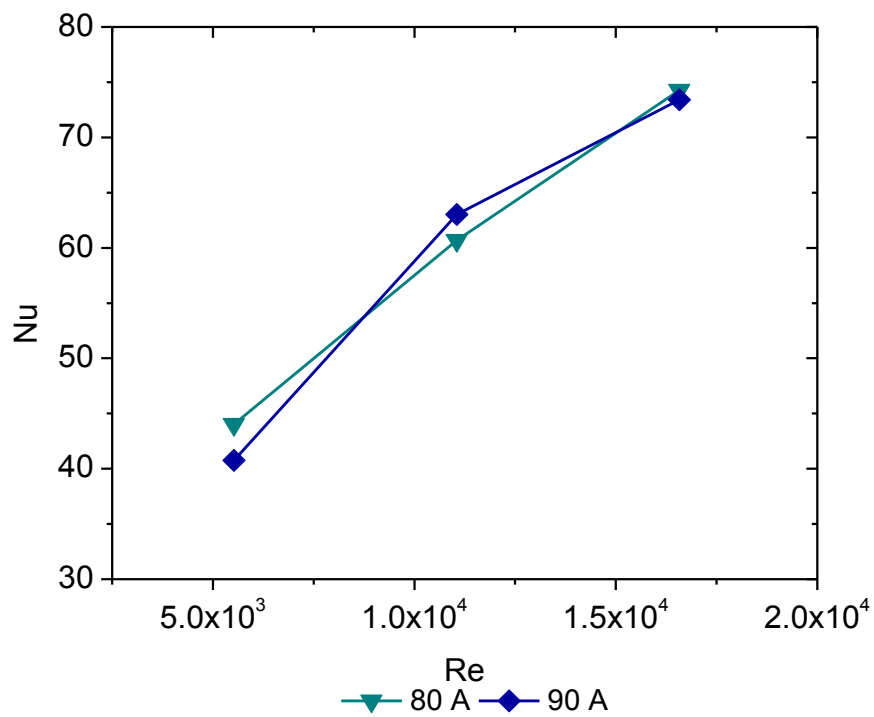


Fig. 3.7 Experimental results for diameter = 2mm and nozzle to target distance = 14 mm



**Fig. 3.8 Experimental results for diameter = 2mm and nozzle to target distance = 19 mm**



**Fig. 3.9 Experimental results for diameter = 2mm and nozzle to target distance = 24 mm**

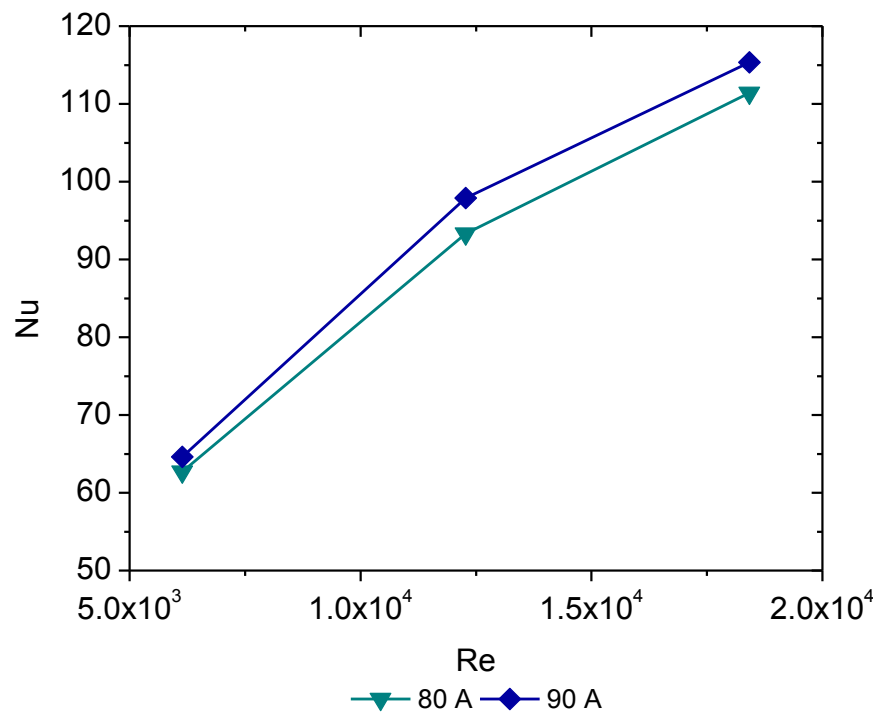


**Fig. 3.10 Experimental results for diameter = 3 mm and nozzle to target distance = 14 mm**

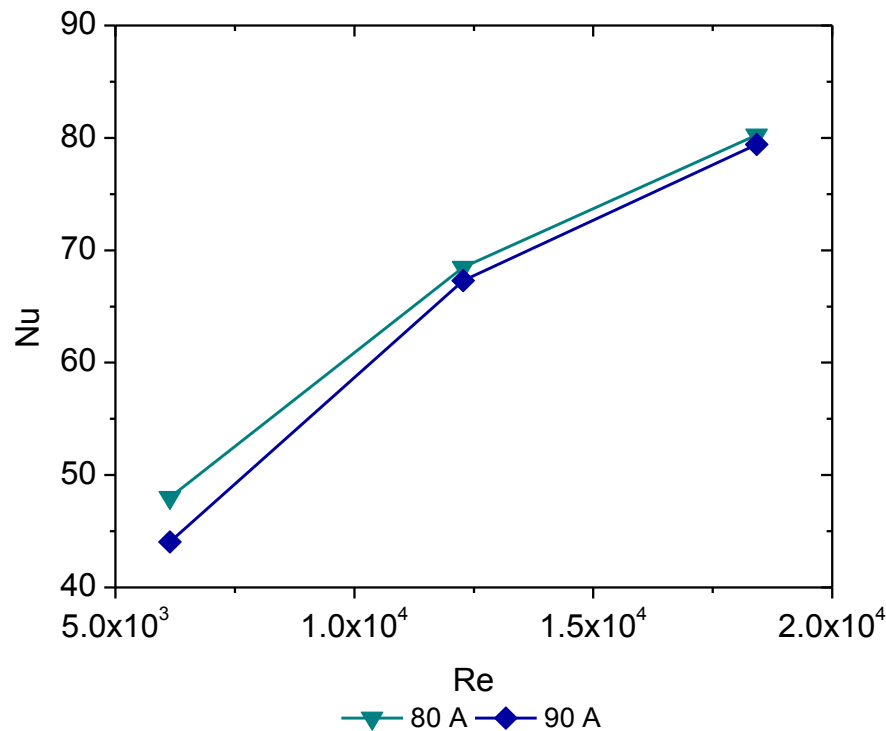


**Fig. 3.11 Experimental results for diameter = 3mm and nozzle to target distance = 19 mm**

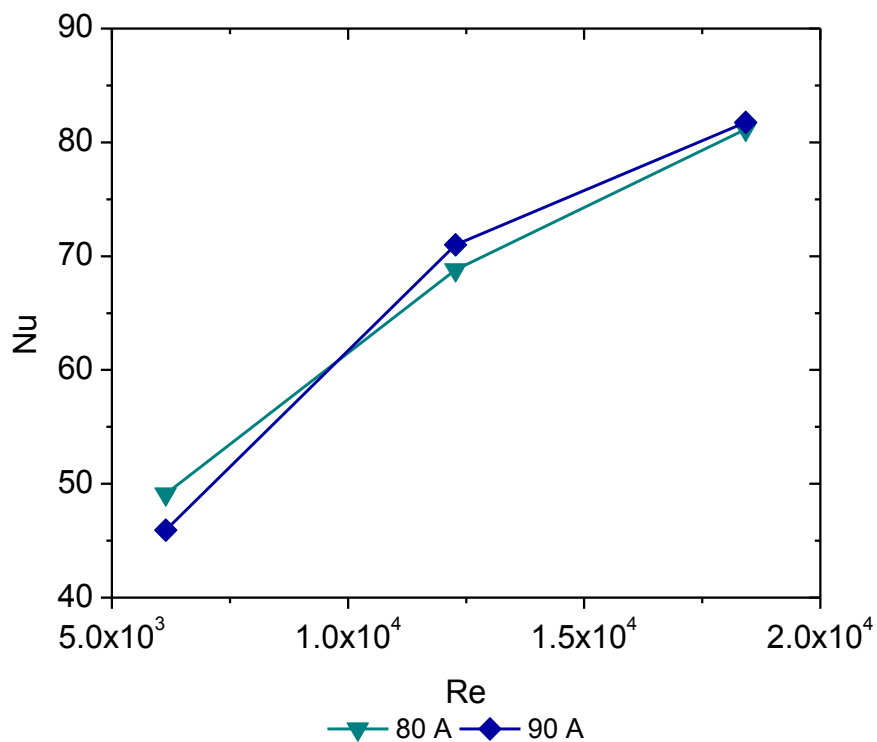


**Fig. 3.12 Experimental results for diameter = 3mm and nozzle to target distance = 24 mm**

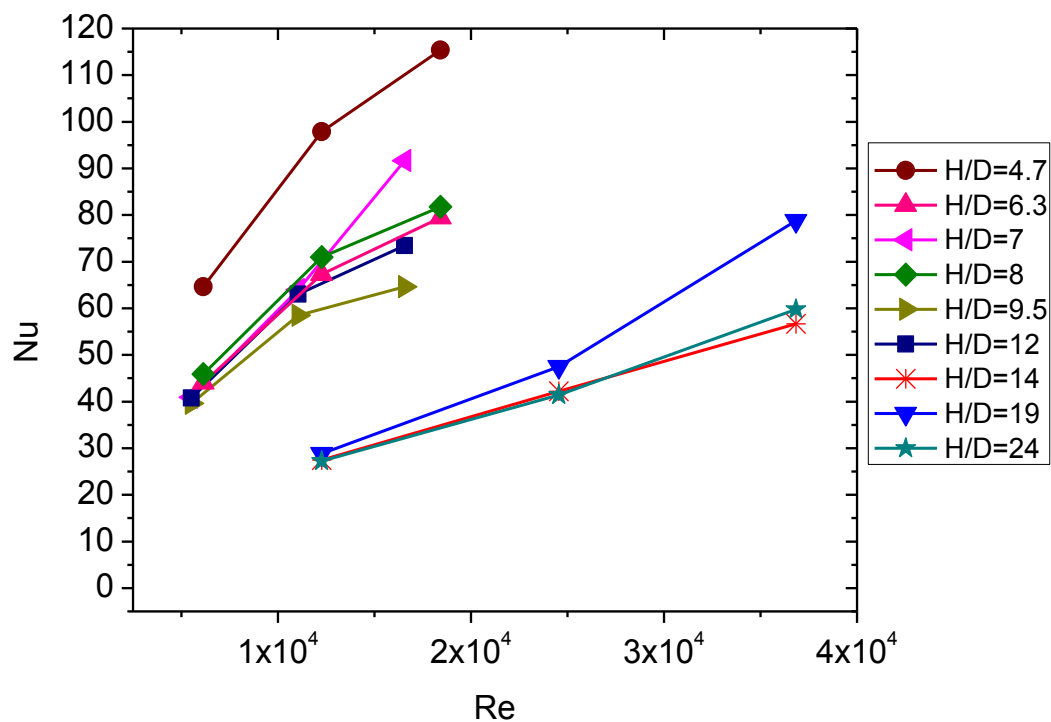


**Fig. 3.13 Nu Vs Re for different H/D ratios**



numbers are lower compared to the target distance of 19 mm. The maximum Nusselt number in this case is only 60.

Similar results are given in Figs. 3.7, 3.8 and 3.9 for nozzle diameter equal to 2 mm and Figs. 3.10, 3.11 and 3.12 for nozzle diameter equal to 3 mm respectively. Even though Reynolds number is same with increased diameter the mass flow rate increases. For example when diameter increases two times, the mass flow rate also increases two times for the same Reynolds number. As a result of this fact, the Nusselt number increases with jet diameter even for identical Reynolds number.

For nozzle diameter equal to 1mm, the Nusselt number is maximum for the target distance of 19 mm. But with increased diameter the maximum Nusselt number occurs for a shorter target distance of 14 mm.

For nozzle diameter equal to 1 mm as can be seen from Figs. 3.4 to 3.6, the slope of the second part is higher than the first part. That is when the Reynolds number is increased, the increase in the Nusselt number is more. Whereas for a nozzle diameter equal to 3 mm, as can be seen from Figs. 3.10 to 3.12, the slope of the second part is lower than the first part. That is when the Reynolds number is increased, the increase in the Nusselt number is less. Therefore in the lower diameter by increasing the Reynolds number we can get good improvement in the Nusselt number. This is true for the case of nozzle diameter equal to 2 mm also. In this case, as can be seen from Figs. 3.7 to 3.9, the slope of the second part is higher than the first part for nozzle to target distance equal to 14 mm. At larger distances the slope of the second part is lower than the first part.

The variation of average Nusselt number with respect to Reynolds number for different ratios of distance between nozzle & target ( $H$ ) and nozzle diameter ( $D$ ) is plotted in Fig. 3.13 for all the above experimental studies. As the  $H/D$  ratio decreases from the maximum value of 24, the average Nusselt number shows an increasing trend reaching the maximum average Nusselt number for the lowest  $H/D$  ratio of 4.7. This is more clearly seen in Fig. 3.14 for Reynolds number equal to 12280. Incropera et. al., [104] reports that to get maximum average Nusselt number, the optimum value of  $H/D$  is approximately equal to 5. This matches well with the present experimental results. Optimum length of the target plate =  $L = 1.4 H$ . This is equal to 19.6 mm, which also matches with the specimen length of 20 mm.

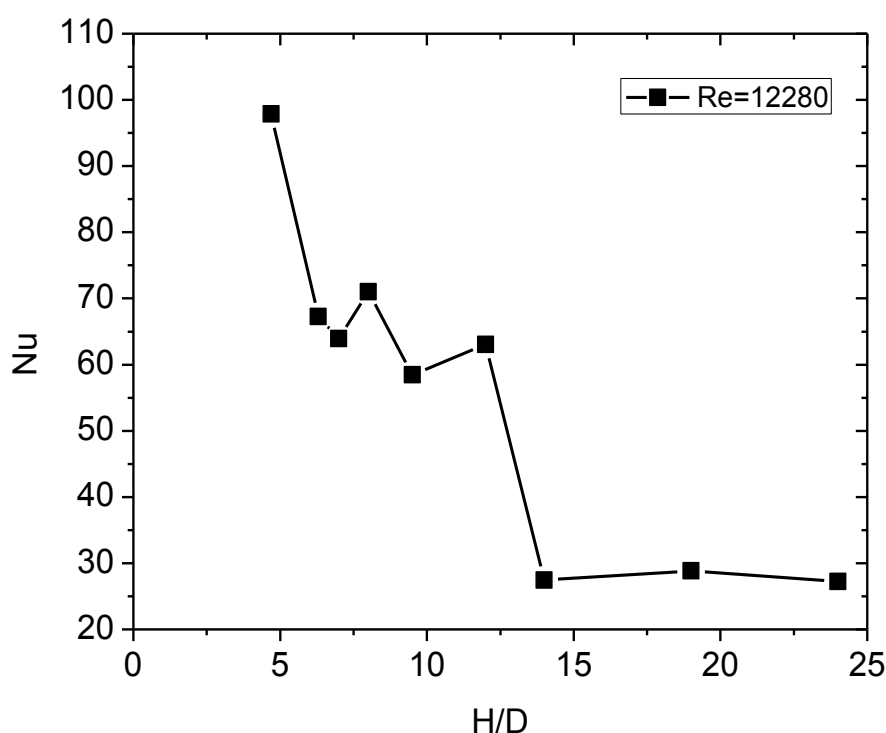


**Fig. 3.14 Nu Vs H/D ratio for Re = 12280**

### 3.3 Empirical correlations

A number of authors experimentally and numerically studied various aspects of jet impingement heat transfer: jet Reynolds number from low to high, jet height to jet diameter,

radial distance, Prandtl number, effect of entrainment on heat transfer, effect of temperature difference between jet and ambient air, cross flow, effect of confinement, angle of jet impingement, jet impingement over a flat surface and curved surface, effect of mesh screen in front of jet nozzle, effect of staggered array and inline array of impinging jets and also effects of nozzle shapes. A detailed review of heat and mass transfer between impinging gas jets and solid surfaces is carried out by Martin [70]. He proposed the following correlation for array of round nozzles:

$$\text{Nu}_{\text{average}} / \text{Pr}^{0.42} = K_A(H/D, f) G(H/D, f) F(\text{Re})$$

$$K_A \left( \frac{H/D}{0.6/\sqrt{f}} \right) = 1 \quad \text{for } \left( \frac{H/D}{0.6/\sqrt{f}} \right) < 1$$

$$K_A \left( \frac{H/D}{0.6/\sqrt{f}} \right) = \left( \frac{H/D}{0.6/\sqrt{f}} \right)^{-0.3} \quad \text{for } \left( \frac{H/D}{0.6/\sqrt{f}} \right) \geq 1$$

$$G(H/D, f) = 2\sqrt{f} \frac{1-2.2\sqrt{f}}{1+0.2\left(\frac{H}{D}-6\right)\sqrt{f}}$$

$$F(\text{Re}) = 0.5 \text{Re}^{2/3}$$

Range of validity:

$$2000 \leq \text{Re} \leq 100,000$$

$$0.004 \leq f \leq 0.04$$

$$2 \leq H/D \leq 12$$

H – Nozzle to target distance

D – Diameter of the nozzle

f – Relative nozzle area

– Ratio of the nozzle exit cross section to the area of the square attached to it.

The Nusselt numbers calculated using this correlation are also given in Fig. 3.4 to 3.7. The experimental predictions are 50 to 70% higher compared to the empirical correlations. The specimen is heated by passing electric current at low voltage through the specimen. In order to have uniform heating two copper plates are attached at both the ends as shown in Fig. 3.1c. These copper plates act as fins and dissipate heat. This leads to additional heat transfer from the specimen. This could be the reason for the difference between experiment and prediction by Martin's correlation. In the experiment thermocouples are used for the temperature measurements. The thermocouple tips are spot welded to the specimen. These thermocouple tips and leads close to the specimen promote additional turbulence which will increase the heat removal from the specimen. This also could be one of the reasons for the difference between experiment and prediction by Martin's correlation.

The heat loss from test sample through the copper plates has been estimated by assuming the copper plates as fins for one typical case as shown in Appendix - B. It is found that the experimental Nusselt number reduces from 57.3 to 33.1 when heat loss effect through copper plates taken into account. This compares very close to Martin's correlation value of 30. The difference is only 9.45%, which is within the experimental uncertainty of  $\pm 15\%$ .

### 3.4 Cooling by slot air jets

Fig. 3.15 shows the variation of average Nusselt number Vs Reynolds number for a slot width of 1 mm and a nozzle to target distance of 14 mm. As expected the Nusselt number

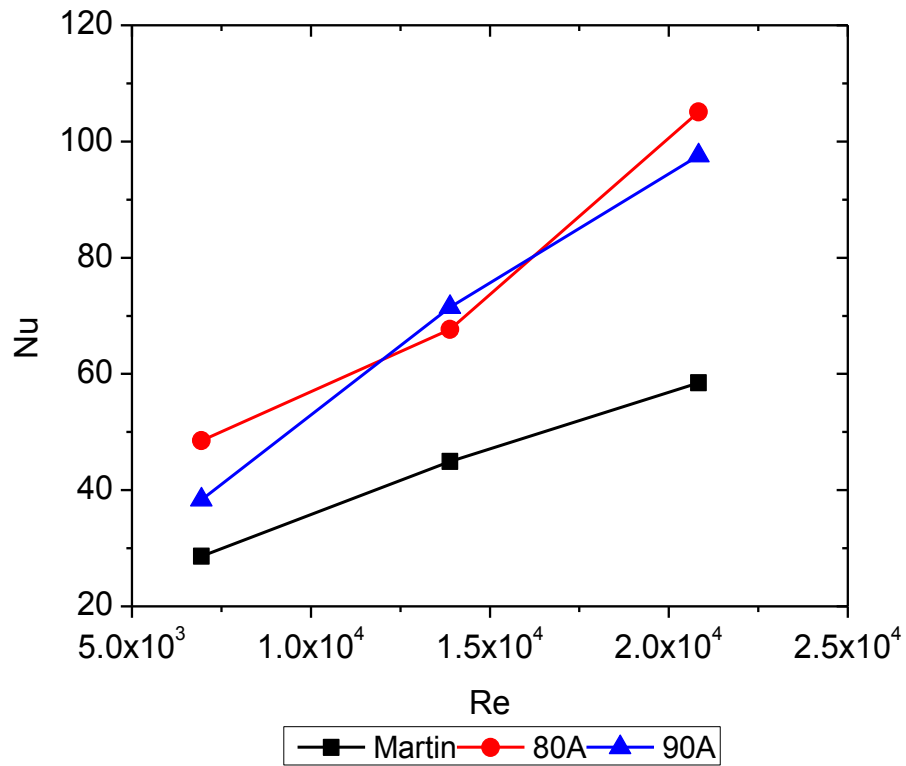


**Fig.3.15** Experimental results for slot width = 1 mm and jet to nozzle distance = 14 mm

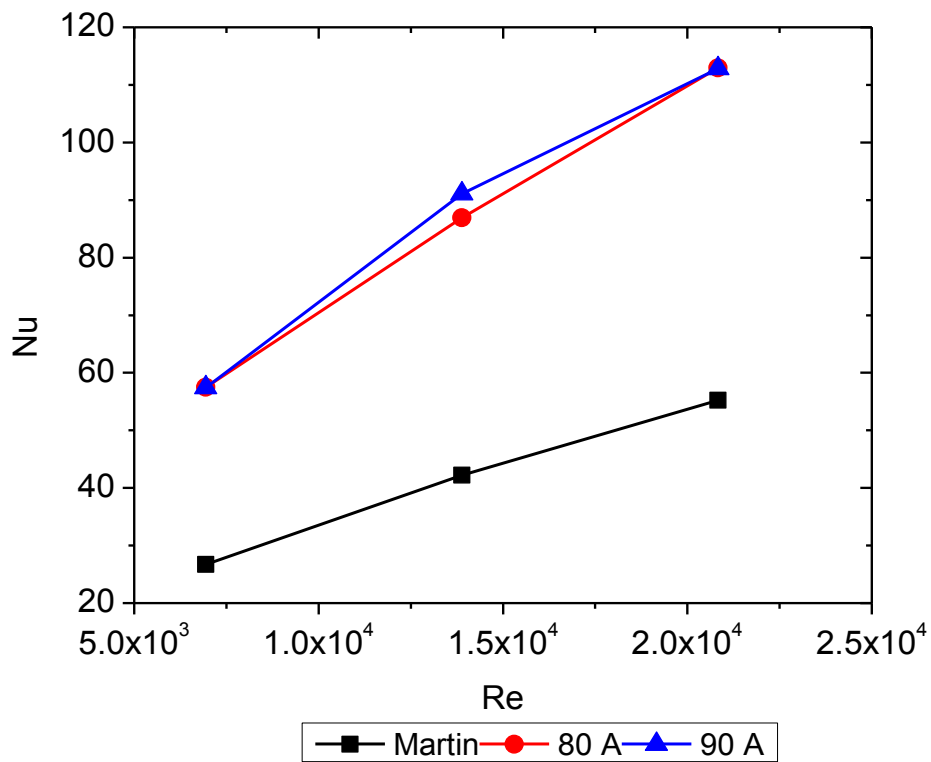


**Fig.3.16** Experimental results for slot width = 1 mm and jet to nozzle distance = 19 mm

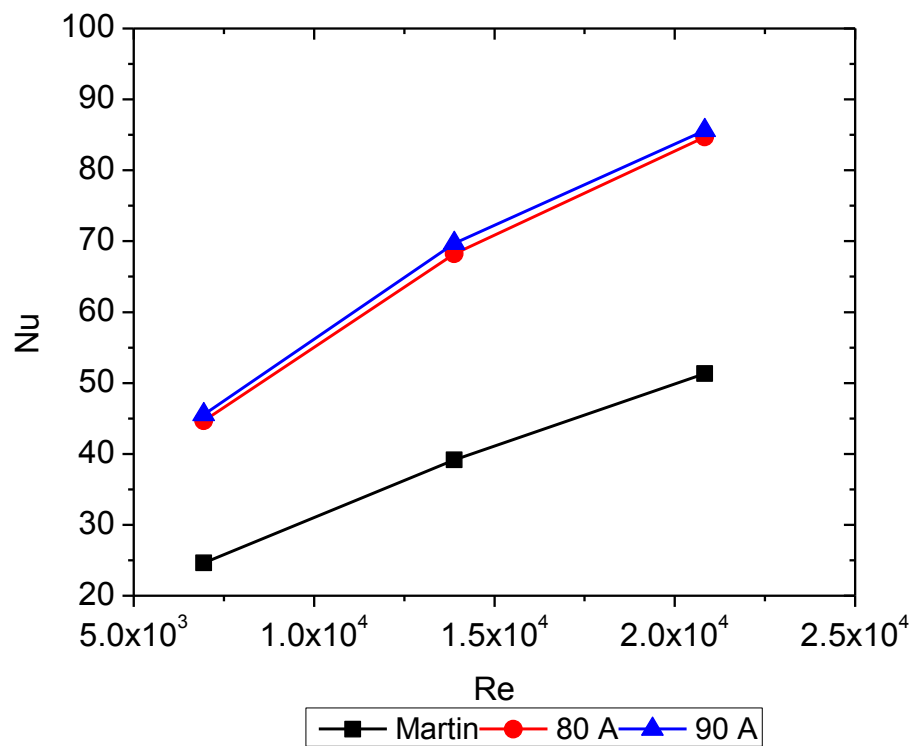


Fig.3.17 Experimental results for slot width = 1 mm and jet to nozzle distance = 24 mm

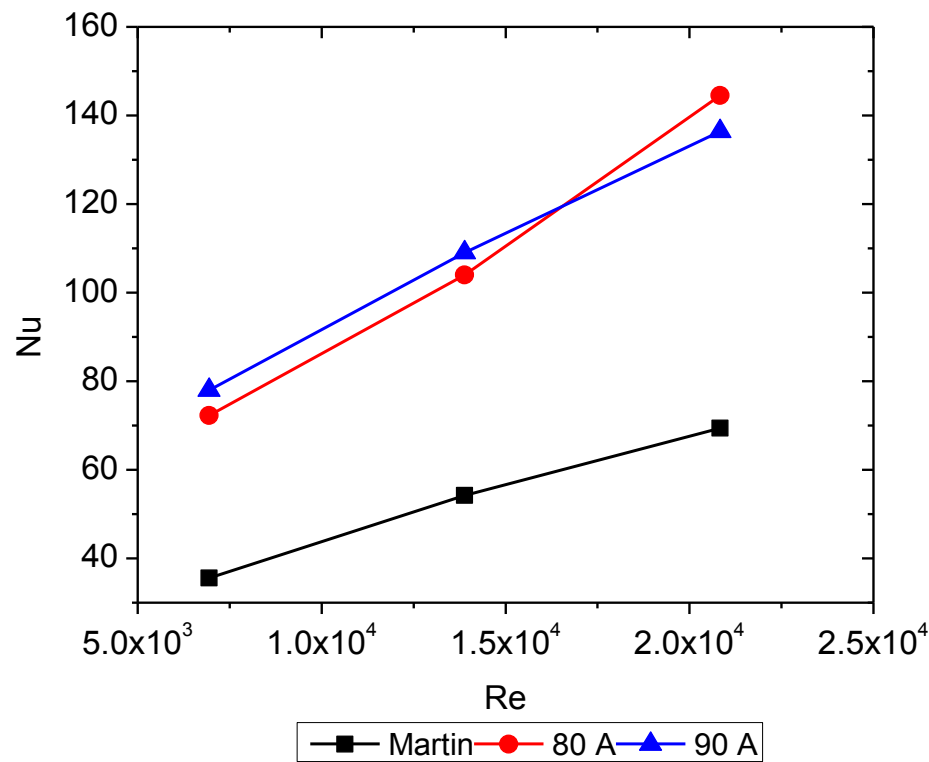
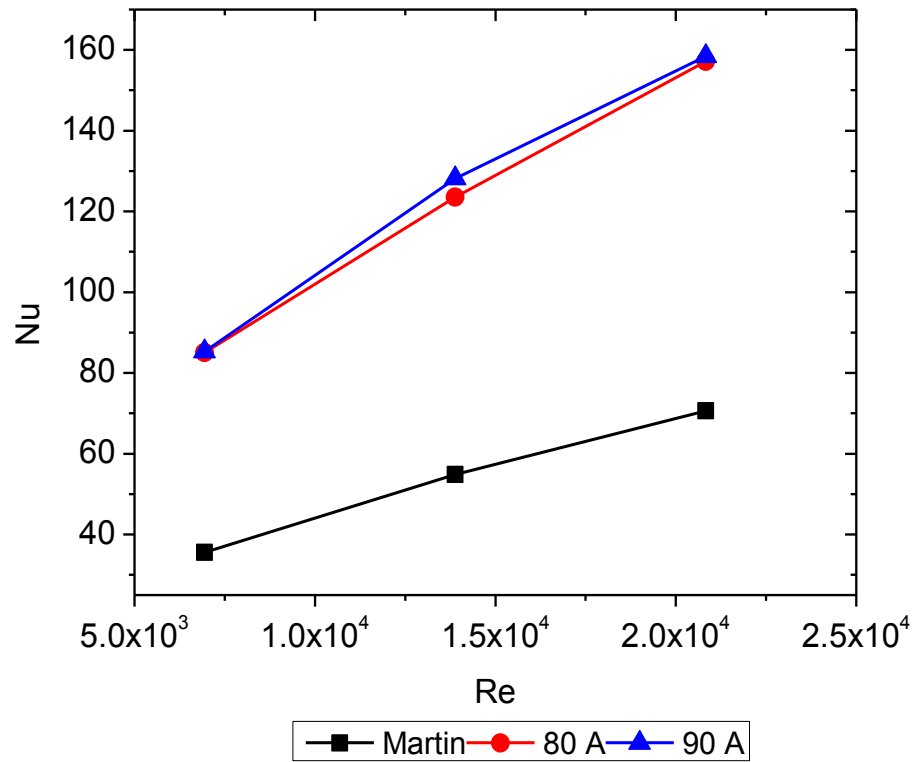
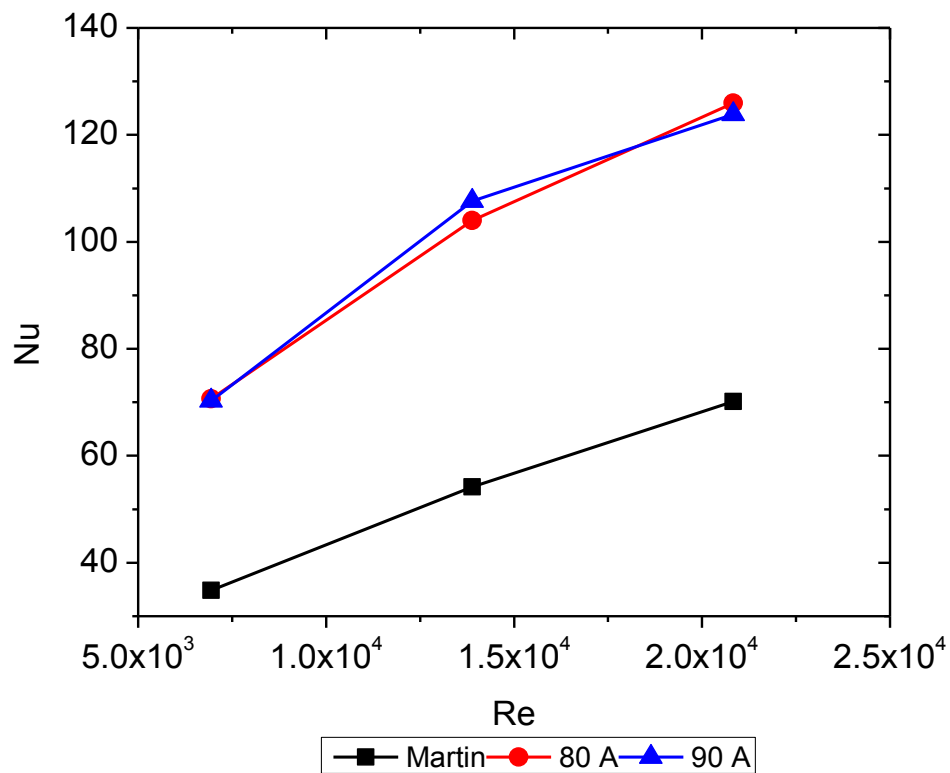


Fig.3.18 Experimental results for slot width = 2 mm and jet to nozzle distance = 14 mm



**Fig.3.19** Experimental results for slot width = 2 mm and jet to nozzle distance = 19 mm



**Fig.3.20** Experimental results for slot width = 2 mm and jet to nozzle distance = 24 mm

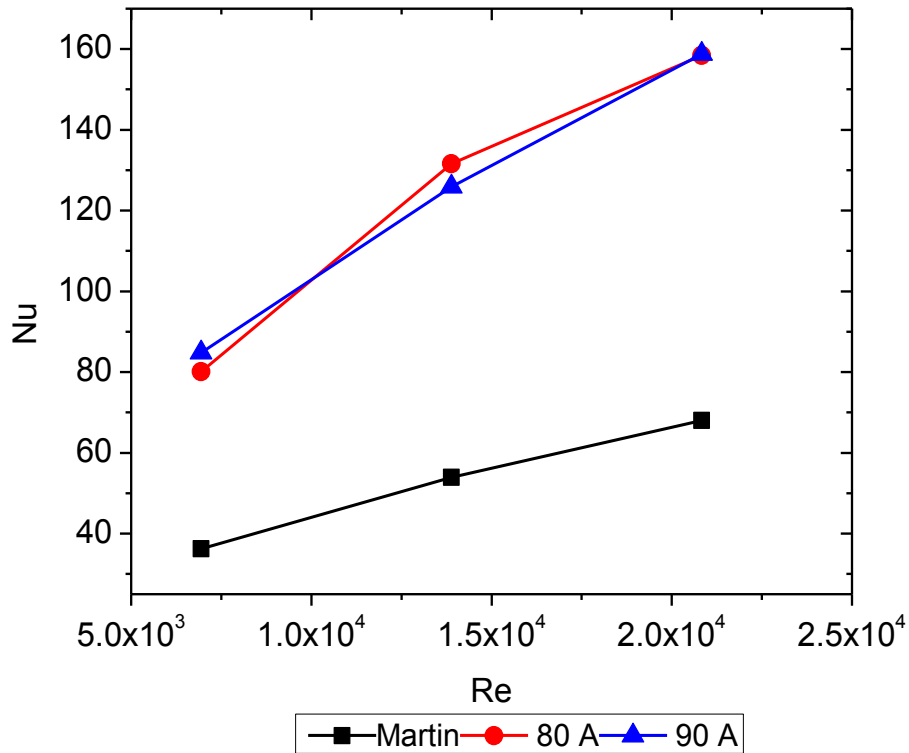


**Fig.3.21** Experimental results for slot width = 3 mm and jet to nozzle distance = 14 mm

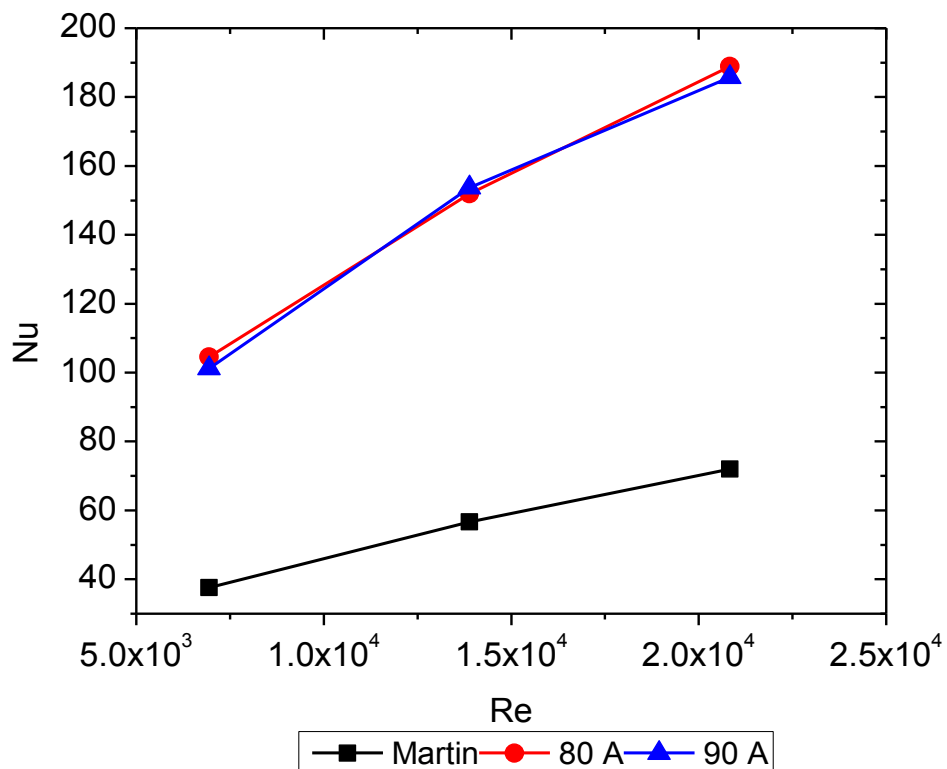


**Fig.3.22** Experimental results for slot width = 3 mm and jet to nozzle distance = 19 mm



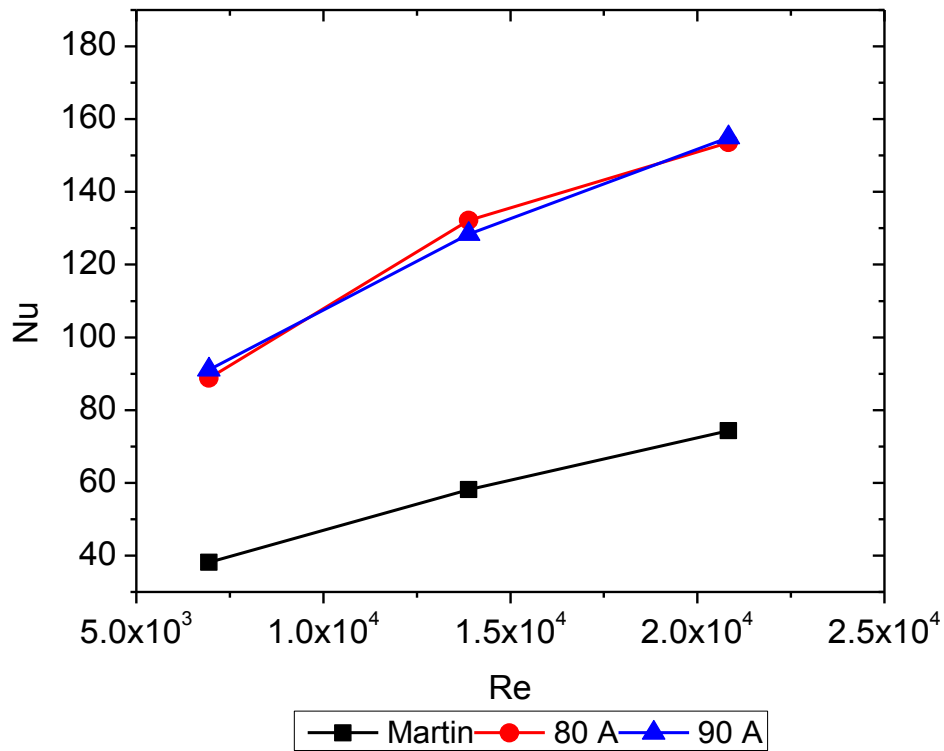


Fig.3.23 Experimental results for slot width = 3 mm and jet to nozzle distance = 24 mm

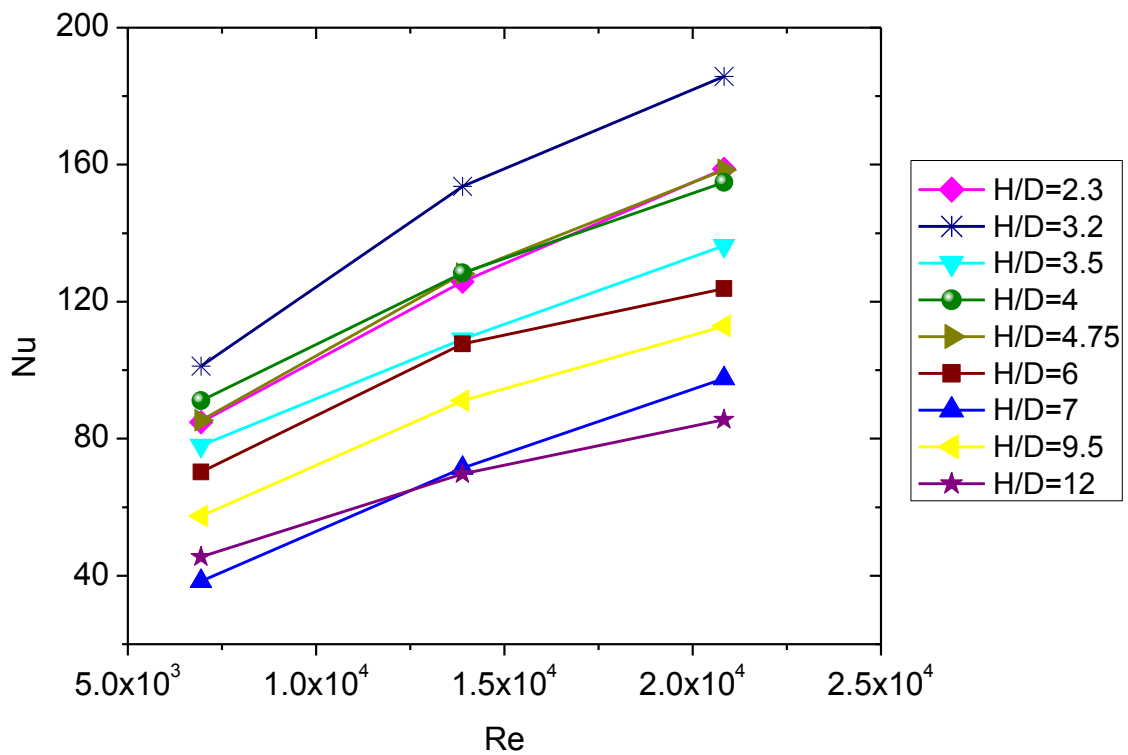
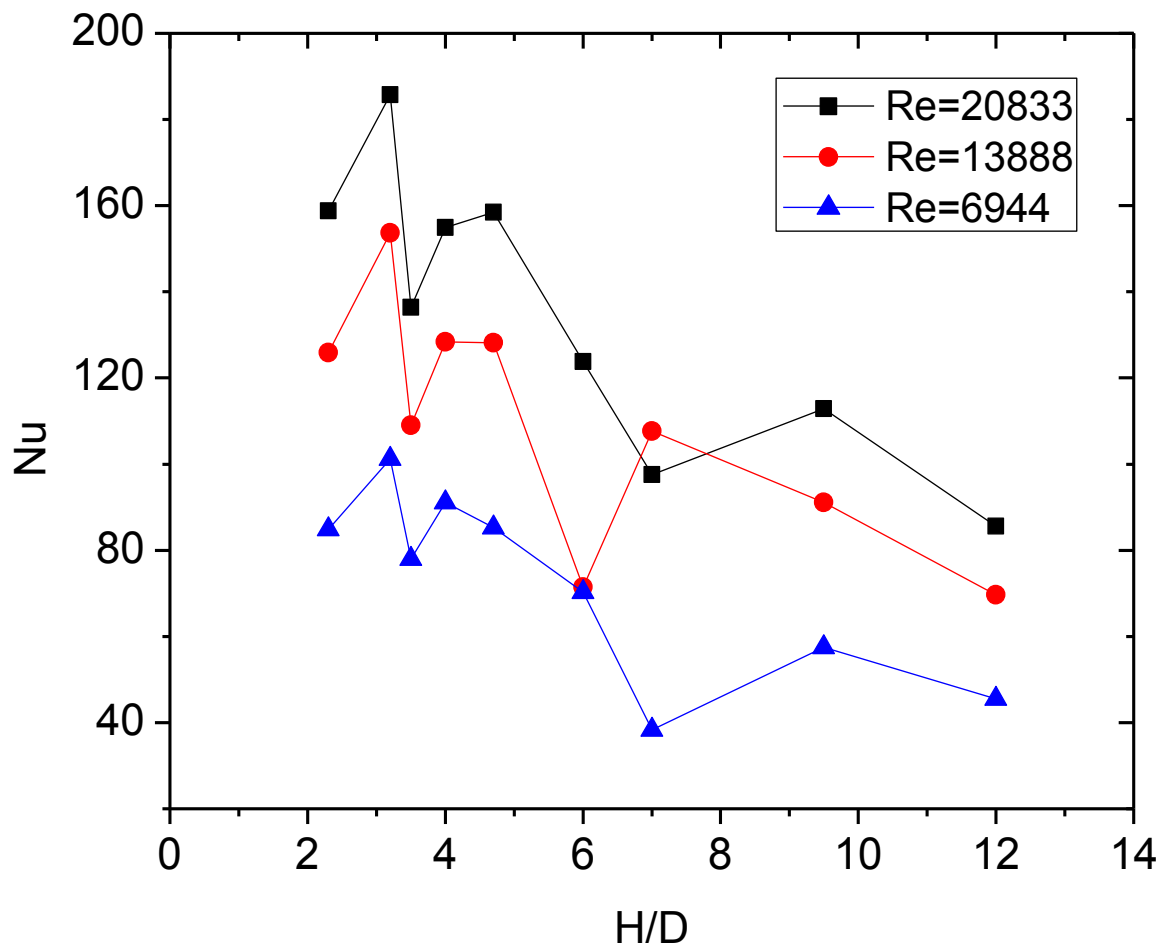


Fig.3.24 Nu Vs Re for different H/D ratios



**Fig. 3.25 Nu Vs H/D ratio**

increases with Reynolds number. Two cases have been studied with current equal to 80 A and 90 A. The temperature of the sample is around 90 °C depending on the applied current. The power transferred is about 14 W. Fig. 3.16 shows the results for the case where the nozzle to target distance is increased from 14 mm to 19 mm. General trend of the results is similar to that presented in Fig. 3.15. The results for the cases 80A and 90A are almost matching with each other. In this case the heat removal rate is higher compared to the previous case. For example for 90 A, the maximum Nusselt number obtained for a Reynolds number of 21000 is 112 where as for the nozzle to target distance of 14 mm the corresponding value is less than 100. Fig. 3.17 shows the results of Reynolds number Vs Nusselt number for a nozzle to

sample distance of 24 mm. Compared to Fig. 3.15 and Fig. 3.16, in this case the measured Nusselt number is the lowest. For example, for the case of 90 A the value is 85, whereas the previous values are 98 and 112. This shows the optimum nozzle to sample distance for maximum Nusselt number is 19 mm. Studies have also been carried out for slot width equal to 2 mm and 3 mm in the Reynolds number range from 7000 to 21000 and for current value equal to 80 A and 90 A and the results are given in Fig. 3.18 to Fig.3.23. The variation of Nusselt number with Reynolds number shows similar trends.

The variation of average Nusselt number with respect to Reynolds number for different ratios of distance between nozzle & target (H) and slot width (D) is plotted in Fig. 3.24 for all the above experimental studies. As the H/D ratio decreases from the maximum value of 12, the average Nusselt number shows an increasing trend reaching the maximum average Nusselt number for the H/D ratio of 3.2. With further reduction in H/D ratio, the Nusselt number starts decreasing. This is more clearly seen in Fig. 3.25 where Nusselt number is plotted against H/D ratio for three different Reynolds numbers. Incropera et. al., [104] reports that to get maximum average Nusselt number, the optimum value of H/D is approximately equal to 5. This matches well with the present experimental results for circular jets. But for slot jets the value is 3.2 which is lower than 5.

The following empirical correlation is proposed by Martin [70] for single slot nozzle:

$$\frac{\overline{Nu}}{Pr^{0.42}} = \frac{1.53}{\frac{x}{S} + \frac{H}{S} + 1.39} Re^{m\left(\frac{x}{S}, \frac{H}{S}\right)}$$

$$m = 0.695 - \left( \frac{x}{S} + \left( \frac{H}{S} \right)^{1.33} + 3.06 \right)^{-1}$$

Range of validity:

$$3,000 \leq Re \leq 90,000$$

$$2 \leq x/S \leq 25 \quad (0.125 \geq f \geq 0.01)$$

$$2 \leq H/S \leq 10$$

Where  $f = S / 4x$

$S$  = Hydraulic diameter of slot nozzle ( $S = 2 B$ )

$B$  = Width of the slot nozzle

$H$  = Nozzle to sample distance

$x$  = Sample length / 2

The experimental results are compared with this empirical correlation in Figs. 3.15 to 3.23. Even though the slope of the empirical correlation matches with the experiment, the experimental predictions are approximately 35% to 55% higher compared to empirical correlation. As explained for the circular jet case this may be due to additional heat loss through the copper plates attached at both ends of the specimen. Another reason could be additional turbulence created by the thermocouple tips and lead wires close to the specimen.

### 3.5 Cooling by inclined slot air jets

Experiments are also carried out with inclined slot jet. The angle of inclination is  $50^\circ$  with the horizontal. The slot jets were placed 1 mm away from the end of sample. The jet to target distance is kept at 19 mm. The air flow rates were varied from 5 to  $15 \text{ m}^3/\text{h}$ . Three slot widths of 1 mm, 2 mm and 3 mm were studied. As with the other studies the Nusselt number increases with the Reynolds number. The maximum heat transfer coefficient obtained is  $1053 \text{ W} / \text{m}^2\text{K}$  for the slot width of 1mm.

### 3.6 Comparison

The results shows that for similar conditions circular jets give higher average heat transfer coefficient compare to slot jet. This may be due to the higher air velocity at the nozzle outlet in case of circular nozzles compare to slot nozzles. The maximum average heat transfer coefficient obtained is  $2400 \text{ W / m}^2 \text{ K}$  for the circular jet with nozzle diameter equal to 1 mm and nozzle to target distance of 19 mm. The maximum heat transfer co-efficient obtained for the slot jet is  $1530 \text{ W / m}^2 \text{ K}$  for the case of 1mm nozzle width and 19 mm nozzle to target distance. For the case of inclined slot jet the maximum heat transfer coefficient obtained is  $1053 \text{ W / m}^2 \text{ K}$  for the slot width of 1 mm. In the present experiments the Nusselt number shows an increasing trend with the Reynolds number. Hence there is possibility to further enhance the heat transfer coefficient by increasing the air flow rate.

A comparison of heat transfer characteristics between helium and air system is given in Appendix – C. It is found that heat transfer coefficient in case of helium is almost twice that of air.

### 3.7 Closure

Air jet experiments have been carried out to find out the conditions for getting maximum heat transfer coefficient. From the experiments it is found that circular nozzles give higher heat transfer coefficients compared to slot nozzles under similar conditions. For nozzle diameter equal to 1 mm, the optimum nozzle to target distance is 19 mm, where as for higher diameter the optimum target distance is 14 mm or lower. The maximum Nusselt number is obtained for H/D ratio equal to 4.7. Inclined jets give lower heat transfer coefficient compared to vertical jets. From the various cases studied the maximum heat transfer coefficient is  $2400 \text{ W / m}^2 \text{ K}$  for a nozzle diameter of 1 mm and nozzle to target distance of 19 mm.

With the advancement of computing power, CFD modeling is used for more and more new areas. CFD modeling is a very useful technique to model more realistically the complicated physical phenomena. With a well validated CFD model a number numerical studies can be carried out with less cost and time compared to experiment. CFD model will be very useful to optimize the parameters for identifying the conditions leading to maximum heat transfer coefficient. Hence the next chapter is devoted to the development of the CFD model for the jet cooling phenomena.

\*       \*       \*

# Chapter- 4

## Computational simulation of single jet experiments

### 4.0 Introduction

Experimental studies have been carried out with air jet issuing from a rectangular slot made to impinge on a heated target. The target plate is heated by resistance heating and flow of current and voltage drop across the target are measured to give an estimate of the heat generation in the plate. Experimental studies have been carried out for a wide range of parameters, viz., (i) varying jet flow rate, (ii) magnitude of electrical current, (iii) distance between the jet and target plate and (iv) size of the jet. The size of the target plate considered in these studies is 20 mm X 20 mm with 0.5 mm thickness. Length of the slot jet is 20 mm. Numerical simulation of the phenomenon has been carried out using general purpose CFD code, STAR-CD and the predictions compared against empirical correlations and experimental results. Details of the CFD model and the comparison against experiments and empirical correlations are presented in this chapter.

### 4.1 Modelling details

The length of the jet (20 mm) is large compared to its width (1 to 2 mm). Hence, the flow pattern would be similar along the length of the jet. Therefore, two dimensional section of the jet along the length direction is considered for the analysis. Further, the geometry of the jet is symmetric along the width direction. However, in view of the possible jet instability, full width of the jet is considered for the analysis. Schematic of the geometry along with boundary conditions is shown in Fig. 4.1. Jet is defined through inlet boundary condition and outlet is specified at all the boundary surfaces of the domain. Volumetric heat generation is specified on the target material. The domain size of simulation is 35 mm x 35 mm and specimen is located 5 mm from bottom. At the domain boundary pressure is defined as the boundary condition. There is no restriction on recirculation. Moreover the temperature of air



in the jet and the ambient air temperature are same. Hence, the selected domain size is sufficient enough. Larger domain size will only going to increase the computational time without any additional improvement in the result.

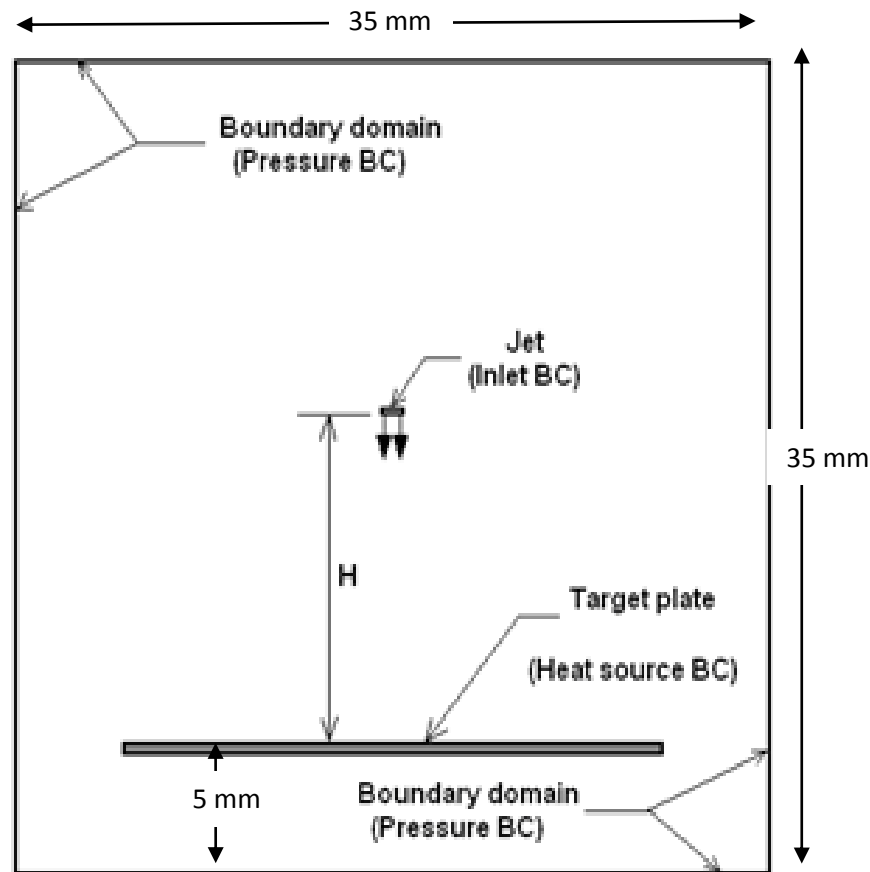
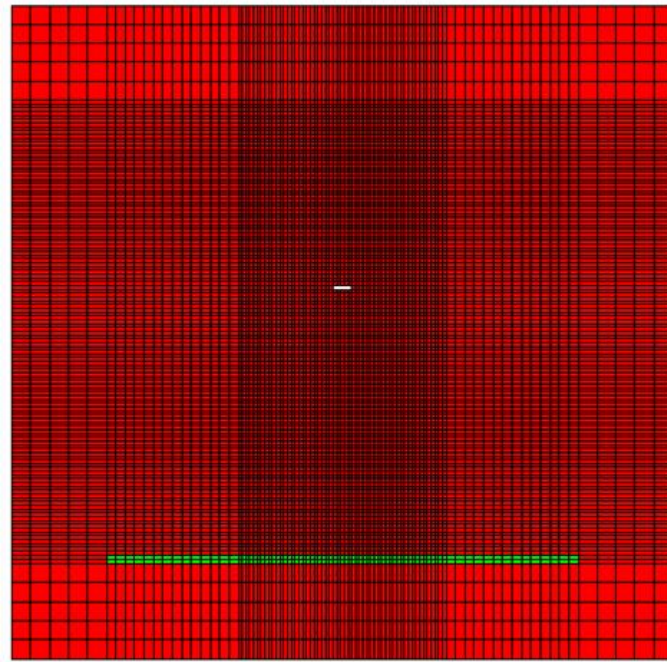


**Fig. 4.1 Schematic of geometry and boundary conditions (BC)**

The geometry of the domain is discretized using structured Cartesian mesh. Two different mesh patterns with 12374 and 49084 control volumes as shown in Fig. 4.2 have been considered for the simulation. For a typical geometrical configuration of the jet with jet velocity of 167 m/s, the average heat transfer coefficient predicted by the coarse and fine mesh models are 605 W/m<sup>2</sup>K and 627 W/m<sup>2</sup>K respectively. Since, the predictions are very close with a deviation of less than 4 %, coarse mesh pattern has been used for further studies. Results of various studies carried out are discussed in the following sections.



(12374 meshes)



(49084 meshes)

**Fig. 4.2 Coarse (top) and fine (bottom) mesh patterns considered for the analysis**

## 4.2 Prediction by various turbulence models

In order to simulate the influence of turbulence on the heat transfer process, various models have been considered. Brief descriptions of various models considered for the study are discussed below.

### 4.2.1 k-ε Model

Among the various turbulence models, k-ε model [97] is one of the most popular and generic models. According to this model, the additional transport equations for turbulent kinetic energy (k) and rate of dissipation of turbulent kinetic energy (ε) are:

$$\nabla \bullet (\bar{V} k) = \nabla \bullet (\nu_k \nabla k) + S_k$$

$$\nabla \bullet (\bar{V} \varepsilon) = \nabla \bullet (\nu_\varepsilon \nabla \varepsilon) + S_\varepsilon$$

Source term in the equation for k ( $S_k$ ) represents sum of turbulent generation by shear & normal stresses, buoyancy force and viscous dissipation of turbulent kinetic energy. Similarly, the source term in the equation for ε ( $S_\varepsilon$ ) represents sum of its production and dissipation analogous to that in the k-equation.

In the above equations, diffusivity term ( $\nu$ ) is given by

$$\nu_k = \frac{\nu_t}{Pr_k} + \nu_l \text{ and } \nu_\varepsilon = \frac{\nu_t}{Pr_\varepsilon} + \nu_l$$

$$\nu_t = \frac{C_\mu k^2}{\varepsilon}$$

where  $C_\mu$  is an empirical constant and Pr is the Prandtl number.

Also in the momentum and energy transport equations,

$$\nu_{eff} = \nu_t + \nu_l \text{ and } \alpha_{eff} = \alpha_t + \alpha_l$$

with,

$$\alpha_t = \frac{\nu_t}{\Pr_t}$$

In the above equations, the subscripts ‘t’ and ‘l’ refer to the turbulent and laminar contributions to a property.

#### 4.2.2 k-ε RNG Model

Minor variations in k-ε model are applied to improve the prediction under specific situation. One such model is known as the Renormalization Group Theory k-ε model (RNG). The RNG model [105] incorporates an additional term in the turbulent energy dissipation equation based on strain rates, and includes adjustments for viscous effects at lower Re and a calculation of turbulent Prandtl number. The governing equations include additional term in ε equation for (i) interaction between turbulence dissipation and mean shear, (ii) the effect of swirl on turbulence, (iii) analytical formula for turbulent Prandtl number and (iv) differential formula for effective viscosity.

#### 4.2.3 Reynolds Stress Model

For better simulation of turbulence, the individual Reynolds stresses may be directly determined by solving their governing transport equations [106]. Reynolds Stress Model (RSM) can predict complex turbulent flows more accurately as it can account better for factors such as anisotropy, streamline curvature, swirl and high rate of strain. RSM directly solves for Reynolds stresses  $\overline{\rho V_i' V_j'}$  using equations of the form,

$$C_{ij} - D_{ij} = P_{ij} + \phi_{ij} - \rho \epsilon_{ij}$$

where  $C_{ij}$  is the convection term,  $D_{ij}$  is the diffusion term,  $P_{ij}$  is the generation term,  $\phi_{ij}$  is the pressure-strain term and  $\rho \epsilon_{ij}$  is the dissipation term. The equations for Reynolds stresses are solved along with the transport equation for k and ε, respectively in the modified form.

#### 4.2.4 Comparison of Predictions

Analysis has been carried out for the case of 1 mm jet width and vertical spacing between the jet and target (H) of 14 mm. Heat generation and inlet temperature of air considered in the analysis are 13.4 W and 23 °C respectively. Convective terms have been resolved using upwind scheme in the simulations. The solution of governing equations representing conservation of mass, momentum, energy and turbulence has been carried out using SIMPLE algorithm. Predicted velocity and temperature distribution in the domain using k- $\epsilon$  RNG model and jet flow rate of 15 m<sup>3</sup>/h are shown in Figs. 4.3 and 4.4 respectively. It can be observed that the jet impinges at the centre of the target and flows parallel to the target in both the directions symmetrically. Due to the increased heat transfer at the region of impingement, the temperature of the target is lower compared to the periphery. Temperature distribution of plate along its length is shown in Fig. 4.5. It can be observed that temperature of plate is minimum at its centre. Heat transfer coefficient of the plate is calculated with respect to the average temperature. Velocity and temperature distribution predicted with other turbulence models are similar. The predicted distribution of axial velocity in the fluid at various distances from the jet is shown in Fig. 4.6. It can be observed that potential cone exists up to 10 mm distance from the jet. The jet spreads by ~ 3 mm when it reaches close to the target located at 14 mm from the jet source.

The predicted values of average temperatures of the plate and heat transfer coefficients for various jet flow rates are given in Table 4.1. The predictions are shown in Fig. 4.7 along those calculated using Martin's correlation [70] and experimental values. It can be observed that predictions by k- $\epsilon$ , k- $\epsilon$  RNG and RSTM model are very close. Compared to Martin's correlation also, these predictions are close with a maximum deviation of less than 30 %. Experimental data also deviates largely from the model predictions and the correlation.

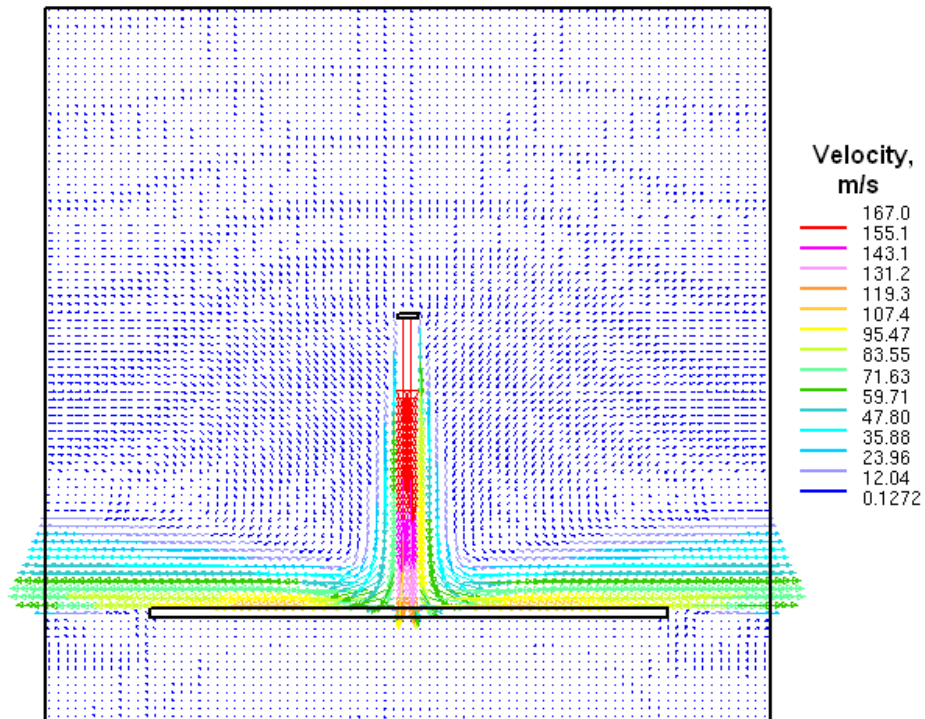


**Fig. 4.3 Predicted velocity distribution for 15 m<sup>3</sup>/h flow rate using k-ε RNG model**

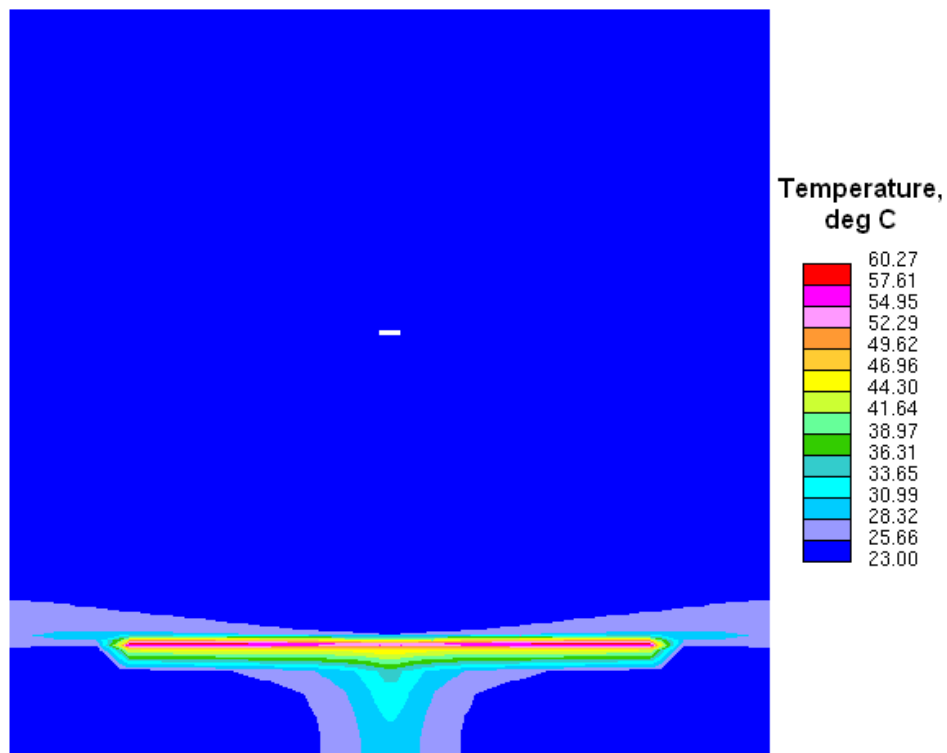


**Fig. 4.4 Predicted temperature distribution for 15 m<sup>3</sup>/h flow rate using k-ε RNG model**

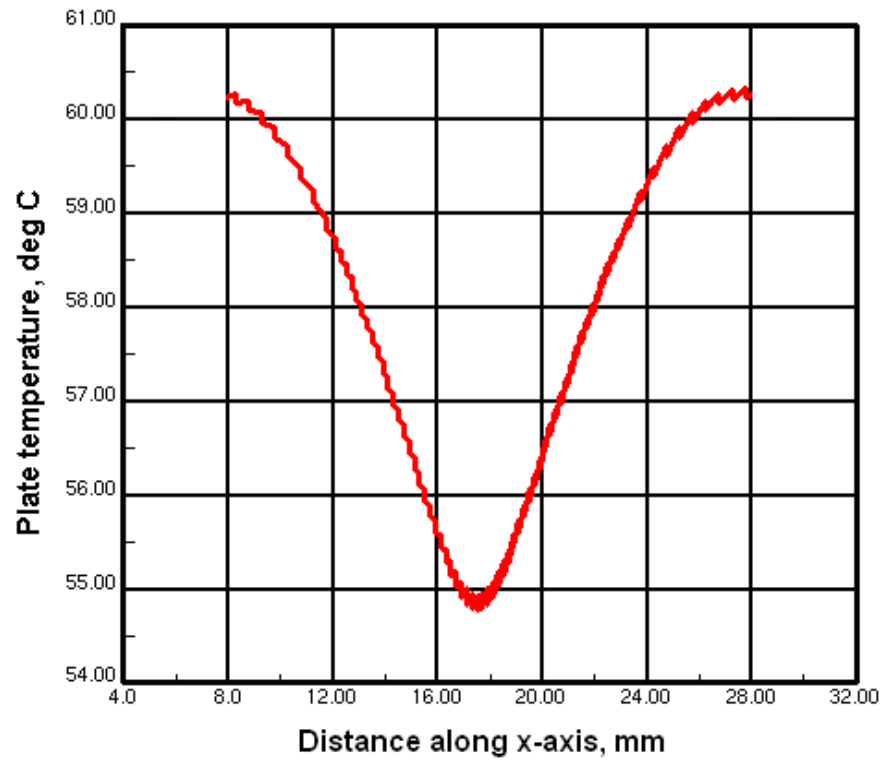


**Fig. 4.5 Temperature distribution along the length of plate**  
(jet flow rate =  $15 \text{ m}^3/\text{h}$  and prediction by k- $\epsilon$  RNG model)

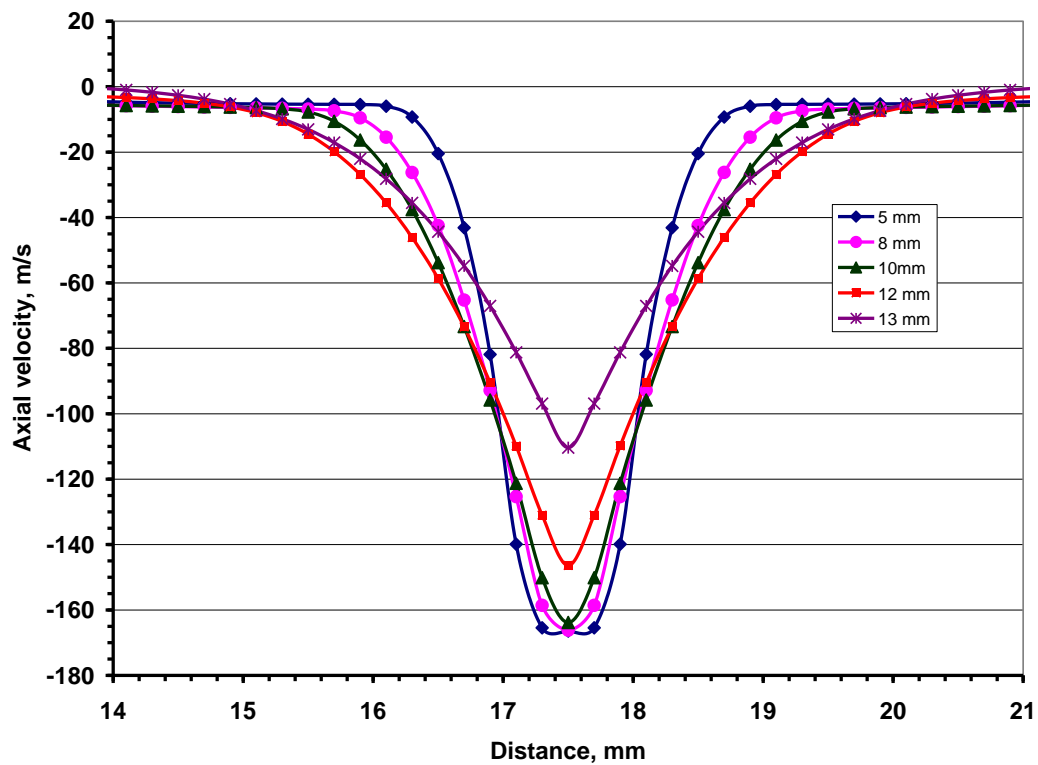


**Fig. 4.6 Axial velocity distribution at different locations from the jet**

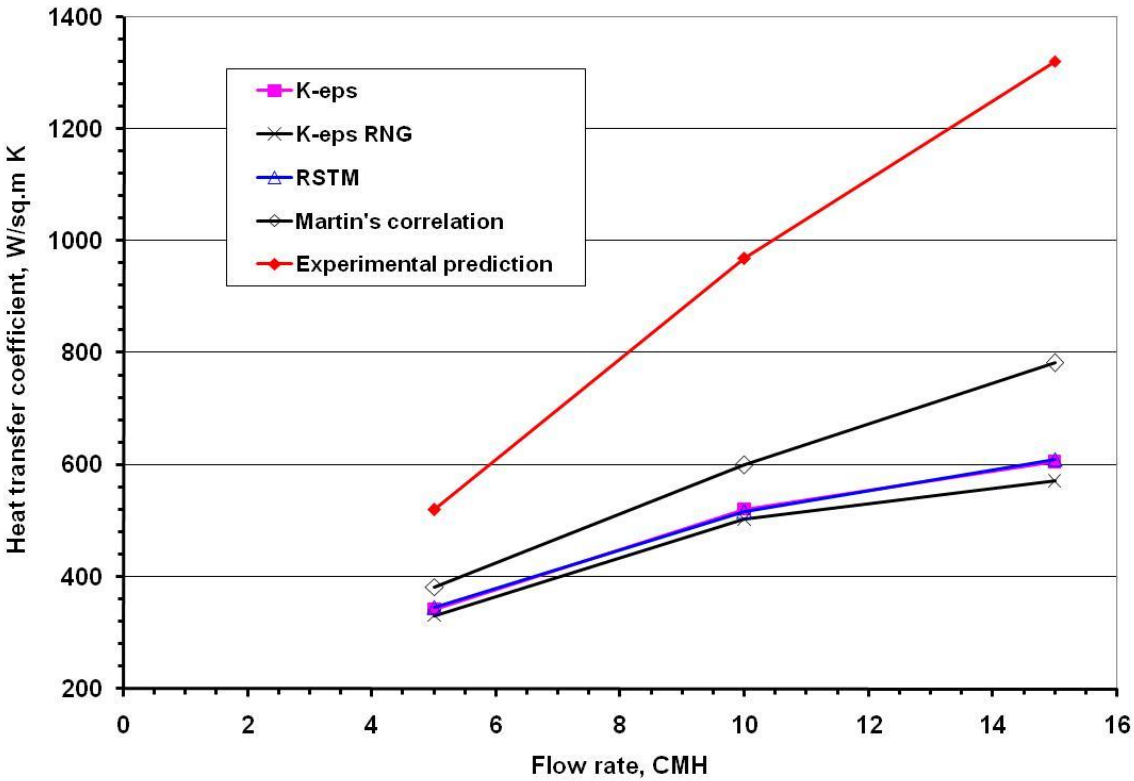


Fig. 4.7 Average heat transfer coefficient predicted by various turbulence models

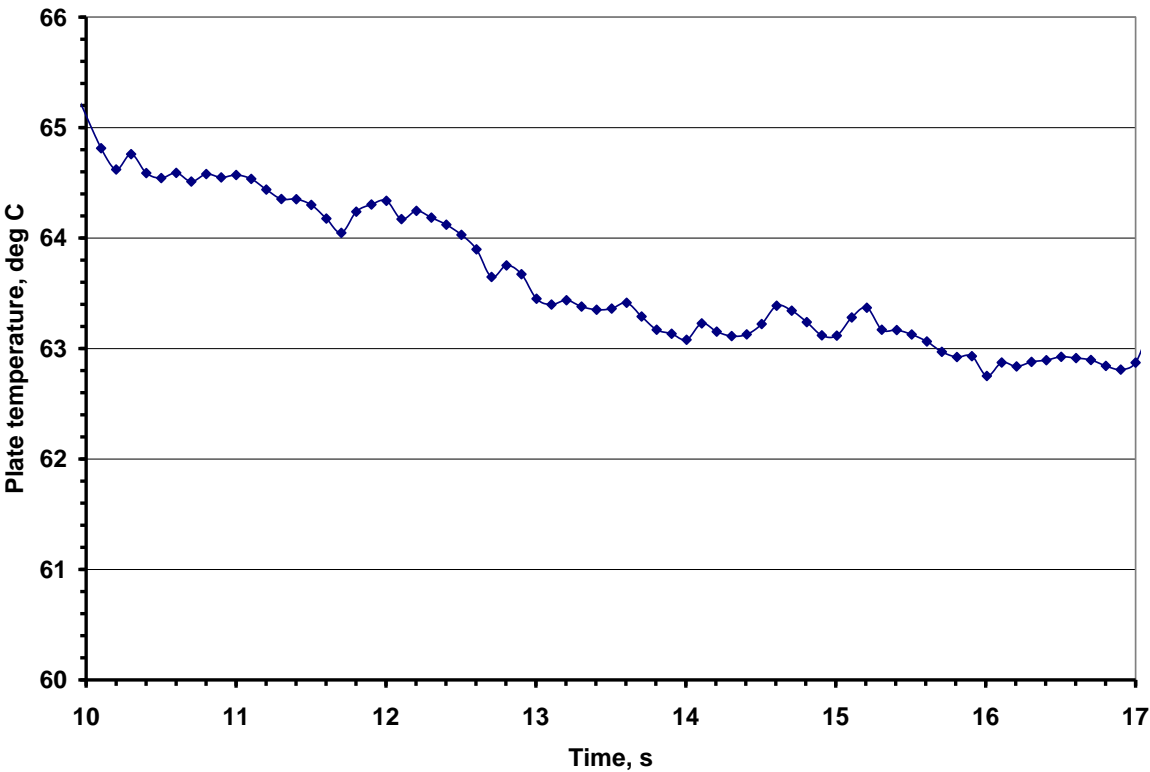


Fig. 4.8 Evolution of average temperature of plate predicted by LES model



**Table 4.1: Estimated values of heat transfer coefficient based on average plate temperature by various turbulence models**

Jet flow rate (m <sup>3</sup> /h)	k-ε model		k-ε RNG model		RSTM model	
	Plate temp. °C	HTC, W/m <sup>2</sup> K	Plate temp. °C	HTC, W/m <sup>2</sup> K	Plate temp. °C	HTC, W/m <sup>2</sup> K
15	58.5	605	60.1	579	58.2	610
10	64.2	521	65.7	503	64.5	517
5	85.7	342	87.9	331	85	346

In view of the difference in the predictions by various turbulence models, analysis has been repeated by adopting LES model. LES model [78] is known for its accurate simulation of turbulence. Evolution of average temperature of plate predicted by LES model is shown in Fig. 4.8. Flow rate of air considered in this study is 15 m<sup>3</sup>/h. It can be observed that plate temperature stabilizes close to 63 °C with minor oscillations. Temperature oscillations caused due to the oscillating nature of jet flow. The corresponding average heat transfer coefficient is 537 W/m<sup>2</sup>K. This value is close to that predicted by k-ε RNG model. Hence this model is used for further studies.

### 4.3 Parametric study on distance between jet and target

Studies have been carried out by varying the distance between the jet and target plate (H). Three different values, viz., 14 mm, 19 mm and 24 mm have been considered. Width of the jet considered in these studies is 1 mm and the analysis is carried out using k-ε RNG model. Jet flow rate considered is 15 m<sup>3</sup>/h. Predicted distributions of velocity and temperature in the domain are shown in Fig. 4.9 to Fig. 4.11. It can be observed that the

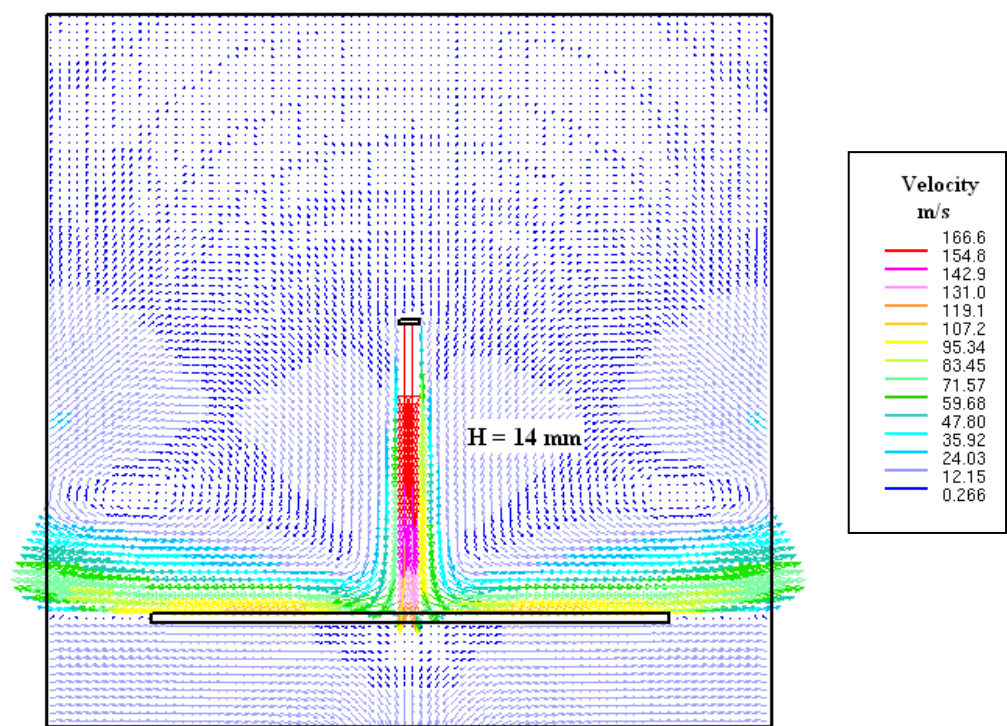


Fig. 4.9a: Velocity distribution for nozzle to target distance = 14 mm

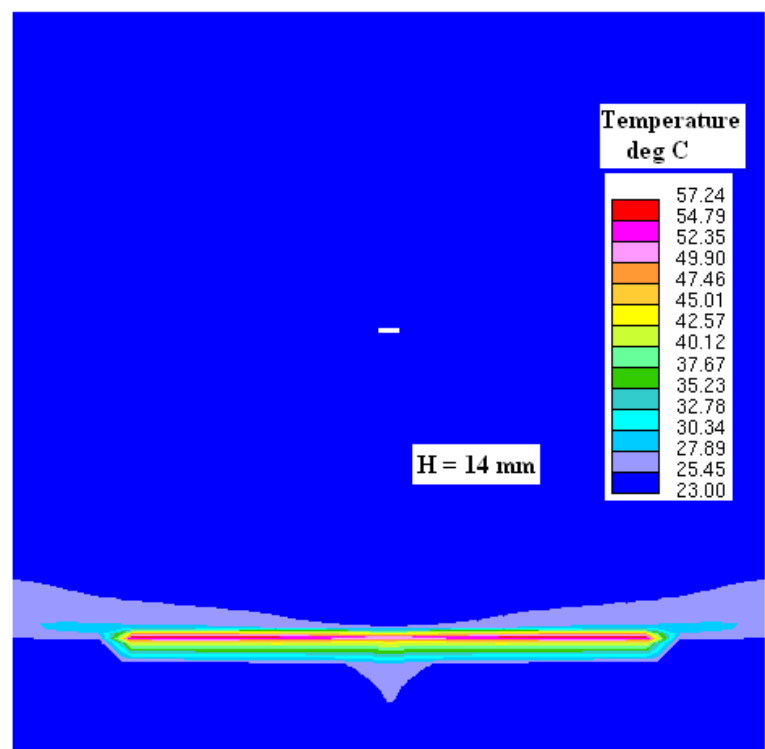


Fig. 4.9b Temperature distribution for nozzle to target distance = 14 mm

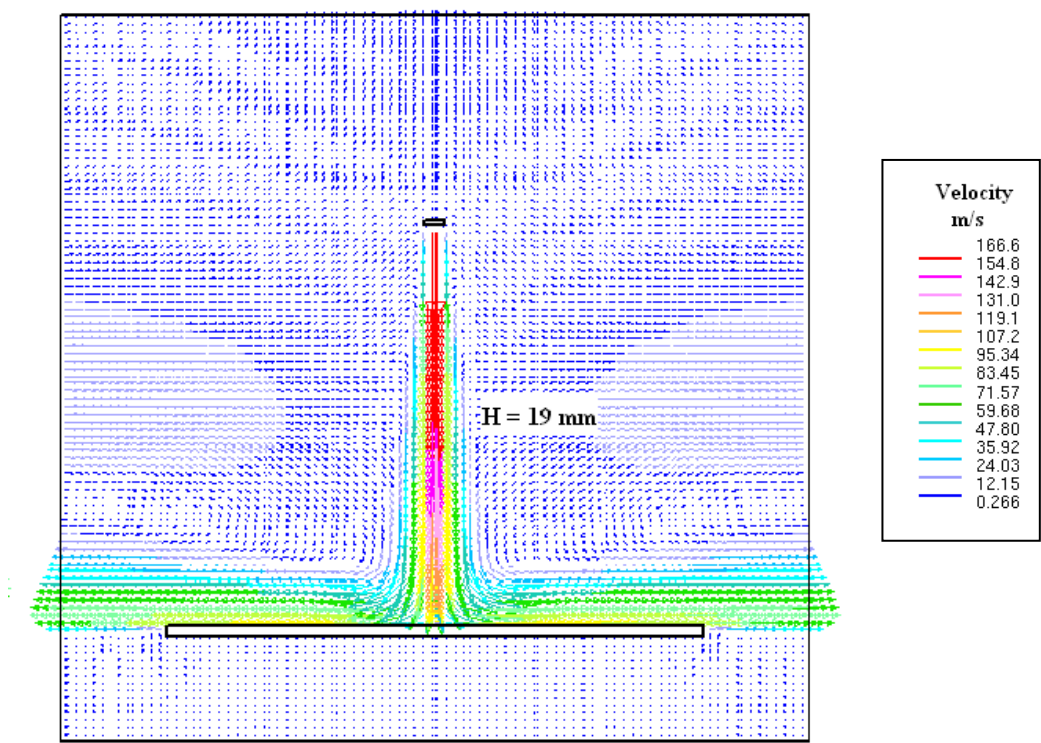


Fig. 4.10a: Velocity distribution for nozzle to target distance = 19 mm

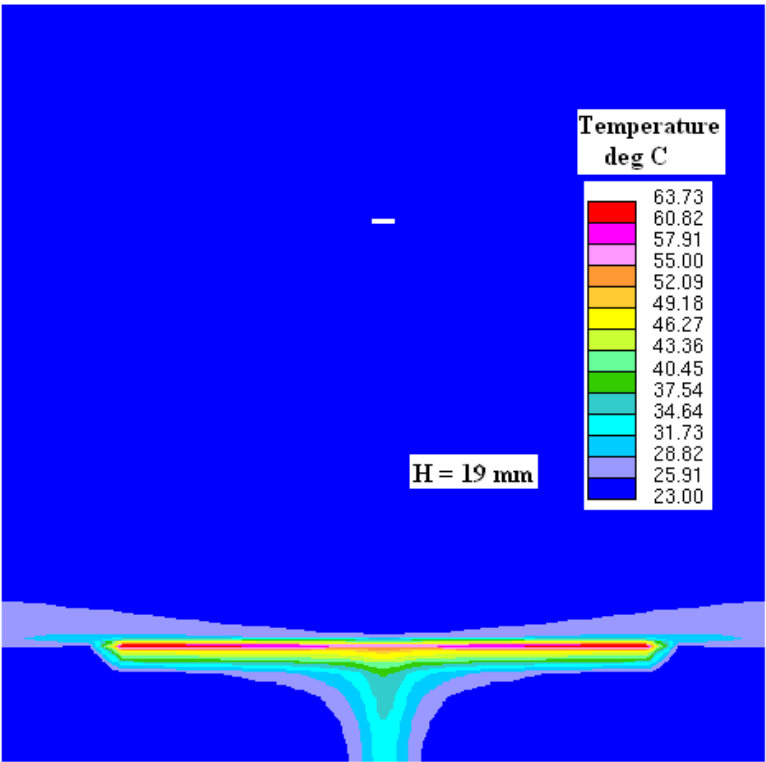


Fig. 4.10b Temperature distribution for nozzle to target distance = 19 mm

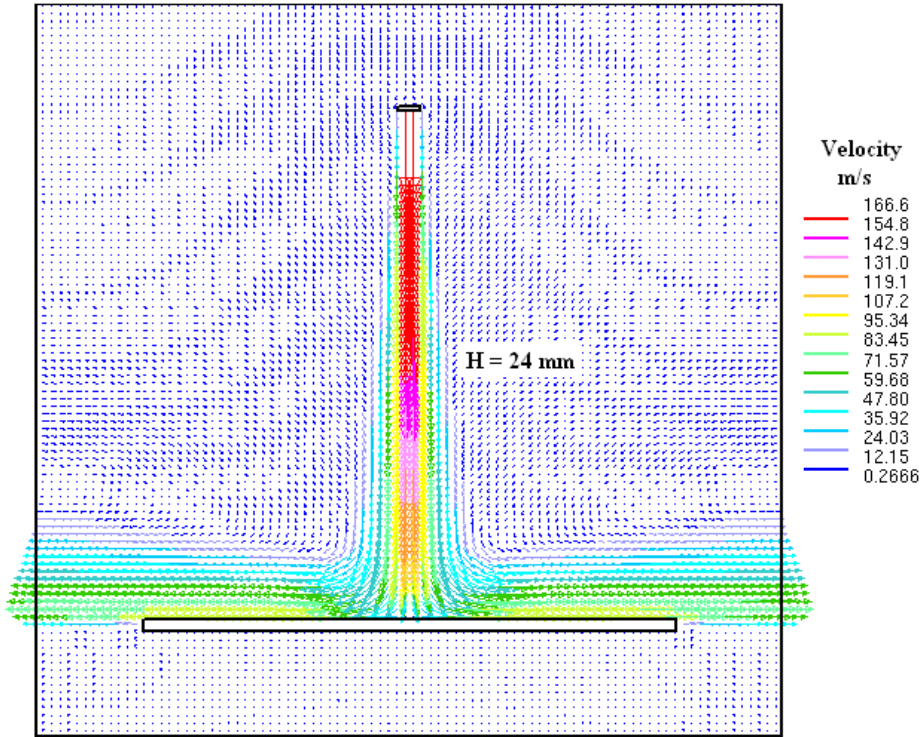


Fig. 4.11a: Velocity distribution for nozzle to target distance = 24 mm

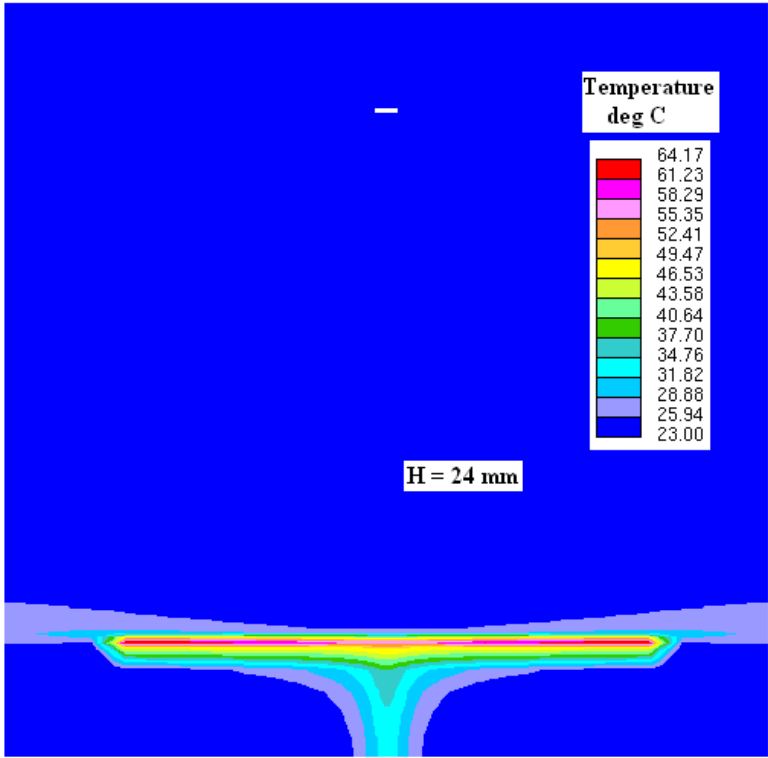
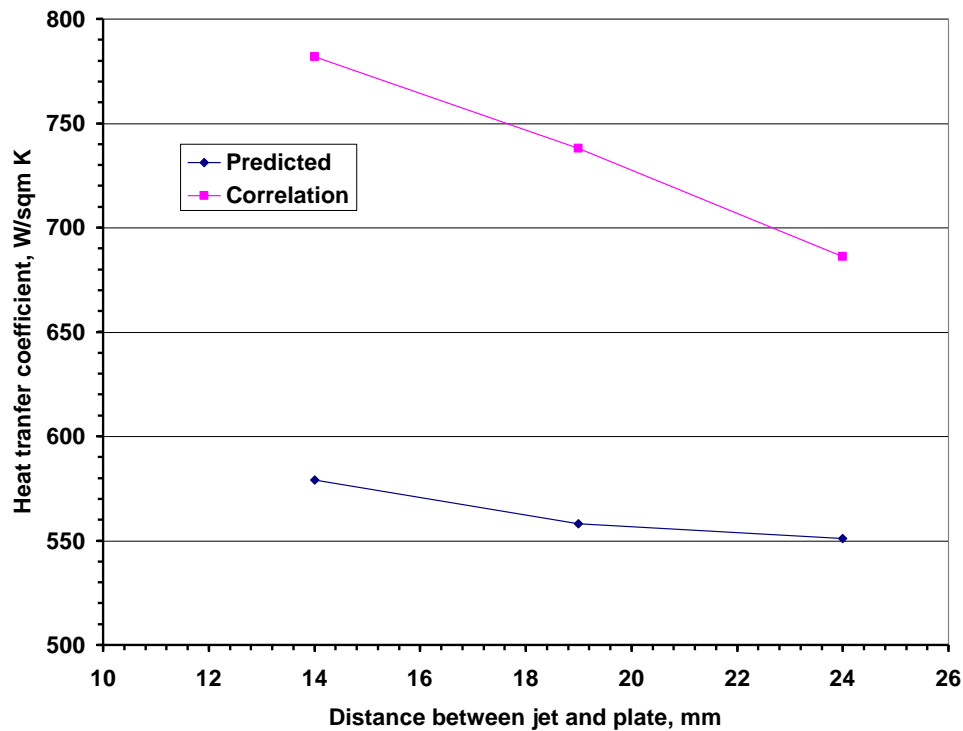


Fig. 4.11b Temperature distribution for nozzle to target distance = 24 mm



**Fig. 4.12 Predicted heat transfer coefficient against distance between jet and target**

**Table 4.2: Heat transfer prediction as a function of distance between jet and target**

Distance between plate and jet	k-ε RNG model		HTC by Martin's correlation(W/m <sup>2</sup> K)
	Plate temp. °C	HTC, W/m <sup>2</sup> K	
14	60.1	579	782
19	61.5	558	738
24	62	551	686

velocity pattern is similar in all the three cases. Average temperatures of plate and heat transfer coefficients are given in Table 4.2. The same data is shown in graphical form in Fig. 4.12 along with those values predicted by Martin's correlation. There is deviation of the order of ~ 30 % between the CFD prediction and the correlation.

#### 4.4 Impingement of two inclined jets

Another case has been analyzed by considering impingement of two inclined jets on the target. The vertical distance of the jets from the target is considered as 14 mm and jet flow rate as  $15 \text{ m}^3/\text{h}$  in these studies. Width of the jet considered is 1 mm. One jet is placed at 1/4th distance of the specimen length from the edge of the plate. Similarly second jet is placed at 1/4th distance of the specimen length from the other edge of the plate. Spacing between the jets is half of the length of the specimen. Three different inclination conditions have been considered for the jet, viz., (i)  $45^\circ$ ,  $52^\circ$  and  $60^\circ$  with the horizontal. It has been found during the simulation that steady state convergence could not be obtained in these cases. Hence, transient study was performed. It was observed that due to the unsteadiness offered due to the interaction between the jets, the jet is not stable. The jet interaction causes only one jet to penetrate and reach the target surface and the flow from the other jet is diverted as shown in Fig. 4.13 to Fig.4.15. Temperature profile predicted is also shown in the same figures.

It can be observed that one jet is effective in producing the impingement action on the plate. Moreover, due to the inclination of the flow velocity with respect to the target, the impingement action is also diluted. Hence, the heat transfer is not that effective compared to that in the case of vertical jet impingement. Predicted values of heat transfer coefficient as function of inclination of the jet is shown in Fig. 4.16. It can be observed that as the inclination of the jet approaches towards vertical, the heat transfer coefficient increases. However, even with two impinging jets,  $60^\circ$  inclined to horizontal, the predicted heat transfer coefficient is less than that of single vertical jet.

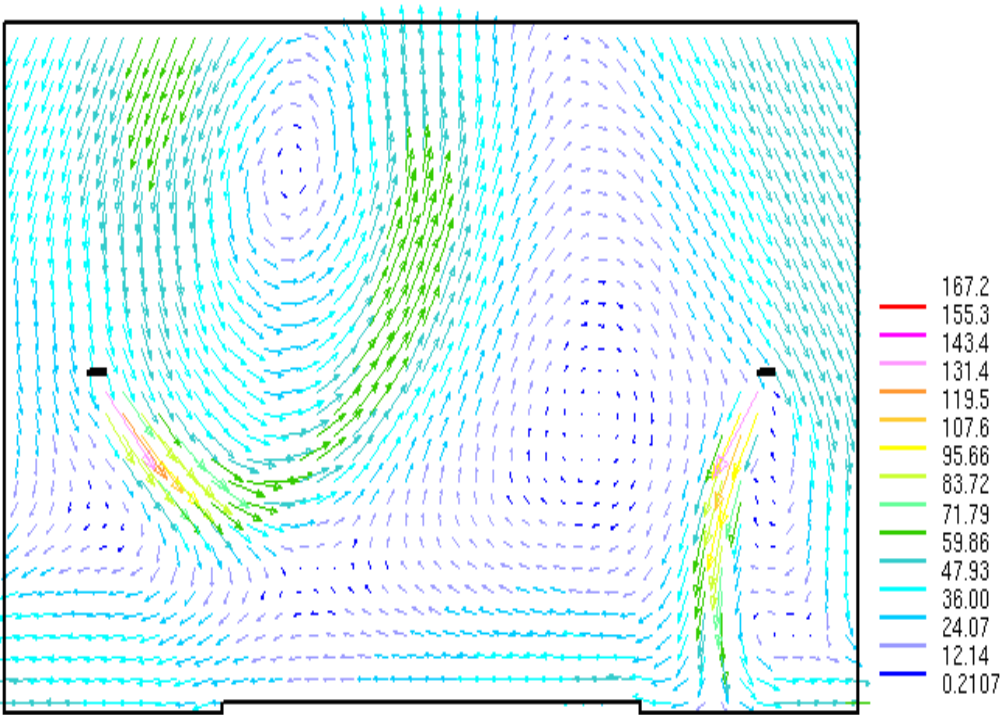


**Fig. 4.13a Predicted velocity distribution with two inclined jets (45°)**

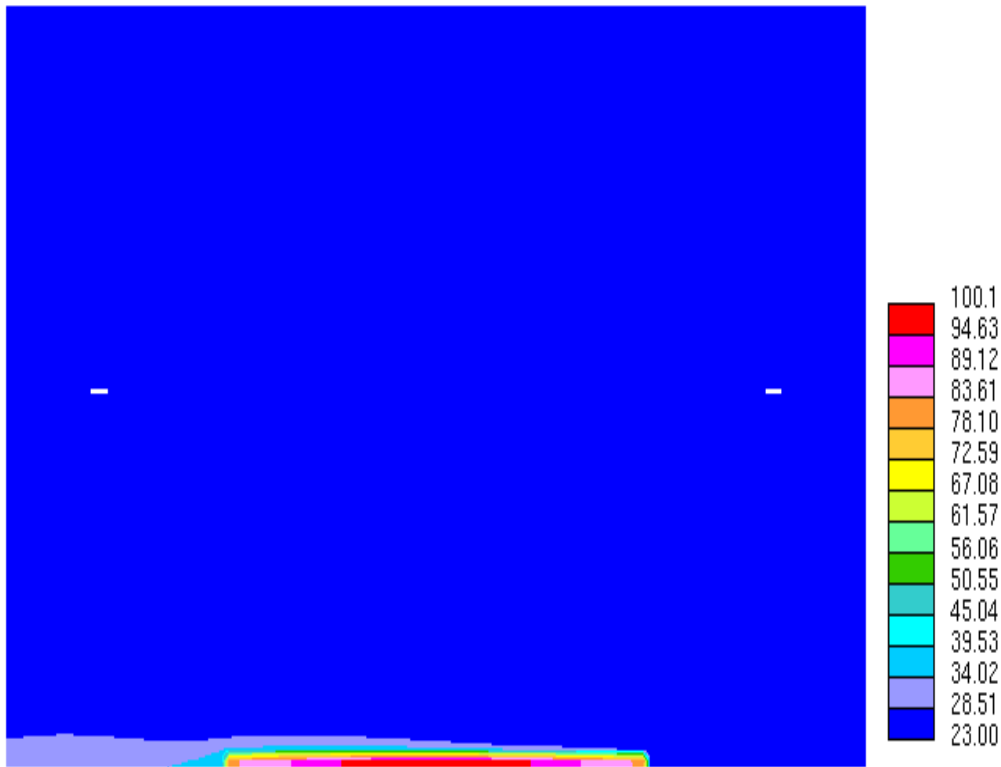


**Fig. 4.13b Predicted temperature distribution with two inclined jets (45°)**

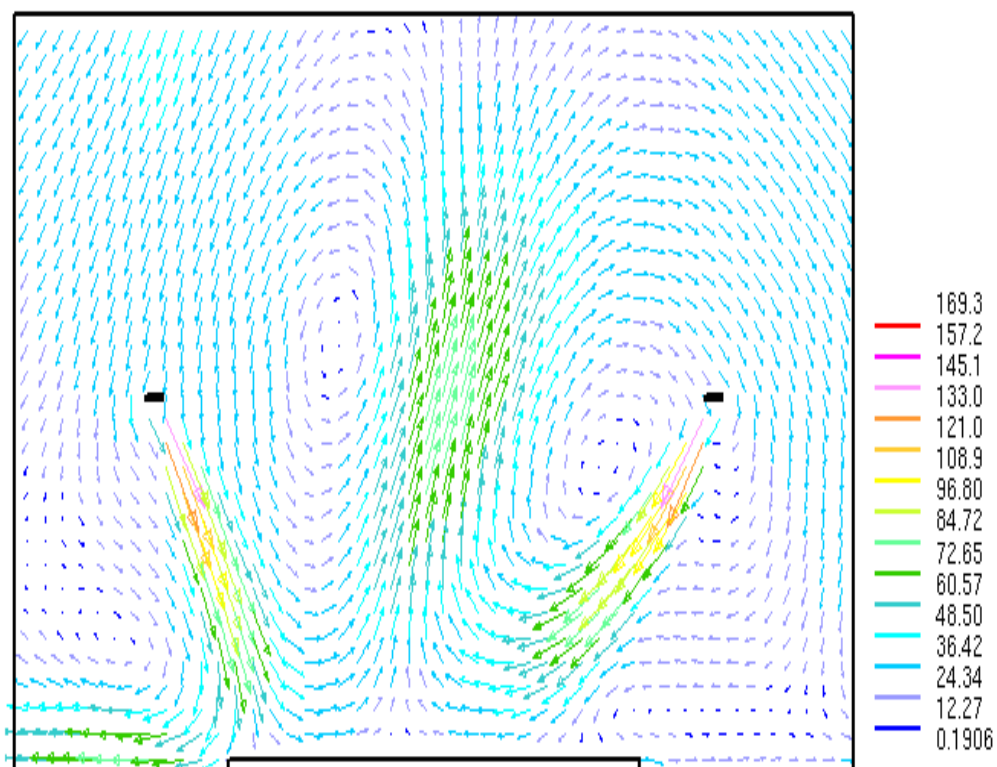


**Fig. 4.14a Predicted velocity distribution with two inclined jets (52°)**

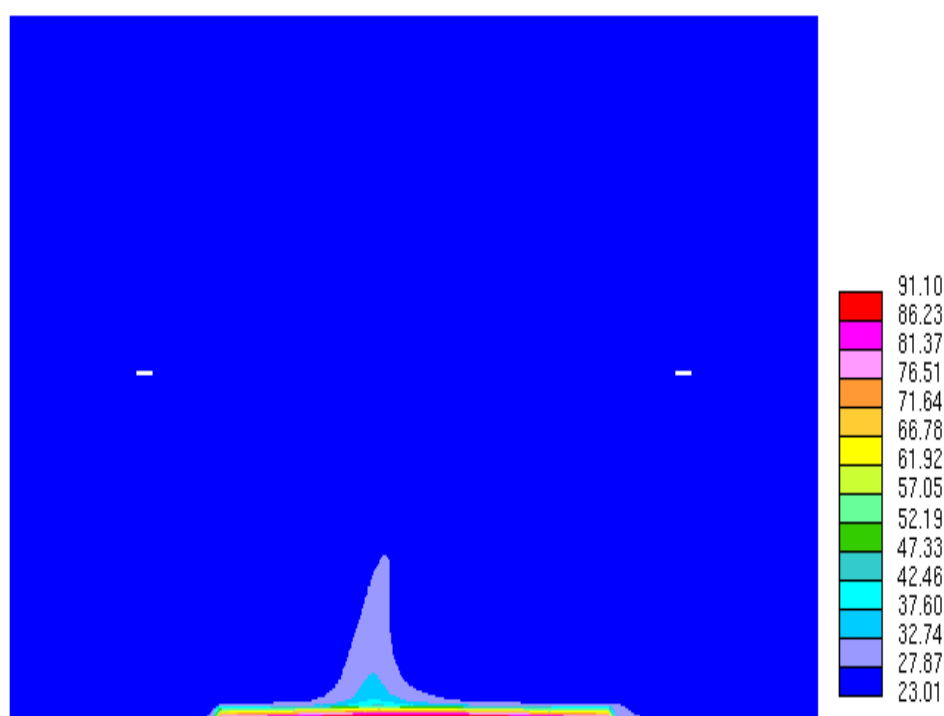


**Fig. 4.14b Predicted temperature distribution with two inclined jets (52°)**



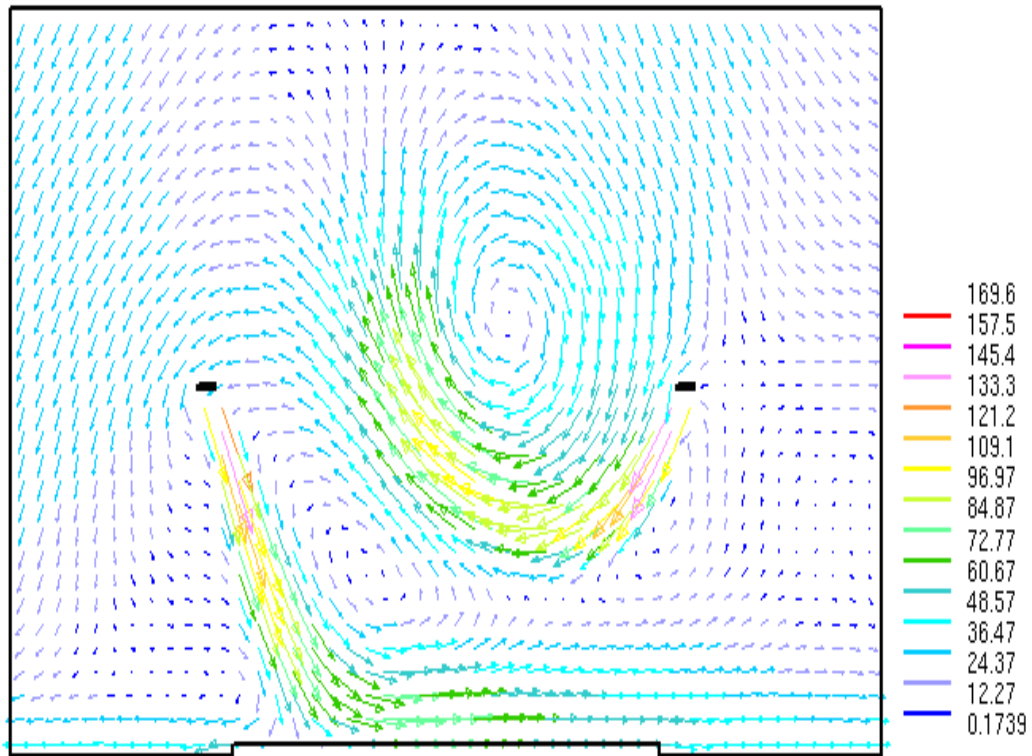


**Fig. 4.15a Predicted velocity distribution with two inclined jets (60°)**

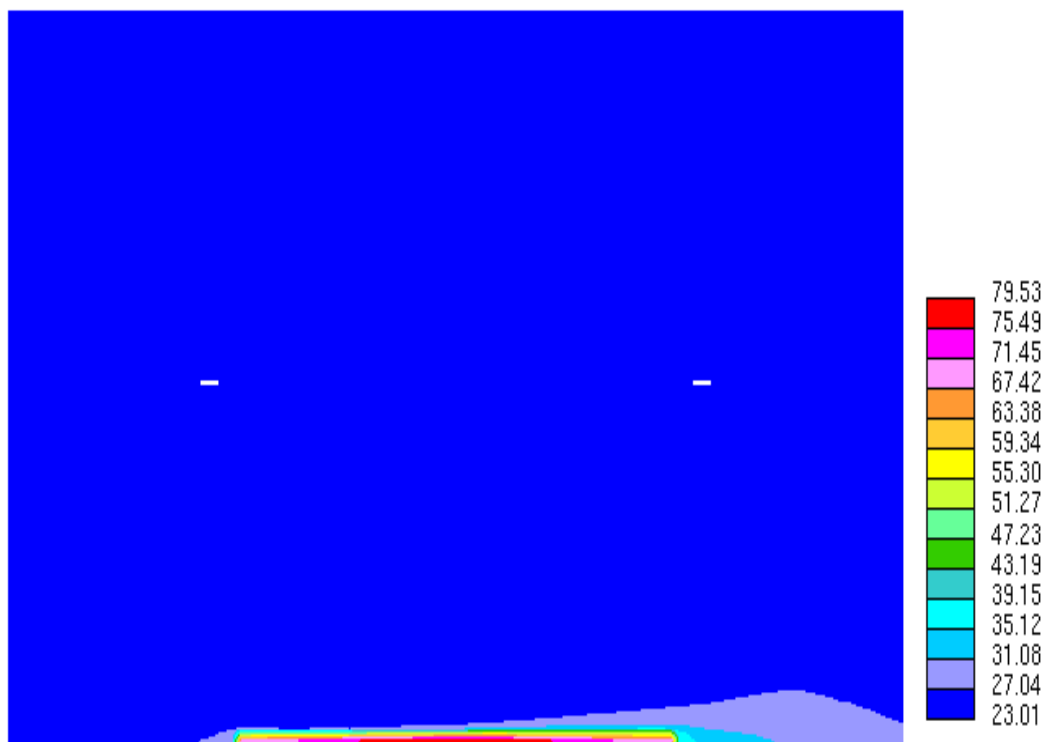


**Fig. 4.15b Predicted temperature distribution with two inclined jets (60°)**

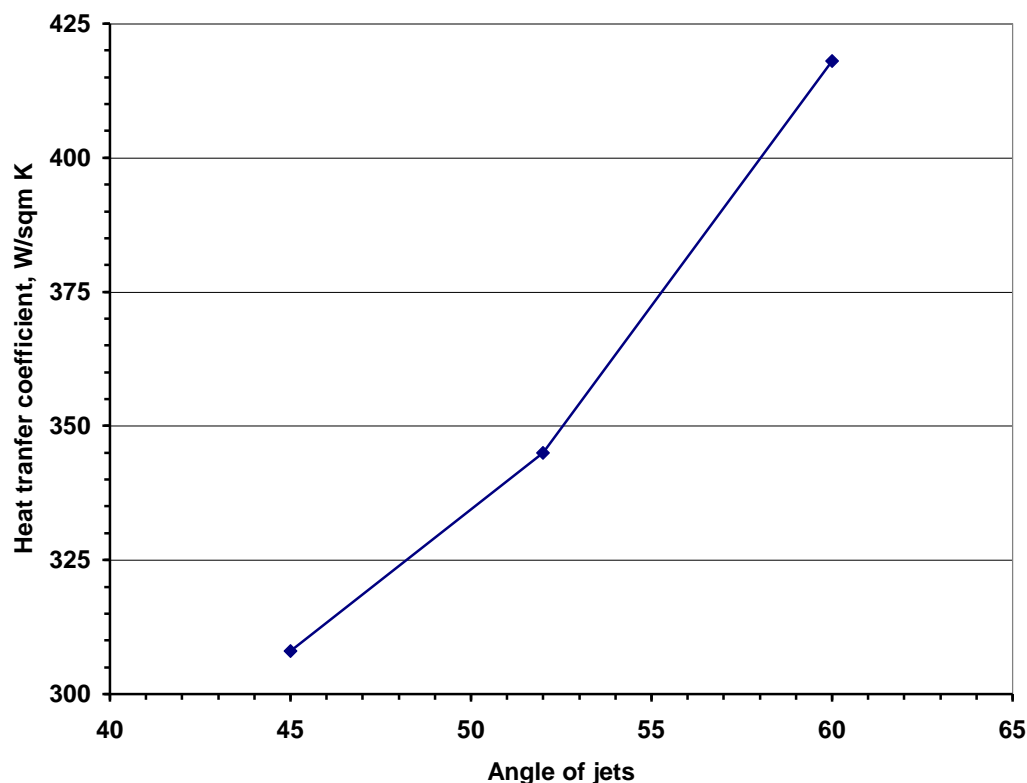


**Fig. 4.16 Heat transfer coefficient variation against angle of inclination of two jets**

#### 4.5 Effect of compressibility

In the above studies, the velocity of air reaches to about 160 m/s. This is almost 50% of sound velocity in air. In this range of velocity the effect of compressibility of air need to be taken into account in the analysis. Hence analysis has been carried out with compressibility effect taken into account. The results show that the maximum pressure drop of air within the domain of study is only 5000 Pa. With compressibility effect the reduction in heat transfer coefficient is only 3.6%. This leads to an increase of about 2.9% in the sample average temperature. Hence studies are continued with incompressible model.

#### 4.6 Closure

A two-dimensional CFD model has been developed for analyzing the jet cooling phenomena. Various turbulence models, viz., k- $\epsilon$ , k- $\epsilon$  RNG and Reynolds Stress Model have

been studied. Based on the predictions,  $k-\varepsilon$  RNG model has been selected for further studies. Air jet experiments have been simulated using the developed 2-D CFD model. The CFD results are also compared with the Martin's empirical correlation. CFD results are  $\sim 30\%$  lower compare to Martin's empirical correlation. Another numerical study using the CFD model has been carried out where two inclined jets are impinging on one side of the target plate. The results show that because of jet interaction only one jet was able to penetrate and reach the target surface and the flow from the other jet is deflected away from the target surface. Due to this effect, the predicted heat transfer coefficient is less than that of a single vertical jet.

So far experimental and numerical studies have been carried out for fundamental understanding of jet cooling phenomena and also for identifying the conditions leading to maximum heat transfer coefficient. In the next chapter the developed 2-D CFD model is used for modeling the spallation target cooling system. Using the CFD model, the heat transfer from the specimen and the temperature difference across the specimen are estimated. Further numerical studies are carried out to reduce the temperature difference across the sample.

\* \* \*

# Chapter- 5

## **Spallation target cooling system**

### **5.0 Introduction**

In this chapter a brief description of the spallation target cooling circuit is given. The need for the cooling system and the envisaged cooling scheme are explained. The heat removal capacity of the helium cooling system under different jet velocities and specimen temperatures are calculated using Martin's correlation and CFD model. Further the CFD model is used for estimating the temperature difference across the sample. Various numerical studies using the CFD model are carried out to find the cooling scheme which gives less temperature difference across the specimen.

### **5.1 Spallation target helium cooling system**

The DAE medical cyclotron will provide proton beam with energy varying between 18 MeV and 30MeV and current up to 200  $\mu$ A. This will be used for radiation damage studies on nuclear structural materials and radiochemistry experiments. Fig. 5.1 shows the schematic of the target chamber which is used for carrying out the irradiation studies. The target chamber is a cylindrical vessel closed at the top and bottom. It has various ports on the side for different purposes as shown in Fig. 5.1. A closed loop helium cooling system (Fig. 5.2) has been envisaged to meet the cooling requirements of irradiation targets with heat generation limited to a maximum of 1 kW. Helium is selected in view of its good heat transfer properties and its inertness against proton environment. Helium jets are injected through slot nozzles of 3 mm width on the surface of the specimen at an angle  $45^{\circ}$ . The impinging pitch of nozzles is 10 mm and for enhanced cooling, jets impinge on both the surfaces of the specimen as shown in Fig. 5.3a and Fig. 5.3b is conceived. In order to show the cooling scheme clearly the specimen is shown in horizontal condition in Fig. 5.3a.

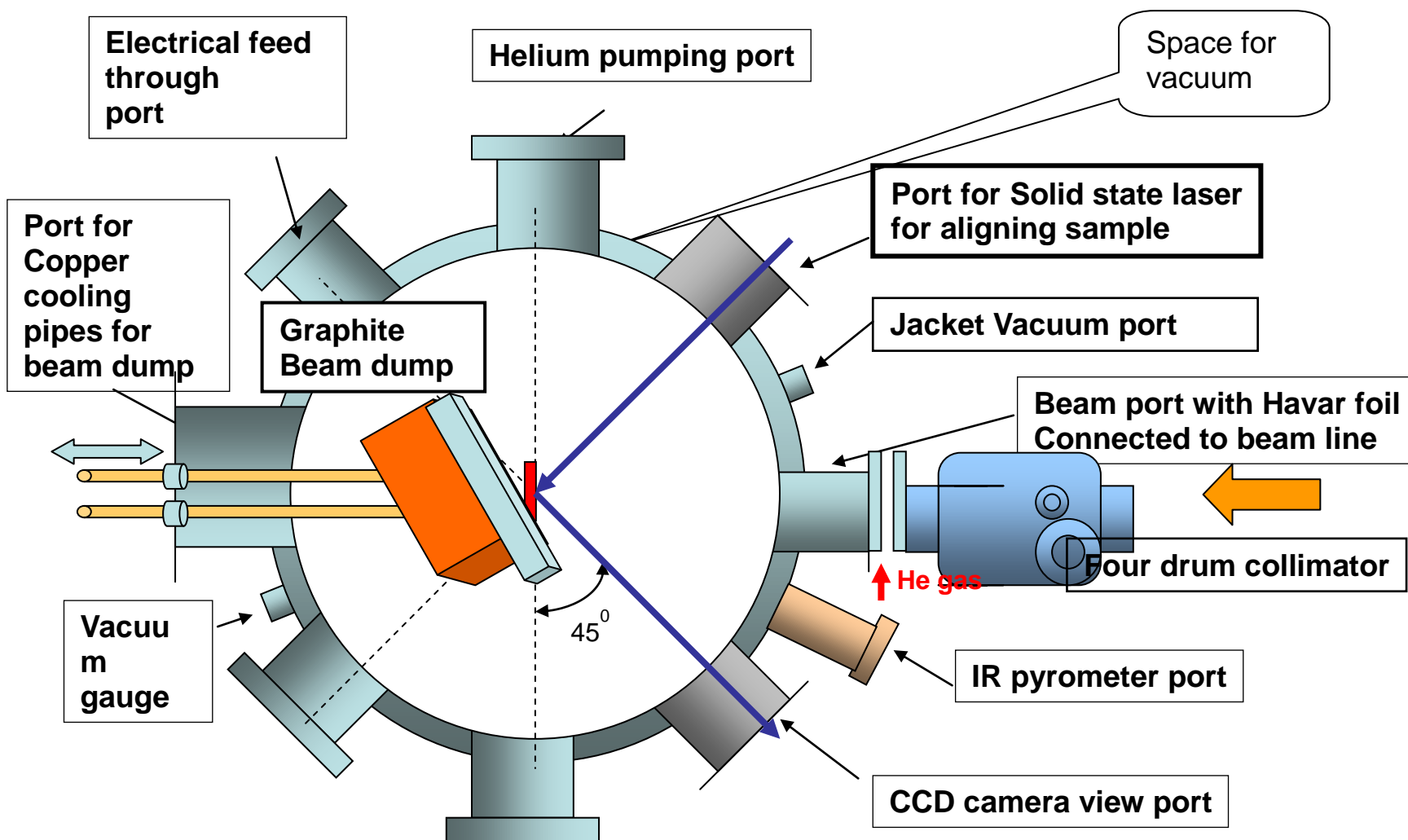
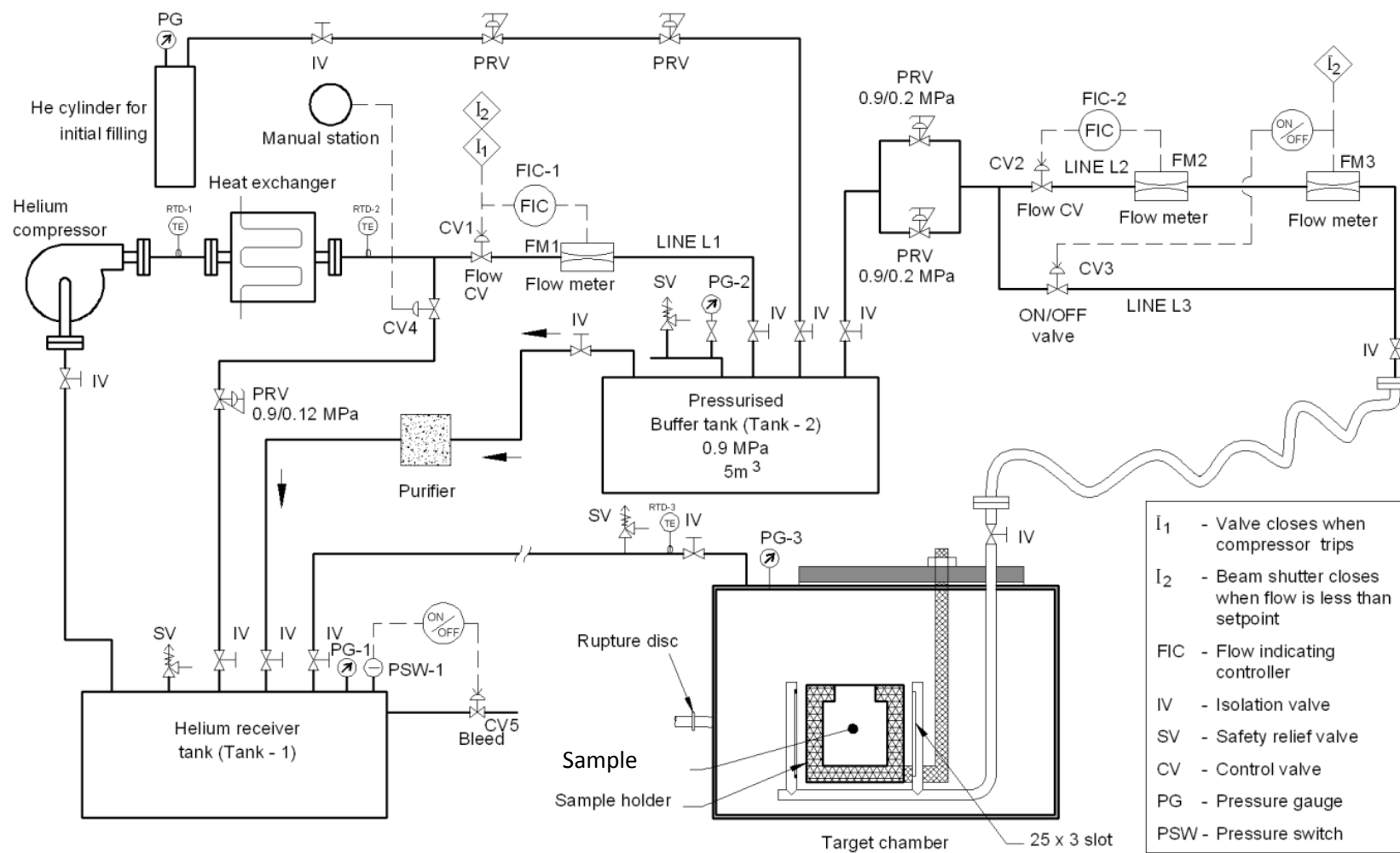
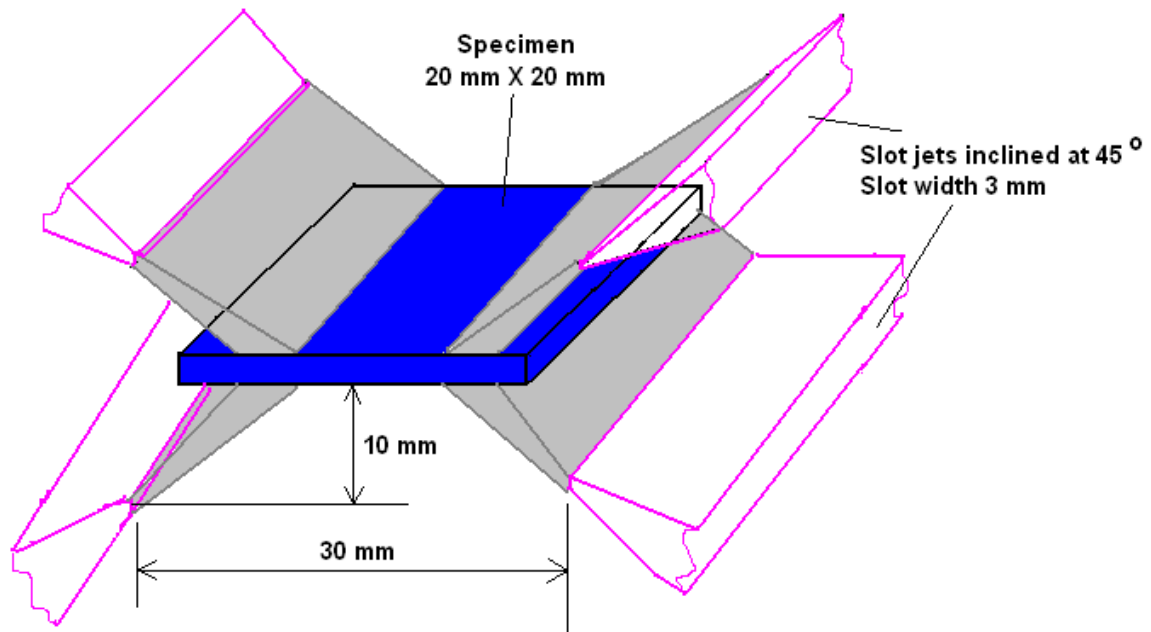


Fig. 5.1 Schematic of the target chamber for irradiation of specimen



**Fig. 5.2 Schematic of helium cooling circuit for spallation target cooling**



**Fig. 5.3a Envisaged cooling arrangement for the specimen**

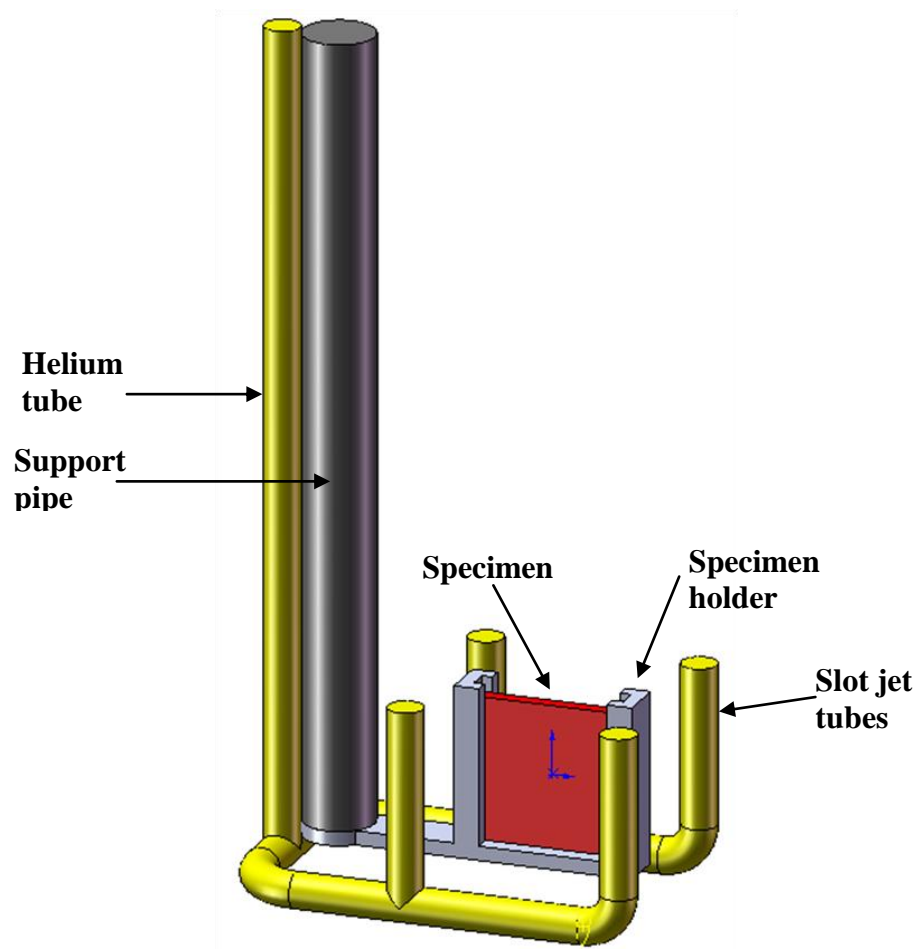


**Fig. 5.3b Envisaged cooling arrangement for the specimen**



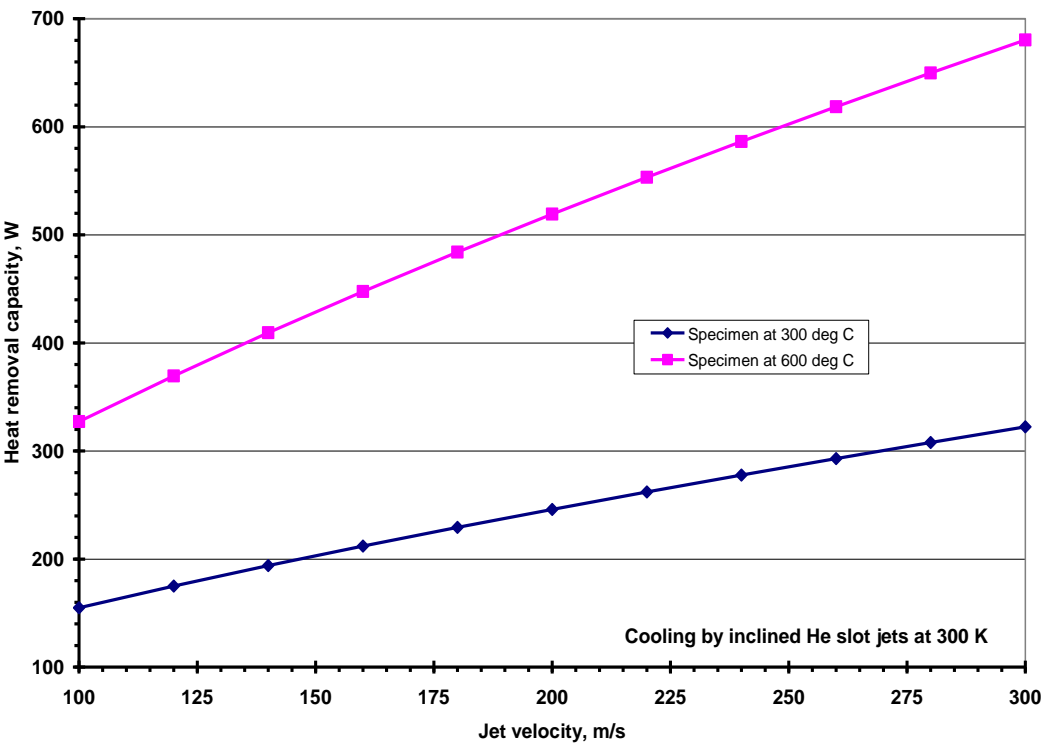


Fig. 5.4 Heat removal capacity of jet cooling arrangement with helium

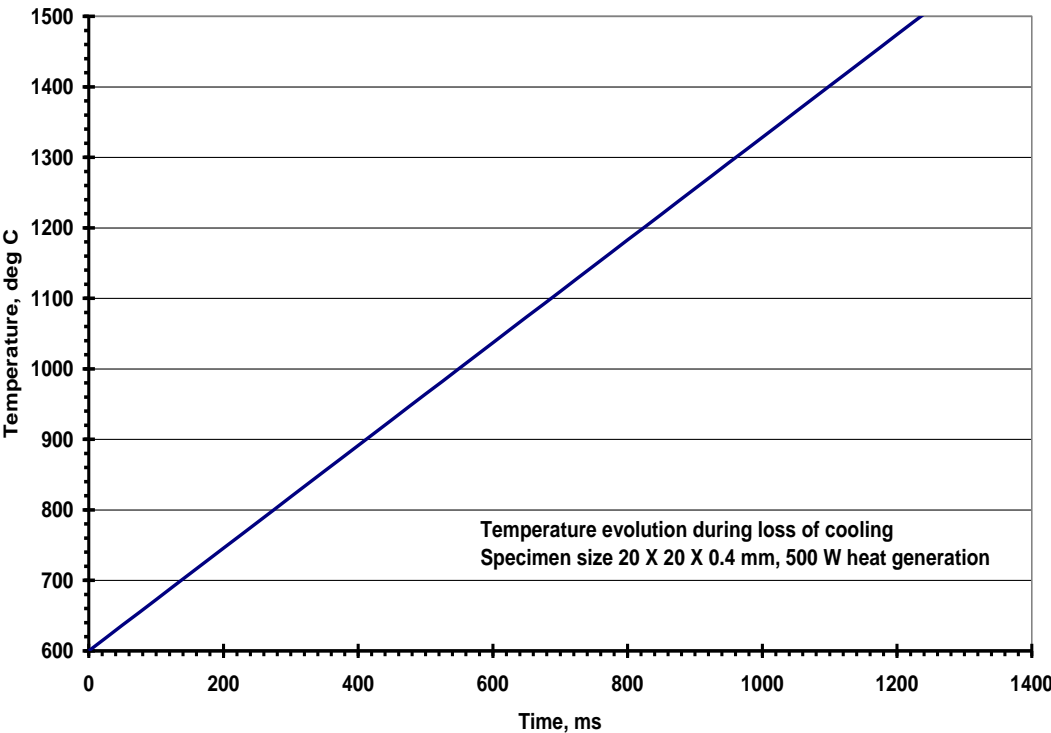


Fig. 5.5 Evolution of specimen temperature in case of loss of cooling

Actually the specimen is in vertical condition as shown in Fig. 5.3b. It is inserted from the top flange into the target chamber (Fig. 5.1) vertically and removed after irradiation from the top remotely. Heat removal capacity of the jet cooling arrangement as a function of specimen temperature with 300 K helium jet are calculated using the Martin's correlation and are shown in Fig. 5.4. About 680 kW heat is removed when the specimen temperature is maintained at 600 °C with jet velocity equal to 300 m/s. The coolant temperature rise estimated while removing 500 W heat generated in the specimen with 200 m/s jet is 13 K.

In order to establish the time available for taking safety action, transient evolution of temperature of specimen in case of loss cooling has been calculated. The size and power generated in the specimen considered are 20 X 20 X 0.4 mm and 500 W respectively. The evolution of specimen temperature after the cooling is lost and heat continues to be generated due to irradiation is shown in Fig. 5.5. It can be seen from the figure that specimen temperature increases to melting point within ~ 1.2 s. In order to avoid this, the heat generation in the specimen should be stopped quickly by cutting the beam current in case of loss of cooling. To avoid loss of cooling during irradiation a buffer tank (tank-2) with 5 minute storage capacity is provided. To reduce the volume of the tank helium is stored at a pressure of 0.9 MPa abs. Fig.5.2 shows the flow diagram of helium cooling circuit for spallation target cooling. Helium pressure is reduced from 0.9 MPa to 0.2 MPa through two parallel pressure reduction valves. Two valves are provided so that even when one valve malfunctions the other valve will supply the helium. Further there are two lines LINE L2 and LINE L3 for supplying helium to the target chamber. Normally the flow is through LINE L2. Control Valve CV2 is adjusted to send the required flow through LINE L2. The flow is also monitored by flow meter FM3. If the flow goes below the predetermined value due to malfunction of flow meter FM2 or control valve CV2 then on/off valve CV3 will be opened

automatically to maintain the helium cooling of the sample for another 5 minutes. Same time signal will be sent to stop the beam current. Two helium compressors are used to pressurize the spent helium again back to buffer tank. Through all these arrangements continuous supply of helium for cooling the sample is ensured for a minimum period of 5 minutes.

## 5.2 CFD simulation for estimation of heat removal capacity

CFD simulation of the inclined slot jet cooling scheme proposed for the target samples of cyclotron have been carried out. The proposed scheme adopts helium jets impinging on target plates from either side. The width of the jet proposed for the cooling is 3 mm. Length of the slot jet (20 mm) is large compared to its width. Hence, the geometrical configuration can be approximated to be 2-dimensional along a plane cut across its width. Geometry and boundary conditions of the model used for the analysis are shown in Fig. 5.6. The objective of the first part of the study is to estimate the heat removal capacity for various values of jet velocity. The second part of the study is to optimize the jet angle for minimizing temperature variation in the target plate. Therefore, the model used for the first study does not consider the solid material of the target plate. Heat source for this calculation is simulated by specifying isothermal boundary condition at the surface of the target plate. Surface temperature of target plate is considered as 300 °C and inlet temperature of helium jet is considered as 30 °C. Turbulence in the flow is modeled based on k- $\epsilon$  RNG model.

Velocity distribution predicted for a jet velocity of 200 m/s and angle of inclination of jet of 45° is shown in Fig. 5.7. It can be observed that the velocity is pattern is symmetric about both the central axes of the plate. Smooth expansion of the jet can be observed and the recirculation rolls generated are also symmetric. The corresponding distribution of temperature of helium is shown in Fig. 5.8. Predicted heat removal capacity of the cooling

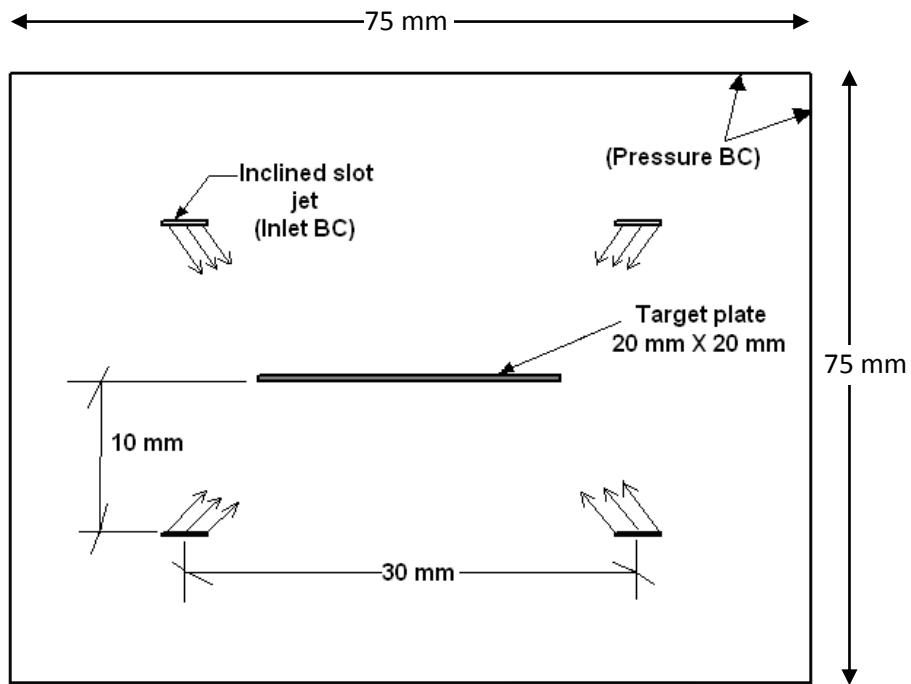


**Fig. 5.6 Schematic of the CFD model for analysis of target cooling**

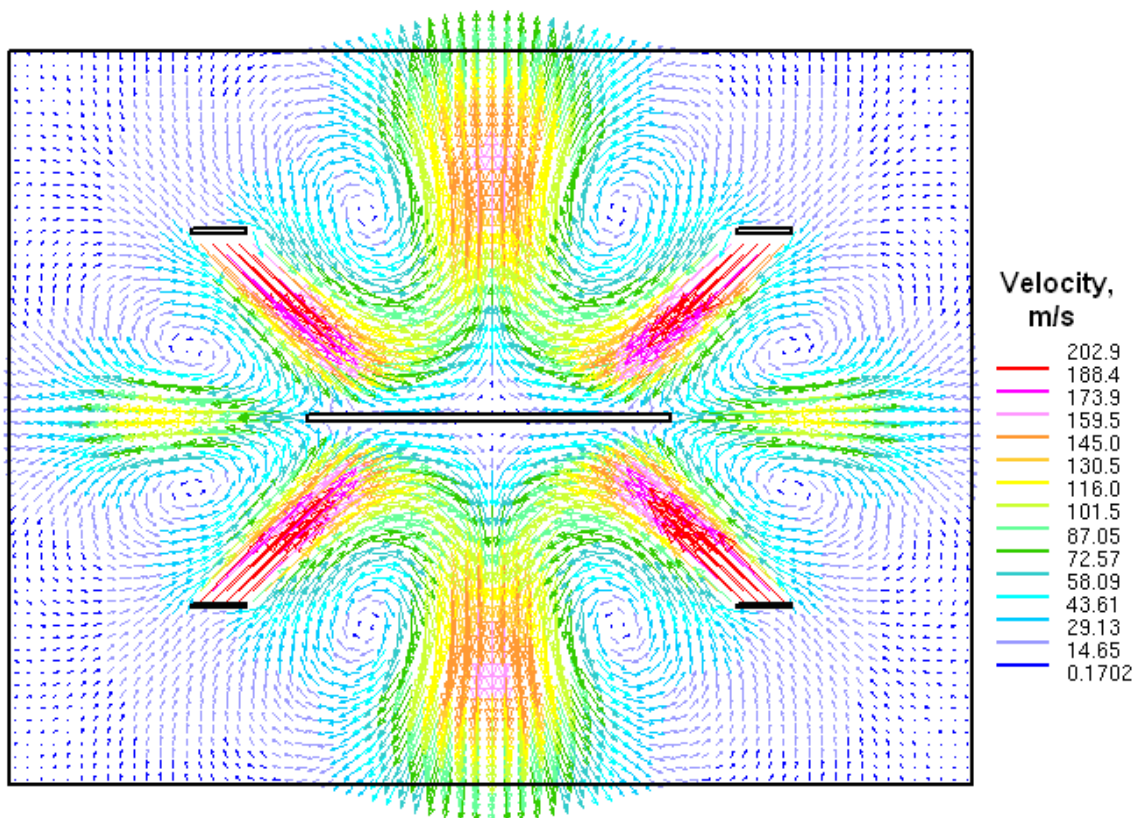


**Fig. 5.7 Velocity pattern with 45° inclined jets and jet velocity of 200 m/s**

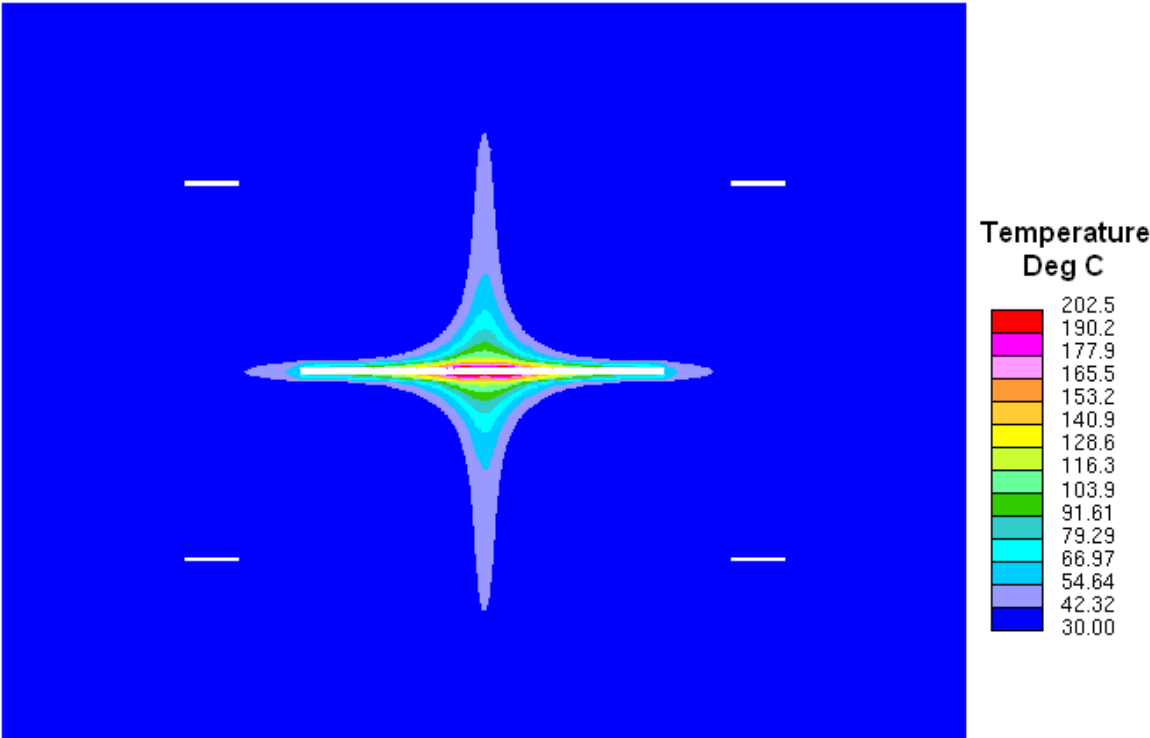


Fig. 5.8 Temperature distribution with 45° inclined jets and jet velocity of 200 m/s

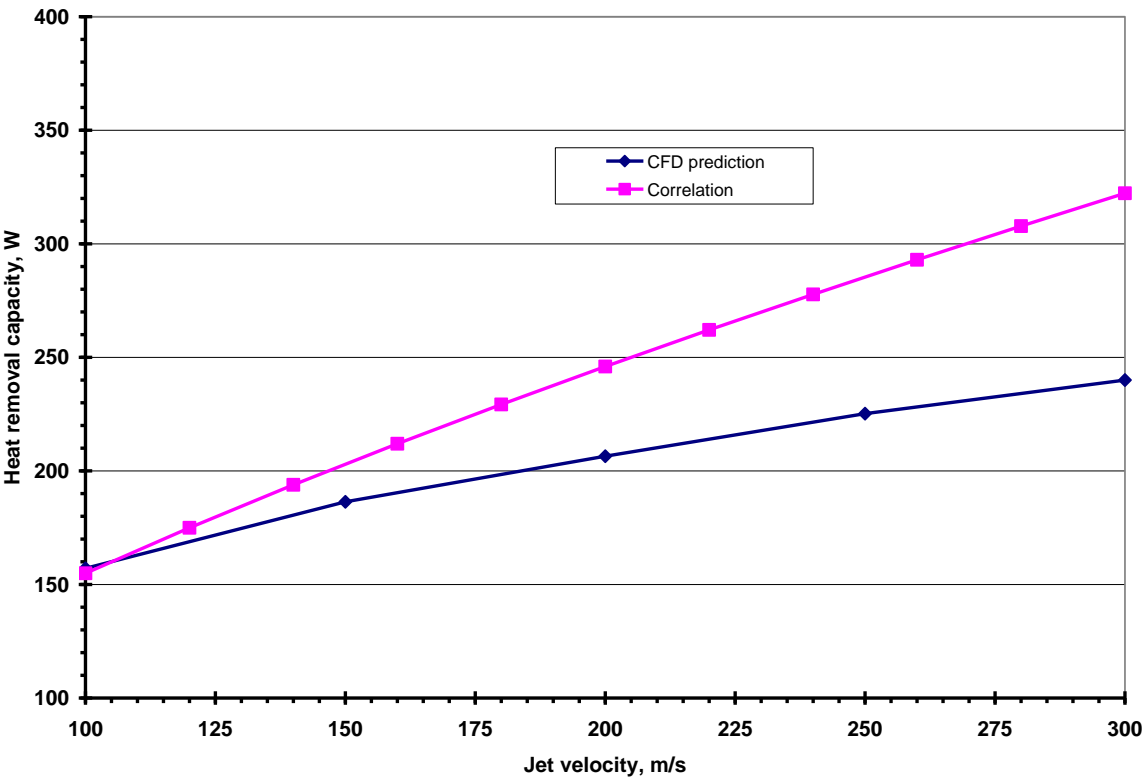


Fig. 5.9 CFD prediction of heat removal capacity of inclined slot jet cooling system

scheme with all jets inclined at an angle of  $45^\circ$  with the plate is shown in Fig. 5.9. Also shown in this figure are the heat removal capacity estimated based on Martin's correlation for array of slot jets. In order to consider the inclination of the jets, the distance between the jet and plate in the correlation is considered as the inclined distance measured along the jet direction. It can be observed that predictions are very close when the jet velocity is 100 m/s. As the jet velocity increases CFD under predicts the heat transfer by about 25 %.

### 5.3 CFD simulation for estimation of temperature difference

Another study has been carried out by using conjugate heat transfer model with target plate modeled as a solid. Heat generated in the target plate is considered as a uniformly distributed heat source and jet velocity considered is 200 m/s. The angle of inclination of jets considered is  $45^\circ$ . Predicted temperature distribution along the length of the plate is shown in Fig. 5.10. It can be observed that there is large variation in temperature of the order of  $200^\circ\text{C}$  in the target plate. Temperature variation of this order is not acceptable for metallographic investigations. One possible reason for this deviation is impingement point of jets on either side of the plate is the same. In order to make each jet to impinge at different points the inclination of two jets are changed to  $30^\circ$  and other two jets retained at  $45^\circ$  inclination. The predicted velocity distribution in the domain is shown in Fig. 5.11. The temperature distribution along the length of the plate is shown in Fig. 5.10. It can be observed that there is reduction in the temperature variation. However, still the variation is large to be acceptable for the experimental studies. The interaction between the jets injected from one side of the target plate could be another reason for the large temperature variation of the target plate. In order to eliminate the interaction between the jets, analysis has been carried on a configuration with only two jets (one jet on either side of the plate). Angle of inclination of the jets is retained as  $45^\circ$  in this case. The predicted velocity distribution is shown in Fig.

5.12. It can be observed that jets do not interact in this case and there smooth flow all over the length of the plate. Temperature distribution along the length of the target plate (Fig. 5.10) showed that the plate temperature is nearly uniform except at the tip of the plate with a maximum variation of 20 °C only. The predicted velocity distribution for four jet configuration is depicted in Figs. 5.7 & 5.11. It can be observed that there is a stagnation zone between the two jets on both the sides of the plate. This leads to increase in the plate temperature in this zone (Fig. 5.8). This in turn increases the mean temperature of the target plate leading to reduction in the average heat transfer coefficient. With two jets one jet on each side of the target at opposite edges, uniform cooling of the target without any local hotspot is achieved. Hence, a large average heat transfer coefficient on the target is achieved. Therefore, the configuration with two jets one on either side can be selected for the target plate cooling in the cyclotron.

Due to the reduction in the number of jets, there is a concern that the heat removal capacity of the cooling jets may get affected seriously. In order to ascertain this, analysis has been carried out by modeling the plate as isothermal boundary at 300 °C. Two inclined jets at 45° are only considered in this case. The predicted heat removal capacity as function of jet velocity is shown in Fig. 5.13. Also shown in the same figure is the heat removal capacity for the case with 4 inclined jets. It can be observed due to the elimination of interaction between jets, there is ~ 10 % improvement in the heat removal capacity.

## 5.4 Closure

Spallation target cooling system along with helium cooling circuit is explained in this chapter. Safety provisions incorporated in the cooling circuit are also explained. Martin's

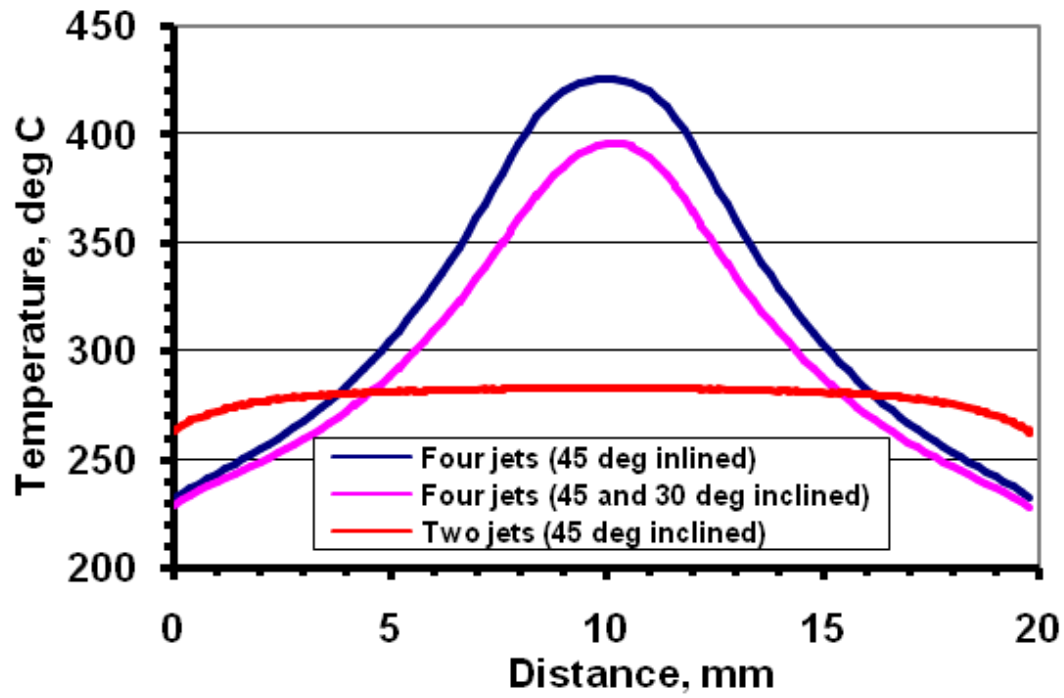


Fig. 5.10 Predicted temperature distribution along the length of plate

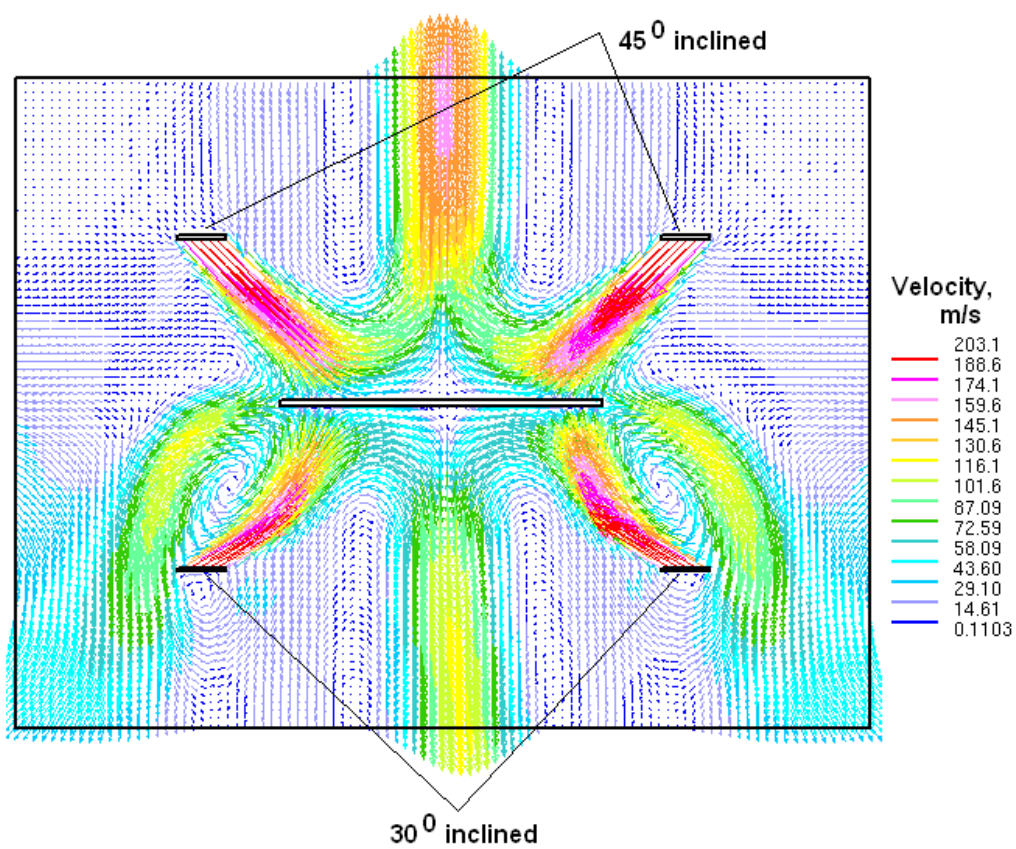


Fig. 5.11 Predicted velocity distribution with two jets inclined at  $30^\circ$  and other two at  $45^\circ$



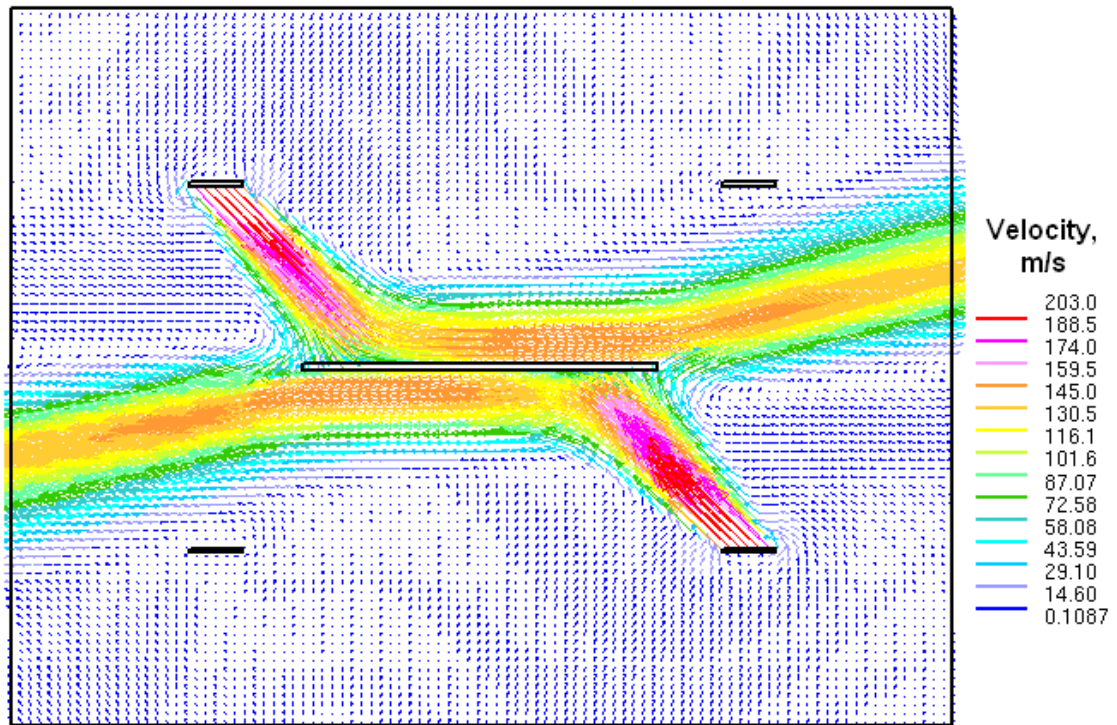


Fig. 5.12 Predicted velocity distribution with two jets inclined at  $45^\circ$

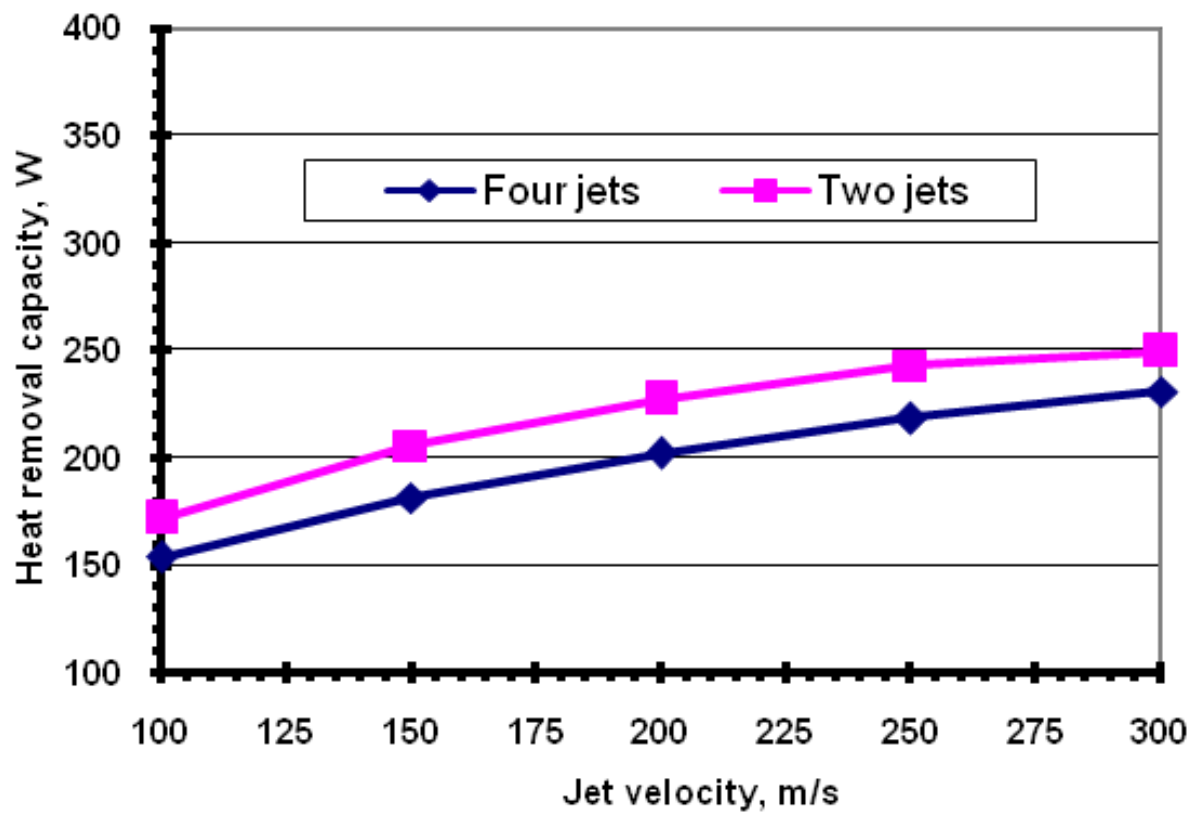


Fig. 5.13 Predicted heat removal capacity for different configurations of jets

empirical correlation is used for estimating the heat removal capacity for specimen temperatures of 300 °C and 600 °C with helium jet velocity varying from 100 to 300 m/s. The maximum heat removal capacity is found to be about 700 kW with an inlet helium temperature of 27 °C. With CFD simulation it is found that the envisaged cooling scheme with two jets on each side of the specimen gives a large temperature difference of 200 °C across the specimen. This is mainly due to the interaction of the spent flow. From the numerical studies, it is found that with two jets one on each side of the specimen, the temperature difference across the sample reduces to 20 °C. Also, due to the elimination of interaction between jets, there is ~ 10 % improvement in the heat removal capacity.

In order to confirm the numerical predictions, multiple air jet experiments are carried out. Details of these experiments are given in the next chapter.

\* \* \*

# Chapter- 6

## **Experimental studies with multiple air jets**

### **6.0 Introduction**

Irradiation specimen cooling by using two jets is found to be good compared to four jets. Numerical studies carried out using the CFD code shows that for the two jets case heat transfer coefficient is more. Moreover the temperature difference across the sample is also less for the two jets case. In the present chapter multiple air jets experiments are carried out to confirm the numerical predictions. In the single air jet experiments, described in chapter 3, the power source used is not sufficient. It has a capacity of only 30 V and 100 A. With 15 m<sup>3</sup>/hr air flow rate when 90 A current is supplied, the specimen is heated to a maximum temperature of 37 °C (Appendix B). In the present multi jet experiments a higher power source of 4 V and 7000 A is used. With this power source the temperature can be increased to the desired values.

In the single air jet experiments, described in chapter 3, four thermocouples are used to measure the temperatures. The thermocouple tips are spot welded to the specimen. These thermocouple tips and thermocouple leads close to the specimen promote additional turbulence which will influence the experimental results. In the present multi air jet experiments, infrared thermal imaging technique is used to measure the specimen surface temperature. This is a non intrusive type of temperature measurement. Moreover, it gives the temperature distribution of the entire surface of the specimen.

### **6.1 Thermal imaging [107 - 109]**

Every physical body emits electromagnetic radiation spontaneously and continuously with energy proportional to its surface temperature. The distribution of wave lengths present

in this radiation spectrum may fall in infrared, visible range, ultraviolet or even X-ray wave length range. Plank's law describes the distribution of radiation intensity from a black body and the same is mathematically expressed as

$$I_{\lambda} = \frac{2\pi hc^2}{\lambda^5 \left( e^{\frac{hc}{\lambda KT}} - 1 \right)} Wm^{-2} Sr^{-1} \mu m^{-1}$$

Where

- $I_{\lambda}$  is the spectral intensity
- $h$  is the Planks constant
- $c$  is velocity of light in space
- $\lambda$  is the wave length of electromagnetic radiation
- $T$  is the absolute temperature
- $K$  is the Boltzmans's constant

Fig. 6.1 shows the spectral radiation intensity of a black body plotted as a function of absolute temperature and corresponding wave lengths. From the figure it can be observed that the wave length corresponding to maximum radiation emittance is unique for a surface and it depends only on surface temperature. This wavelength with which maximum radiation emittance occurs can be derived by differentiating Planks equation with respect to  $\lambda$  and setting the derivative equal to zero. The resulting relation is known as Wien's displacement law and the same is given as

$$\lambda_{\max} = \frac{2898}{T} \mu m$$

Integrating Plank's equation with respect to  $\lambda$  between zero to infinity for constant

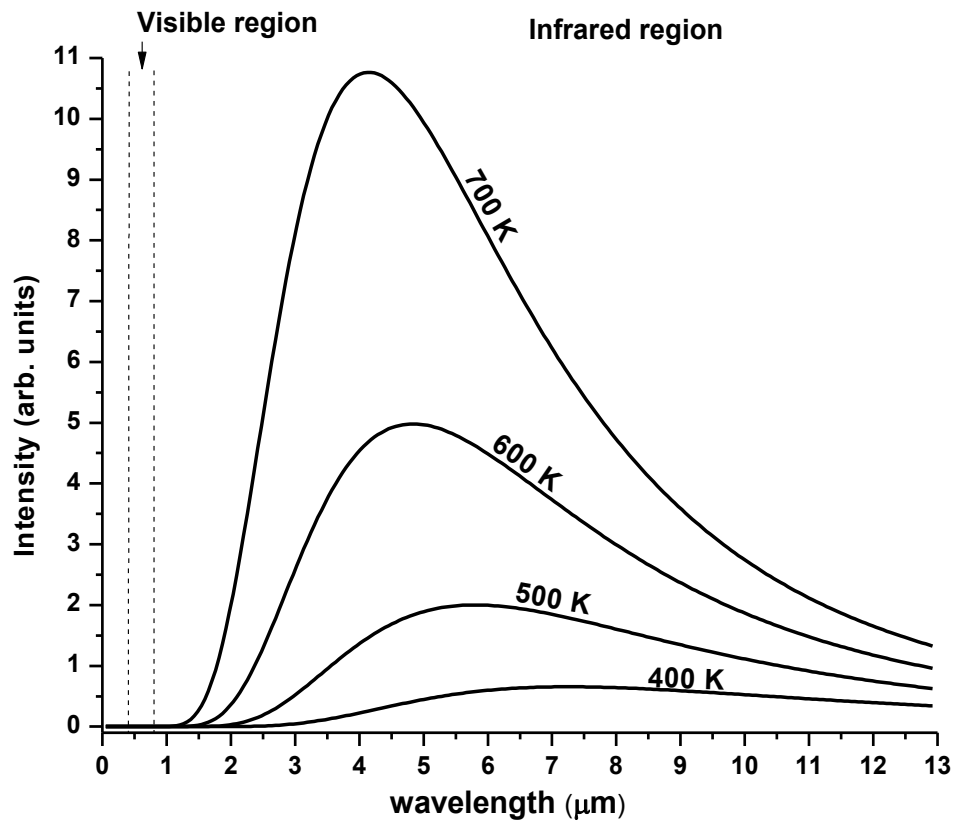


**Fig.6.1 Spectral radiation intensity of a black body for different temperatures**

absolute temperature,  $T$  gives the total radiant flux emitted by a surface. This is known as Stephan-Boltzmann law and it is expressed as

$$\Phi = \int_0^{\infty} I_{\lambda} d\lambda = \epsilon \sigma T^4 \quad W / m^2$$

Where

- $\Phi$  is the total radiant flux
- $\sigma$  is Stephen- Boltzmann constant
- $\epsilon$  is relative emissivity of the surface

Using the above described physical phenomena the temperature of a surface can be accurately estimated with the knowledge of the emissivity of the irradiative surface. This

technique of measuring surface temperature is known as infrared thermal imaging (IRTI) technique. Most of the measuring surfaces of normal engineering, medical and environmental application emit radiation in the infrared region and hence the term 'infrared' in the name of the technique. Using this technique the temperature distribution of a surface can be accurately established with high level of accuracy. In recent days, infrared thermal imaging is successfully utilizing in the field of engineering research, environmental surface temperature mapping over very large area using satellites, as a non-destructive testing method, condition monitoring of machineries, medical diagnosis etc.

Infrared thermal imaging is a fast, cost effective way to perform detailed thermal analysis. A typical IRTI system essentially consists of an infrared camera, control unit, image acquisition and analysis unit. The important part of the system is image acquisition and analysis unit which also known as IR scanner. The IR scanner unit converts the electromagnetic infrared radiation emitted by a surface into electronic image signals in digital format. These signals amplified and transmitted to output devices as spatial distribution of temperature in two dimensional surfaces. A true thermal image is a gray scale image with hot items shown in white and cold items in black. This in turn is converted to color maps corresponding to the temperature range using appropriate processors. This creates industry-standard image formats, such as the Tagged Image File Format (TIFF), permit files to work with a wide array of commercially available software packages. In quantitative IRTI systems thermal images are temperature calibrated using an internal black body reference. Present day IRTI systems have a temperature resolution of less than 0.1K and a spatial resolution as fine as 15 $\mu$ m. Dynamic speed of these cameras is more than 320 frames per second. The main advantages of IRTI system are:

- Non-contact and non-intrusive method

- Capability to scan from distance
- Ability to provide full field image
- Real time capability
- Less systematic measurement errors compared to direct methods

The main disadvantage of IRTI is that it is a surface measurement technique. Internal temperature distribution of a body cannot be quantified with this technique.

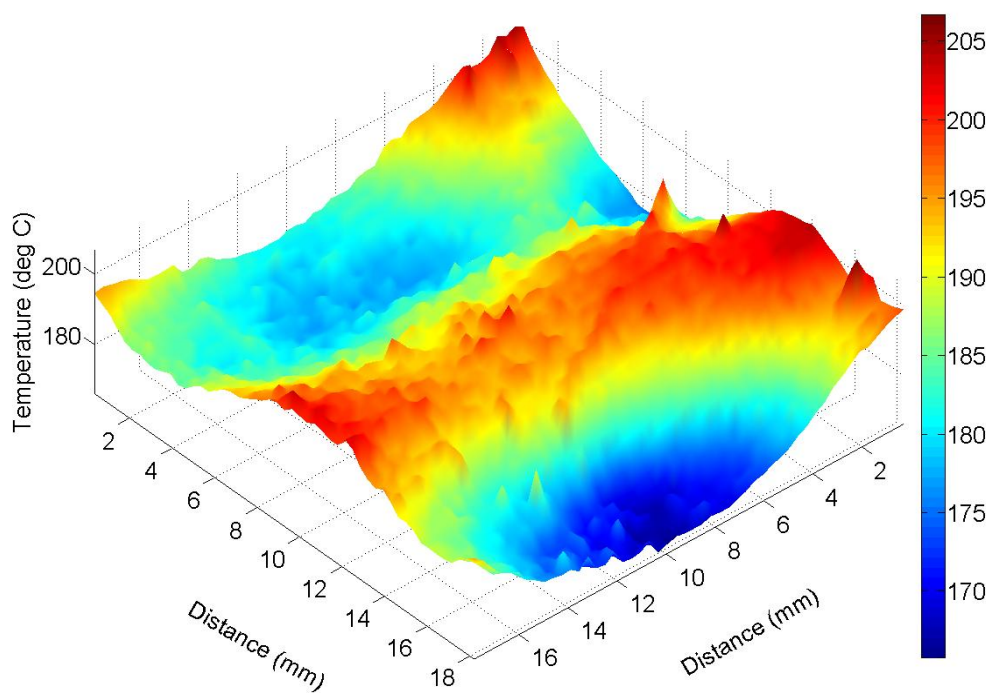
## 6.2 Experiments with four and two air jets

To confirm the numerical results for multiple jets, slot air jet experiments were carried out with four and two air jets with angle of inclination equal to  $45^\circ$ . Total air flow rate is maintained at  $9.25 \text{ m}^3/\text{hr}$ . The current passing through the sample is kept at 150 A. After attaining the steady state, the temperature fields on the specimen were obtained using thermal imaging. The model of thermal imaging camera used for jet impingement studies is Flir make T400 with accuracy of  $\pm 1\%$  or  $\pm 1^\circ\text{C}$ . Thermal resolution of the camera is  $0.01^\circ\text{C}$ . Surface temperature of the sample with four and two slot air jets at steady state are depicted in Fig.6.2 and Fig. 6.3 respectively. The voltage drop measured across the sample is 235 mV and 239 mV respectively.

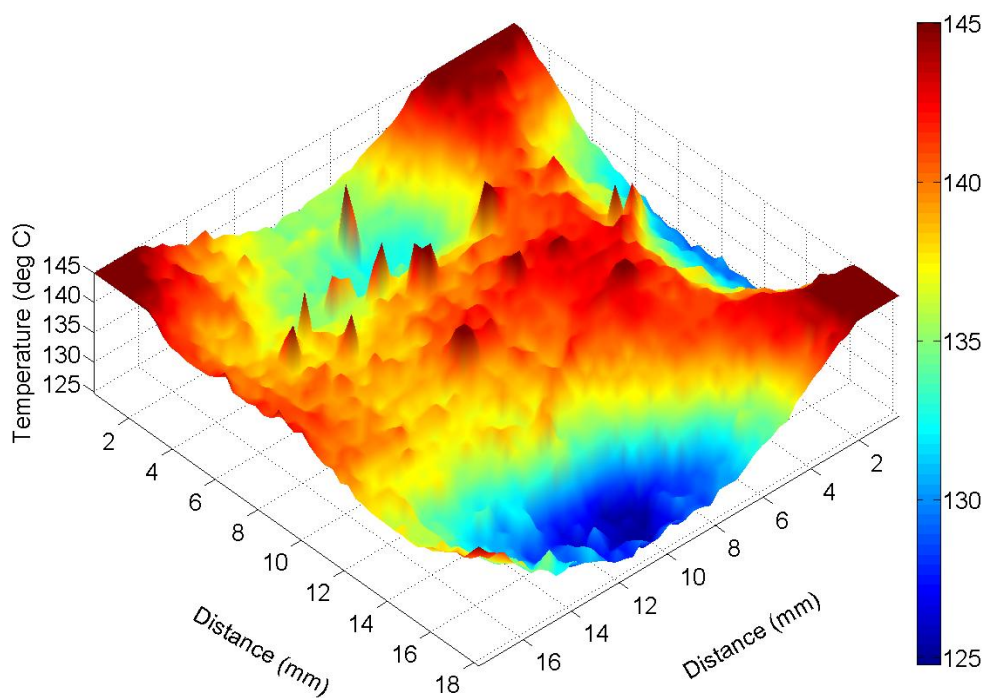
Four jets cooling (Fig. 6.2) gives a maximum temperature of  $207^\circ\text{C}$  and temperature variation of  $42^\circ\text{C}$ . For the case of two jets cooling one on each side (Fig. 6.3) the maximum temperature is  $145^\circ\text{C}$  and the temperature difference is only  $20^\circ\text{C}$ . This clearly shows advantage of two jets cooling compared to four jets as predicted by numerical analysis.

Figure 6.5 shows the average temperature of the sample for the above cases studied. The average temperature of the sample reduces from  $190^\circ\text{C}$  (cooling with four jets) to  $140^\circ\text{C}$





**Fig. 6.2** Surface temperature ( $^{\circ}\text{C}$ ) of the sample with four air jets



**Fig. 6.3** Surface temperature ( $^{\circ}\text{C}$ ) of the sample with two air jets

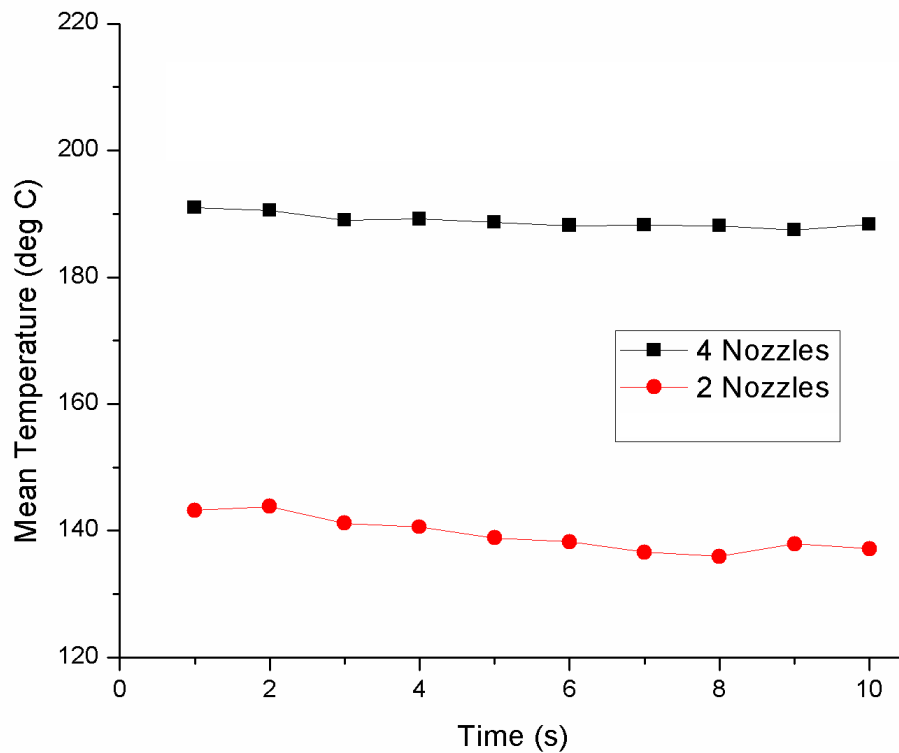


**Fig. 6.4 Average temperature of the specimen**

(cooling with two jets). This also confirms that cooling with two jets placed diagonally opposite side is more effective. Based on the current and voltage measured, the heat transfer coefficient for the case with four jets is determined to be  $275 \text{ W/m}^2\text{K}$  and for two jets, the value is  $407 \text{ W/m}^2\text{K}$ . This is 48% higher than that of the four jets case.

### 6.3 Closure

In this chapter details of the multi jet air experiments are given. In these experiments thermal imaging technique is used to measure the surface temperature of the specimen. Also higher power source of 4 V and 7000 A is used for heating the specimen. Experiments show that having two jets one on each side of the specimen is a better configuration. This configuration gives higher heat transfer coefficient and also lower temperature difference

across the specimen. This configuration is recommended for the spallation target cooling of cyclotron.

\* \* \*

# Chapter- 7

### Conclusions and scope for future work

Spallation target cooling in cyclotrons involves high heat fluxes of the order of 15 MW/m<sup>2</sup>. From a comprehensive literature review it is found that for high heat flux applications jet impingement method can be used. Helium jet impingement cooling has been selected for heat removal up to about 1 kW. Even though the amount of heat removal is less, helium cooling system is a simple system due to its non-radioactive nature. First an experimental facility has been established to carryout various jet cooling experiments with air as the cooling medium. The air flow rate was varied from 0 to 15 m<sup>3</sup>/hr. Thin specimen of the order of 20 mm x 20 mm x 0.5 mm have been heated by joule heating. The current has been increased from 0 to 7000 A. Using the experimental facility various single and multi jet air cooling experiments have been carried out. Slot jet and single array of circular jet nozzles have been used. Temperature measurements have been carried out using thermocouples and infrared thermal imaging technique.

The jet cooling phenomena are also simulated numerically using two-dimensional computational fluid dynamic analyses. Commercially available CFD code is used for this purpose. An investigation of the performance of various turbulence models shows that prediction of heat transfer behavior by eddy viscosity models, viz., k- $\epsilon$  and k- $\epsilon$  RNG are close to those predicted by Reynolds Stress models and large eddy simulation. Parametric study by varying the distance between jet and target plate has also been performed to ascertain the influence. Studies on multiple inclined jets impinging on a target plate show that the interaction between jets makes the thermal hydraulic behavior unsteady. Flow from one jet is found to mask that from the other jet. Hence, the heat transfer is not that effective compared to that in the case of vertical jet impingement. As the inclination of the jet approaches

towards vertical, the heat transfer coefficient increases. However, even with two impinging jets,  $60^\circ$  inclined to horizontal, the predicted heat transfer coefficient is less than that of single vertical jet.

From the correlations available in literature, Martin correlation is selected and is compared with the experimental as well as numerical results. Experiments indicate that Martin correlation under predicts the heat transfer coefficient by 26% to 70%. Two dimensional computational fluid dynamic studies predictions are 30% lower compared to Martin correlation. Hence prediction by Martin correlations lies between experimental and numerical predictions. Further, the CFD studies indicate that cooling by two jets one on either side is more effective in heat removal compared to four jets on all the sides due to the effect of spent flow. This configuration also gives low temperature difference across the sample. Multi air jet experiments also confirms that two jet cooling gives higher heat transfer coefficient compared to four jet cooling and also more uniform temperature distribution across the specimen. Hence this configuration is recommended for spallation target cooling in cyclotrons.

### **Scope for Future work**

Two jets case with each jet on either side of the sample is studied with  $45^\circ$  jet angle. This study can be carried out for various angles to see any possibility of for further minimizing the temperature difference across the specimen. The numerical results presented here are with two-dimensional CFD model. Similar studies can be carried out with three-dimensional CFD model to confirm the two-dimensional assumption. For ease of simulation, numerical studies have been carried out for slot jet. Similar studies can be carried out for circular jets which need three dimensional simulation.

Even though helium jet cooling is simple and non-radioactive the amount of heat removal by helium is limited to less than 1 KW. For higher heat transfer coefficient cooling by water jet can be used. If water jet comes into contact with the proton beam it will become radioactive. This will make the whole water circuit including pump, valves etc., radioactive. Hence care has to be taken to avoid any accidental contact with proton beam. This calls for another good conducting material in between specimen and water. Normally the specimen is attached to one end of copper tube and water flows inside the copper tube. This avoids direct contact of water with proton beam. By going for water jet cooling high heat transfer coefficient can be obtained between copper and water. This can be increased further by going for boiling water. But the main issue with this type of arrangement is the contact resistance between specimen and copper tube which will be limiting the heat transfer.

For still higher heat removal other cooling methods like liquid metal cooling can be used. This will have additional complications like handling of liquid metals. In case of any accidental leakage this will contaminate the whole system. Hence, care has to be taken in the system design and operation.

\* \* \*

## References:

1. I. Mudawar, Assessment of High-Heat-Flux Thermal Management Schemes, 2001, IEEE Trans. Compon. Packag. Technol. 24, 122–141.
2. N. Gayathri., P. Barat, P. Mukherjee, S. K. Bandhopadhyaya, P. Sen, M. Bhattacharya and K.G.M. Nair, 2006, Materials science activities with the DAE medical cyclotron, Progress Report, VECC-PR-2006, 169-172.
3. X. Liu, J.H. Lienhard, Extremely high heat flux removal by sub cooled liquid jet impingement, 1992, Fundamentals of Sub cooled Flow Boiling, 217, ASME, HTD, 11–20.
4. B.W. Blackburn, J.C. Yanch, R.E. Klinkowstein, 1998, Development of high-power water cooled Beryllium target for use in accelerator based Boron neutron capture therapy, Med. Phys. 25, 1967–1974.
5. J.H. Lienhard, 1995, Liquid Jet Impingement, Chapter in: C.L. Tien (Ed.), Annual Review of Heat Transfer, 6, Begell House, New York.
6. Y. Mitsutake, M. Monde, 2003, Ultra high critical heat-flux during forced flow boiling heat transfer with an impinging jet, Trans. ASME 125, 1038–1044.
7. L. Zhen-Hua, T. Tie-Feng, Q. Yu-Hao, 2004, Critical heat flux of steady boiling for sub cooled water jet impingement on the flat stagnation zone, Heat Transfer 126, 179–183.
8. K. Sato, A. Furutani, M. Saito, M. Isozaki, K. Suganuma, S. Imahori, 1991, Melting attack of solid plates by a high-temperature liquid jet [II] – Erosion behavior by a molten metal jet, Nuclear Engineering & Design, 132, 171–186.
9. B.W. Blackburn, J.C. Yanch, 1999, Liquid Gallium cooling for a high power Beryllium target for use in accelerator Boron neutron capture therapy (ABNCT), Proc. Eighth Workshop on Targetry and Target Chemistry, St. Louis, Missouri.



10. B.W. Blackburn, 2002, High-power target development for accelerator based neutron capture theory, Ph.D. Thesis, MIT, Boston, MA.
11. A. Miner, U. Ghoshal, 2004, Cooling of high power density micro devices using liquid metal coolants, *Appl. Phys. Lett.* 85, 506–508.
12. Peter Jung, Jochen Viehweg and Christian Schwaiger, 1978, Cooling and temperature stabilizing of thin specimens for mechanical measurements under light ion bombardment, *Nuclear Instrument and methods*, 154, 207-212.
13. P. Jung, A. Schwarz and H.K. Sahu, 1985, An apparatus for applying tensile, compressive and cyclic stresses on foil specimens during light ion irradiation, *Nuclear Instruments and Methods in Physics Research A* 234, 331-334.
14. K. Thomsen, L. Buligins, M. Butzek, G. Heidenreich, F. Heinrich, M. Magán, E. Pitcher, Target cooling options for neutron sources at high power densities, *Physics Procedia* 60 ( 2014 ) 83 – 90.
15. J Jurns, J Ringné, H Quack, P Arnold, J.G. Weisend, D. Lyngh, Spallation target cryogenic cooling design challenges at the European Spallation Source IOP Conf. Series: Materials Science and Engineering 101(2015) 012082
16. M. Molana and S. Banooni, 2013, Investigation of Heat Transfer Processes Involved Liquid Impingement Jets: A Review, *Brazilian Journal of Chemical Engineering*, Vol. 30, No. 3, 413 – 435.
17. N. Zuckerman and N. Lior, 2006, Jet Impingement Heat Transfer: Physics, Correlations and Numerical Modeling, *Advances in Heat Transfer*, Vol. 39, 565-631.
18. XXI Fluid Mechanics Conference IOP Publishing Journal of Physics: Conference Series 530 (2014) 012038 doi:10.1088/1742-6596/530/1/012038
19. J. Ferrari, N. Lior and J. Slycke, 2003, An evaluation of gas quenching of steel rings by multiple-jet impingement, *J. Mater. Process. Technol.* 136, 190–201.

20. J.C. Han, S. Dutta and S. Ekkad, 2000, Gas Turbine Heat Transfer and Cooling Technology, Taylor & Francis, New York.
21. K. Jambunathan, E. Lai, M.A. Moss and B.L. Button, 1992, A review of heat transfer data for single circular jet impingement, *Int. J. Heat Fluid Flow* 13 (2), 106–115.
22. R.J. Goldstein, A.I. Behbahani and K.K. Heppelmann, 1986, Stream wise distribution of the recovery factor and the local heat transfer coefficient to an impinging circular air jet, *Int. J. Heat Mass Transfer*, 29, 1227–1235.
23. J.P. Bouchez and R.J. Goldstein, 1975, Impingement cooling from a circular jet in a cross flow, *Int. J. Heat Mass Transfer*, 13, 719–730.
24. E.M. Sparrow, R.J. Goldstein and M.A. Rouf, 1975, Effect of nozzle surface separation distance on impingement heat transfer for a jet in a cross flow, *J. Heat Transfer* 97, 528–533.
25. R.J. Goldstein, K.A. Sobolik and W.S. Seol, 1990, Effect of entrainment on the heat transfer to a heated circular air jet impinging on a flat surface, *J. Heat Transfer* 112, 608–611.
26. E.M. Sparrow, Z.X. Xu and L.F.A. Azevedo, 1987, Heat transfer for circular jet impingement on a confined disk with annular collection of the spent air, *J. Heat Transfer* 109, 329–335.
27. R.J. Goldstein and J.F. Timmers, 1982, Visualization of heat transfer from arrays of impinging jets, *Int. J. Heat Mass Transfer* 25 (12), 1857–1868.
28. R.J. Goldstein and M.E. Franchett, 1988, Heat transfer from a flat surface to an oblique impinging jet, *J. Heat Transfer* 110, 84–90.
29. L. Huang and M.S. EL-Genk, 1994, Heat transfer of an impinging jet on a flat surface, *Int. J. Heat Mass Transfer* 37 (13), 1915–1923.

30. D. Lytle and B.W. Webb, 1994, Air jet impingement heat transfer at low nozzle-plate spacing, *Int. J. Heat Mass Transfer*, 37 (12), 1687–1697.
31. C.Y. Li and S.V. Garimella, 2001, Prandtl-number effects and generalized correlations for confined and submerged jet impingement, *Int. J. Heat Mass Transfer*, 44, 3471–3480.
32. S.V. Garimella and R.A. Rice, 1995, Confined and submerged liquid jet impingement heat transfer, *J. Heat Transfer*, 117, 871–877.
33. J.A. Fitzgerald and S.V. Garimella, 1998, A study of the flow field of a confined and submerged impinging jet, *Int. J. Heat Mass Transfer*, 41, 1025–1034.
34. M. Angibletti, R.M. Di Tommaso, E. Nino and G. Ruocco, 2003, Simultaneous visualization of flow field and evaluation of local heat transfer by transitional impinging jet, *Int. J. Heat Mass Transfer*, 46, 1703–1713.
35. V. Narayanan, J. Seyed-Yagoobi and R.H. Page, 2004, An experimental study of fluid mechanics and heat transfer in an impinging slot jet flow, *Int. J. Heat Mass Transfer* 47, 1827–1845.
36. D.W. Zhou and S.J. Lee, 2004, Heat transfer enhancement of impinging jets using mesh screens, *Int. J. Heat Mass Transfer*, 47, 2097–2108.
37. A.M. Huber and R. Viskanta, 1994, Effect of jet-jet spacing on convective heat transfer to confined impinging arrays of axisymmetric air jets, *Int. J. Heat Mass Transfer*, 37 (18), 2859–2869.
38. J.Y. San and M.D. Lai, 2001, Optimum jet-to-jet spacing of heat transfer for staggered arrays of impinging air jets, *Int. J. Heat Mass Transfer*, 44, 3997–4007.
39. B.P.E. Dano, J.A. Liburdy, K. Kanokjaruvijit, 2005, Flow characteristics and heat transfer performance of a semi-confined impinging array of jet: effect of nozzle geometry, *Int. J. Heat Mass Transfer*, 48, 691–701.

40. D. B. Tuckerman, and R.F.W. Pease, 1981, High Performance Heat Sink for VLSI, IEEE Electron Dev. Let., EDL-2, no. 5, 126– 129.
41. R.J. Phillips, 1987, Forced Convection, Liquid Cooled, Microchannel Heat Sinks, M.S. Thesis, Dept. of Mechanical Engineering, Massachusetts Institute of Technology, Cambridge, MA.
42. M.E. Steinke, and S.G. Kandlikar, 2004, Review of Single-Phase Heat Transfer Enhancement Techniques for Application in Microchannels, Minichannels and Microdevices, International Journal of Heat and Technology, vol. 22, no. 2, 3–11.
43. S.G. Kandlikar and W.J. Grande, 2004, Evaluation of Single Phase Flow in Microchannels for High Flux Chip Cooling Thermohydraulic Performance Enhancement and Fabrication Technology, Heat Transfer Engineering, vol. 25, no. 8, pp. 5–16.
44. E.G. Colgan, B. Furman, M. Gaynes, W. Graham, N. LaBianca, J.H. Magerlein, R.J. Polastre, M.B. Rothwell, R.J. Bezama, R. Choudhary, K. Martson, H. Toy, J. Wakil, J. Zitz and R. Schmidt, 2005, A Practical Implementation of Silicon Microchannel Coolers for High Power Chips, Invited Paper presented at IEEE Semi-Therm 21, San Jose, 15–17 March 2005, 1–7.
45. S.G. Kandlikar and H.R. Upadhye, 2005, Extending the Heat Flux Limit with Enhanced Microchannels in Direct Single-Phase Cooling of Computer Chips, Invited Paper presented at IEEE Semi Therm 21, San Jose, 15–17 March 2005, 8–15.
46. H. Pokharna, K. Masahiro, E. DiStefanio, R. Mongia, J. Crowley Barry, W. Chen, and M. Izenson, 2004, Microchannel Cooling in Computing Platforms: Performance Needs and Challenges in Implementation, Keynote Paper, ASME Paper No. ICMM2004-2325, Second International Conference on Microchannels and Minichannels, 17–19 June 2004, Rochester, NY, 109–118.

47. P. Norajitra, S.I. Abdel-Khalik, L.M. Giancarli and P. Sardain, 2008, Divertor conceptual designs for a fusion power plant *Fus. Eng. Des.* 83 (7), 893-902.
48. S. K. Das, U. Stephen, Wenhua Yu Choi, T. Pradeep, 2007, *Nanofluids: Science and Technology*, First ed., John Wiley & Sons.
49. A. Sergis and Y. Hardalupas, 2011, *Nanoscale Research Letters*, 6(1), 391.
50. Huseyin Bostanci, 2010, High heat flux spray cooling with ammonia on enhanced surfaces, Ph.D. Thesis, University of Central Florida ,Orlando, Florida.
51. M. Hashimoto, H. Kasai, K. Usami, H. Ryoson, K. Yazawa, J.A. Weibeland S.V. Garimella, 2010, Nano-structured two-phase heat spreader for cooling ultra-high heat flux source, *Proceedings of the 14th International Heat Transfer Conference, IHTC14* August 8-13, 2010, Washington, DC, USA.
52. M.G. Izenon and J.L. Martin, 1996, Optimal thermal hydraulic performance for helium cooled divertors, *Fusion Technology*, 29, 545 -558.
53. J.H. Rosenfeld and M. T. North, 1995, Porous media heat exchangers for cooling of high-power optical components, *Optical Engineering* 34 (2), 335-341.
54. B.W. Webb and C.F. Ma, 1995, Single phase liquid jet impingement heat transfer, *Advances in Heat Transfer* 26, 105-217.
55. D.Y. Lee and K. Vafai, 1999, Comparative analysis of jet impingement and microchannel cooling for high heat flux applications, *International Journal of Heat and Mass Transfer*, 42 , 1555 – 1568.
56. H. Bostanci, D.P. Rini, J.P. Kizito, Virendra Singh, Sudipta Seal, L.C. Chow, 2014, High heat flux spray cooling with ammonia: Investigation of enhanced surfaces for HTC, *International Journal of Heat and Mass Transfer*, 75, 718-725.
57. S.V. Ravikumar, J.M. Jha, A.M. Tiara, S.K. Pal and S. Chakraborty, 2014, Experimental investigation of air-atomized spray with aqueous polymer additive for

- high heat flux applications, *International Journal of Heat and Mass Transfer* 72, 362–377.
58. G.R. Warrier, C.J. Kim and Y.S. Ju, 2014, Microchannel cooling device with perforated side walls: Design and modeling, *International Journal of Heat and Mass Transfer* 68, 174–183.
  59. J. Filipovic, F.P. Incropera and R. Viskanta, 1995, Quenching phenomena associated with a water wall jet: 1. Transient hydrodynamic and thermal conditions, *Expt. Heat Transfer* 8, 97–117.
  60. S. Kumagai, S. Suzuki, Y. Sano and M. Kawazoe, 1995, Transient cooling of a hot metal slab by an impingement jet with boiling heat transfer, in: *ASME/JSME Thermal Engineering Conference*, vol. 2, 1995.
  61. E. Hall, P. Incropera and R. Viskanta, 2001, Jet impingement boiling from a circular free-surface jet during quenching: Part 1—single-phase jet, *ASME J. Heat Transfer* 123, 901–910.
  62. T. Semenic and I. Catton, 2009, Experimental study of biporous wicks for high heat flux applications, *International Journal of Heat and Mass Transfer* 52, 5113–5121.
  63. T. Tsukamoto and R. Imai, 2006, Thermal characteristics of a high heat flux micro-evaporator, *Experimental Thermal and Fluid Science* 30, 837–842.
  64. C. Glynn, T. O'Donovan and D.B. Murray, 2005, Jet Impingement Cooling, *Proceedings of the 9th UK National Heat Transfer Conference*, Manchester, England, 5-6.
  65. J.Y. San and W.Z. Shiao, 2006, Effects of jet plate size and plate spacing on the stagnation Nusselt number for a confined circular air jet impinging on a flat surface, *Int. J of Heat and Mass Transfer*, 49, 3477–3486.

66. P.C. Mishra, S.K. Nayak, D.P. Ghosh, M. Ukamanal, S.K. Nayak and S.K. Sahu, 2013, Effect of Controlling Parameters on Heat Transfer during Jet Array Impingement Cooling of a Hot Steel Plate, *International Journal of Computational Engineering Research*, 3 (8), 51-57.
67. Vadiraj Katti and S.V. Prabhu, 2008, Experimental study and theoretical analysis of local heat transfer distribution between smooth flat surface and impinging air jet from a circular straight pipe nozzle, *International Journal of Heat and Mass Transfer*, 51(17–18), 4480–4495.
68. H. Wang, W. Yu and Q. Cai, 2012, Experimental study of heat transfer coefficient on hot steel plate during water jet impingement cooling, *Journal of Materials Processing Technology*, 212, 1825–1831.
69. Kartik Jujare, Shashank Kumat and Akash Thawkar, 2014, Experimental Investigation of Jet Impingement Cooling On a Ribbed Surface with Holes, *Journal of Engineering Research and Applications*, 4 (1), 256-260.
70. H. Martin, 1977, Heat and mass transfer between impinging gas jets and solid surface, *Adv. Heat transfer*, 13, 1-60.
71. Z. H. Lin, Y. J. Chou and Y. H. Hung, 1997, Heat transfer behaviors of a confined slot jet impingement, *Int. Heat Mass Transfer*, 40 (5), 1095-1107.
72. D.W. Zhou and Sang-Joon Lee, 2007, Forced convective heat transfer with impinging rectangular jets , *Int. Journal of Heat and Mass transfer*, 50, 1916-1926.
73. H. Eren and N. Celik, 2006, Cooling of a heated flat plate by an obliquely impinging slot jet, *International Communications in Heat and Mass Transfer*, 33, 372-380.
74. P. Gulati, V. Katti and S.V. Prabhu, 2009, Influence of the shape of the nozzle on local heat transfer distribution between smooth flat surface and impinging air jet, *Int. Journal of Thermal Sciences*, 48, 602-617.

75. M. Attalla and M. Salem, 2013, Effect of nozzle geometry on heat transfer characteristics from a single circular air jet, *Applied Thermal Engineering*, 51, 723-733.
76. S. Polat, B. Huang, A.S. Majumdar and W.J.M. Douglas, 1989, Numerical Flow and Heat Transfer Under Impinging Jets: A Review, *Annual Review of Heat Transfer*, 2, 157–197.
77. A. N. Kolmogorov, 1941, The local structure of turbulence in incompressible viscous fluid for very large Reynolds number, *Dokl. Akad. Nauk SSSR*, 30, 9–13.
78. J. Smagorinsky, 1963, General Circulation Experiments with the Primitive Equations. 1. The Basic Experiment, *Monthly Weather Review*, 91, 99–164.
79. M. Germano, U. Piomelli, P. Moin and W. Cabot, 1991, A dynamic subgrid-scale eddy viscosity model, *Physics of Fluids*, A3 (7), 1760–1765.
80. F. Nicoud and F. Ducros, 1999, Subgrid-Scale Modeling Based on the Square of the Velocity Gradient Tensor, *Flow Turbulence and Combustion*, 62, 183–200.
81. J. Bardina, J.H. Ferziger and W.C. Reynolds, 1980, Improved subgrid scale models for Large Eddy Simulation, *AIAA paper No. 80*, 1357.
82. S. Liu, C. Meneveau and J. Katz, 1994, On the properties of similarity subgrid-scale models as deduced from measurements in a turbulent jet, *J. Fluid Mech.*, 275, 83-119.
83. A. Leonard, 1974, Energy cascade in large-eddy simulations of turbulent fluid flows, *Adv. In Geophysics*, A 18, 237-248.
84. R.A. Clark, J. H. Ferziger and W. C. Reynolds, 1979, Evaluation of subgrid models using an accurately simulated turbulent flow, *J. Fluid Mech.* 91, 1-16
85. M. Olsson and L. Fuchs, 1998, Large Eddy Simulations of a Forced Semiconfined Circular Impinging Jet, *Physics of Fluids*, 10, 476–486.



86. G. Lodato, L. Vervisch and P. Domingo, 2009, A compressible wall-adapting similarity mixed model for large-eddy simulation of impinging round jet, *Physics of Fluids*, 21, 1–21.
87. A.G. Kravchenko, P. Moin and R. Moser, 1996, Zonal embedded grids for numerical simulations of wall-bounded turbulent flows, *Journal of Computational Physics*, 127, 412–423.
88. M. Hadziabdic and K. Hanjalic, 2008, Vortical structures and heat transfer in a round impinging jet, *J. Fluid Mech.* 596, 221–260.
89. P. Moin and K. Mahesh, 1998, Direct numerical simulation: A tool in turbulence research, *Annu. Rev. Fluid Mech.*, 30, 539–78.
90. R.D. Moser and P. Moin, 1987, The effects of curvature in wall-bounded turbulent flows, *J. Fluid Mech.*, 175, 479–510.
91. H. Choi and P. Moin, 1994, Effects of the computational time step on numerical solutions of turbulent flow, *J. Comp. Phys.*, 113, 1–4.
92. Y. M. Chung and K.H. Luo, 2002, Unsteady Heat Transfer Analysis of an Impinging Jet, *Journal of Heat Transfer*, 124, 1039–1048.
93. E.M. Sparrow and T.C. Wong, 1975, Impingement Transfer Coefficients Due to Initially Laminar Slot Jets, *Int. J. Heat Mass Transf.*, 18, 597–605.
94. Hattori, H., and Nagano, Y., 2004. Direct Numerical Simulation of Turbulent Heat Transfer in Plane Impinging Jet, *International Journal of Heat and Fluid Flow*, vol. 25, pp. 749–758.
95. M. Tsubokura, T. Kobayashi, N. Taniguchi and W.P. Jones, 2003, A Numerical Study on the Eddy Structures of Impinging Jets Excited at the Inlet, *International Journal of Heat and Fluid Flow*, 24, 500–511.

96. S. Satake and T. Kunugi, 1998, Direct Numerical Simulation of an Impinging Jet Into Parallel Disks, *International Journal of Numerical Methods for Heat & Fluid Flow*, 8, 768–780.
97. B.E. Launder and D. B. Spalding, 1974, *Computer Methods in Applied Mechanics and Eng.* 13, 269-289.
98. L. Prandtl, 1925, *Über die ausgebildete Turbulenz*, *ZAMM*. 5, 136-139.
99. A.M.O. Smith and T. Cebeci, 1967, Numerical solution of the turbulent boundary layer equations, Douglas aircraft division report DAC 33735.
100. U. Heck, K. Fritsching and K. Bauckhage, 2001, Fluid flow and heat transfer in gas jet quenching of a cylinder, *Int. J. Numer. Methods Heat Fluid Flow*, 11, 36–49.
101. A.O. Demuren, 1994, Calculations of 3D impinging jets in cross flow with Reynolds stress models, *Heat Transfer in Turbomachinery* (R.J. Goldstein, D.E. Metzger and A.I. Leontiev, eds.), Begell House, Inc., New York, 527–540.
102. T.J. Craft, L.J.W. Graham and B.E. Launder, 1993, Impinging jet studies for turbulence model assessment – II. An examination of the performance of four turbulence models, *Int. J. Heat Mass Transfer* 36, 2685–2697.
103. G. Le Song and M. Prud'homme, 2007, Prediction of Coherent Vortices in an Impinging Jet with Unsteady Averaging and a Simple Turbulence Model, *International Journal of Heat and Fluid Flow*, 28, 1125–1135.
104. Frank P. Incropera and David P. Dewitt, 2009, *Fundamentals of heat and mass transfer*, Wiley India Pvt. Ltd, pp 428-434.
105. D. Choudhury, 1993, Introduction to the renormalization group method and turbulence modeling, *Fluent Inc. Tech. Memorandum TM-107*.
106. B.E. Launder, G. J. Reece and W. Rodi, 1975, Progress in the Development of a Reynolds-Stress Turbulent Closure, *J. of Fluid Mechanics*, 68(3), 537-566.

107. [https://en.wikipedia.org/wiki/Planck%27s\\_law](https://en.wikipedia.org/wiki/Planck%27s_law)
108. B. Venkataraman et al., 2006, Infrared Imaging-an overview on its multifarious possibilities and applications in IGCAR, Journal of Nondestructive Testing & Evaluation, Vol. 5, Issue 2.
109. [https://www.ndeed.org/EducationResources/CommunityCollege/Other%20Methods/IRT/IR\\_index.php](https://www.ndeed.org/EducationResources/CommunityCollege/Other%20Methods/IRT/IR_index.php)
110. [www2.fiu.edu/~dbrookes/ExperimentalUncertaintiesCalculus.pdf](http://www2.fiu.edu/~dbrookes/ExperimentalUncertaintiesCalculus.pdf), Adapted by D. Brookes and M. Kagan (2011).

\* \* \*

## Appendix - A

### Experimental uncertainty [110]

Nusselt number =  $hd/k$

d - diameter of the nozzle

(Since uncertainty in the diameter is very small it is neglected)

k - thermal conductivity of air

(Since uncertainty in the thermal conductivity of air is very small it is neglected)

h - heat transfer coefficient =  $P / \{A (T_{avg} - T_{amb})\}$

P - heat transferred =  $V \times I$

V - voltage

I - current

**Error in power measurement =  $\pm 1.5\%$**

The margin of error for Type K thermocouple used is  $\pm 0.75\%$  or  $\pm 2.2\text{ }^{\circ}\text{C}$ .

Higher value of  $2.2\text{ }^{\circ}\text{C}$  is taken as error for Type K thermocouple.

Error in temperature measurement ( $T_{avg} - T_{amb}$ ):  $2.2 + 2.2 = \pm 4.4\text{ }^{\circ}\text{C}$

(When two measured quantities are subtracted their absolute uncertainties add up).

The maximum temperature of the specimen during experiments  $\approx 100\text{ }^{\circ}\text{C}$

The ambient temperature  $\approx 23\text{ }^{\circ}\text{C}$

The average temperature =  $(100+23) / 2 \approx 60\text{ }^{\circ}\text{C}$

**Relative error in temperature measurement** =  $(4.4 / 60) \times 100 = \pm 7.3\%$

Error in power measurement =  $\pm 1.5\%$

**Error in heat transfer coefficient** =  $7.3 + 1.5 = \pm 8.8\%$

(When two measured quantities are divided their absolute uncertainties add up).

The rotameter used for the air flow measurement has an accuracy of  $\pm 5\%$ .

**Hence the error in the Reynolds number  $\pm 5\%$ .**

From Martin's [70] correlation  $Nu \propto Re^{2/3}$

Error in the Nusselt number due to error in Reynolds number =  $(2/3) \times 5 = 3.3\%$

(When raising a measured quantity to a power, the percent uncertainty should be multiplied by the corresponding factor)

Hence total error in Nusselt number =  $8.8 + 3.3 = 12.1 \approx \pm 15\%$

\* \* \*

## Appendix - B

### Model Calculation for circular air jet (at 90° with horizontal) Target distance 14 mm

#### Reynolds number calculation:

$$D = \text{diameter of the nozzle} = 1 \text{ mm}$$

$$n = \text{number of holes} = 9$$

$$\begin{aligned} a &= \text{area of the nozzle} = \Pi D^2/4 \\ &= 0.7854 \times 10^{-6} \text{ m}^2 \end{aligned}$$

$$\text{Ambient temperature of air} = T_a = 23 \text{ }^\circ\text{C}$$

$$\nu - \text{kinematic viscosity of air} = 16.0 \times 10^{-6} \text{ m}^2/\text{s}$$

$$\begin{aligned} Q &= \text{air flow rate} = 15 \text{ m}^3/\text{hr} \\ &= 15/3600 \\ &= 4.167 \times 10^{-3} \text{ m}^3/\text{s} \end{aligned}$$

$$\begin{aligned} v &= \text{velocity of air} = Q/(n a) \\ &= 4.167 \times 10^{-3} / (9 \times 0.7854 \times 10^{-6}) \\ &= 589.5 \text{ m/s} \end{aligned}$$

$$\begin{aligned} \text{Reynolds number} &= Re = \frac{v D_h}{\nu} \\ &= 589.5 \times 0.001 / 16.0 \times 10^{-6} \\ &= \mathbf{36844} \end{aligned}$$

Similarly for flow rate equal to 10 and 5 m<sup>3</sup>/h, the calculated Reynolds numbers are 24561 & 12280 respectively.

#### Heater Power calculation:

$$\text{Input voltage} = V = 0.15 \text{ v}$$

$$\text{Current} = I = 90 \text{ A}$$

$$\begin{aligned}\text{Power} = P &= V \times I \\ &= \mathbf{13.5 \text{ w}}\end{aligned}$$

### Calculation of average specimen temperature:

Measured temperature at the centre of four quadrants:

$$T_1 = 37^\circ\text{C}$$

$$T_2 = 36^\circ\text{C}$$

$$T_3 = 28^\circ\text{C}$$

$$T_4 = 35^\circ\text{C}$$

$$\begin{aligned}T_{\text{avg}} &= (T_1 + T_2 + T_3 + T_4) / 4 \\ &= \mathbf{34.0^\circ\text{C}}\end{aligned}$$

### Heat transfer through radiation

$\epsilon$  = Emissivity of the sample

$$= 0.2 \text{ (for polished SS 304)}$$

$\sigma$  = Stefan - Boltzmann constant

$$= 5.67 \times 10^{-8} \text{ W / m}^2 \text{ K}^4$$

Heat transfer through radiation:

$$\begin{aligned}P_r &= 2 A \epsilon \sigma \{T_{\text{avg}}^4 - T_a^4\} \\ &= 2 \times 0.02 \times 0.02 \times 0.2 \times 5.67 \times 10^{-8} \times \{(273+34)^4 - (273+23)^4\} \\ &= \mathbf{0.011 \text{ w}}\end{aligned}$$

This value is very small and can be neglected.

### Calculation of heat transfer coefficient:

$$\Delta T = T_{\text{avg}} - T_a$$

$$= 34.0 - 23.0$$

$$= 11.0^{\circ}\text{C}$$

$$\text{Total area of the specimen} = A = 2 \times 20 \times 20$$

$$= 800 \text{ mm}^2$$

$$= 800 \times 10^{-6} \text{ m}^2$$

$$\text{Heat transfer coefficient} = h = P / (A \times \Delta T)$$

$$= 13.5 / (800 \times 10^{-6} \times 11.0)$$

$$= \mathbf{1534 \text{ w / m}^2\text{C}}$$

### **Nusselt number calculation**

$$\text{Thermal conductivity of air} = k = 0.02675$$

$$\text{Nusselt number} = Nu = h D / k$$

$$= 1534 \times 0.001 / 0.02675$$

$$= 57.3$$

$$\text{Nusselt number through Martin's correlation} = 30$$

$$\text{Difference between experiment and Martin's correlation} = 27.3/57.3 \times 100 = 48\%$$

### **Estimation of heat loss through copper plates**

$$\text{Velocity of jet over copper plates front surfaces} = 78 \text{ m/s}$$

$$\text{Natural air velocity over copper plates back side} = 4 \text{ m/s}$$

### **Calculation of heat transfer coefficient over copper plates front surfaces:**

$$\text{Reynolds number} = Re = \frac{V x}{\nu}$$

$$= 78.0 \times 0.045 / 16.0 \times 10^{-6}$$

$$= 219431$$



$$\begin{aligned}
 \text{Prandtl number, } Pr &= \frac{\rho C_p}{k} \\
 &= 1005 * 1.8328 \times 10^{-5} / 0.02675 \\
 &= 0.6885
 \end{aligned}$$

$$\begin{aligned}
 \text{Nussel number, } Nu &= 0.664 * Re^{0.5} Pr^{0.3} \\
 Nu &= 0.664 * 219431^{0.5} 0.6885^{0.3} \\
 &= 278.1
 \end{aligned}$$

$$\begin{aligned}
 h &= 278.1 * 0.02675 / 0.045 \\
 &= 165.3 \text{ W/m}^2\text{K}
 \end{aligned}$$

**Calculation of heat transfer coefficient over copper plates back side:**

$$\begin{aligned}
 \text{Reynolds number} = Re &= \frac{V x}{\nu} \\
 &= 4 * 0.045 / 16.0 \times 10^{-6} \\
 &= 11250
 \end{aligned}$$

$$\begin{aligned}
 \text{Prandtl number, } Pr &= \frac{\rho C_p}{k} \\
 &= 1005 * 1.8328 \times 10^{-5} / 0.02675 \\
 &= 0.6885
 \end{aligned}$$

$$\begin{aligned}
 \text{Nussel number, } Nu &= 0.664 * Re^{0.5} Pr^{0.3} \\
 Nu &= 0.664 * 11250^{0.5} 0.6885^{0.3} \\
 &= 62.97
 \end{aligned}$$

$$\begin{aligned}
 h &= 62.97 * 0.02675 / 0.045 \\
 &= 37.43 \text{ W/m}^2\text{K}
 \end{aligned}$$

**Heat flux calculated from FEM analysis with heat transfer coefficient as boundary condition:**

$$\text{Heat flux on front side surface} = 1756 \text{ W/m}^2$$

Heat flux on back side surface =  $400 \text{ W/m}^2$

$$\begin{aligned}\text{Total heat loss through copper plates } P_c &= (1756 + 400) \times 0.033 \times 0.04 \times 2 \\ &= 5.69 \text{ W}\end{aligned}$$

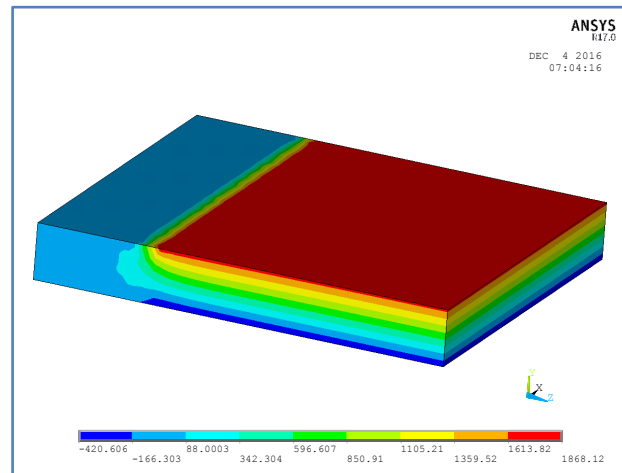


Fig. a: Distribution of surface heat flux over the copper end connection.

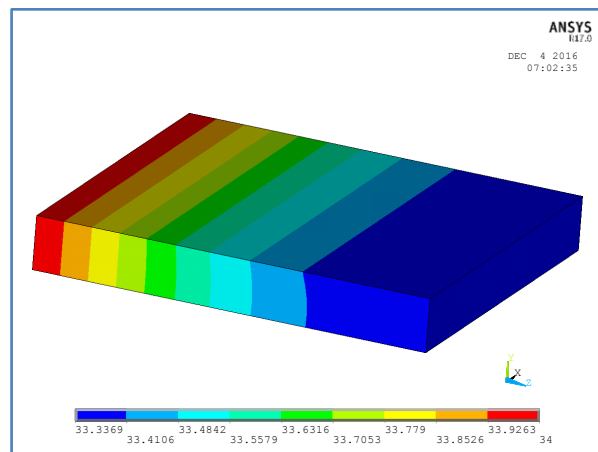


Fig. b: Distribution of temperature over the copper end connection.

#### Calculation of heat transfer coefficient:

$$\begin{aligned}\Delta T &= T_{\text{avg}} - T_a \\ &= 34.0 - 23.0 \\ &= 11.0^\circ\text{C}\end{aligned}$$

$$\begin{aligned}
 \text{Heat transfer coefficient} = h &= P - P_r - P_c / (A \times \Delta T) \\
 &= 7.799 / (800 \times 10^{-6} \times 11.0) \\
 &= \mathbf{886.25 \text{ W / m}^2\text{C}}
 \end{aligned}$$

#### **Nusselt number calculation**

$$\text{Thermal conductivity of air} = k = 0.02675$$

$$\begin{aligned}
 \text{Nusselt number} = Nu &= h D / k \\
 &= 886.25 \times 0.001 / 0.02675 \\
 &= \mathbf{33.13}
 \end{aligned}$$

$$\text{Nusselt number from Martin's correlation} = 30$$

$$\text{Difference between experiment and Martin} = 3.13/33.13 \times 100 = \mathbf{9.45\%}$$

This is within the experimental uncertainty of  $\pm \mathbf{15 \%}$ . Moreover data regarding uncertainty in Martin's correlation is not given in reference [70].

\*      \*      \*

## Appendix – C

### Comparison of heat transfer characteristics between helium and air system

**Martin's correlation for single slot nozzle:**

$$\frac{\overline{Nu}}{Pr^{0.42}} = \frac{1.53}{\frac{x}{S} + \frac{H}{S} + 1.39} Re^{m(\frac{x}{S}, \frac{H}{S})}$$

$$m = 0.695 - \left( \frac{x}{S} + \left( \frac{H}{S} \right)^{1.33} + 3.06 \right)^{-1}$$

Range of validity:

$$3,000 \leq Re \leq 90,000$$

$$2 \leq x/S \leq 25 \quad (0.125 \geq f \geq 0.01)$$

$$2 \leq H/S \leq 10$$

Where  $f = S / 4x$

$S$  = Hydraulic diameter of slot nozzle ( $S = 2 B$ )

$B$  = Width of the slot nozzle

$H$  = Nozzle to sample distance

$x$  = Sample length / 2

For given

$x = 10 \text{ mm}$  &  $w = 3 \text{ mm}$

$$m = 0.695 - \left[ \frac{10}{6} + \left( \frac{14}{6} \right)^{1.33} + 3.06 \right]^{-1}$$

$$m = 0.567$$

**Calculations for Helium Jet:**

*Thermo-physical properties at 300 K*

$$Pr = 0.68$$

$$Re = \frac{vD}{\vartheta}$$

$$Re = 100 \times 0.006 / 122 \times 10^{-6}$$

$$Re = 4918$$

$$\frac{Nu}{0.68^{0.42}} = \frac{1.53}{\frac{10}{6} + \frac{14}{6} + 1.39} \times 4918^{0.567}$$

$$Nu = 29.92$$

$$\text{Heat Transfer Coefficient, } h = 29.92 \times 0.152 / 0.006 = 757 \text{ W/m}^2 \text{ K}$$

### Calculations for air Jet:

*Thermo-physical properties at 300 K*

$$Pr = 0.707$$

$$Re = \frac{vD}{\vartheta}$$

$$Re = 100 \times 0.006 / 15.89 \times 10^{-6}$$

$$Re = 37759$$

$$\frac{Nu}{0.707^{0.42}} = \frac{1.53}{\frac{10}{6} + \frac{14}{6} + 1.39} \times 37759^{0.567}$$

$$Nu = 96.63$$

$$\text{Heat Transfer Coefficient, } h = 96.63 \times 0.0263 / 0.006 = 424 \text{ W/m}^2 \text{ K}$$

### Summary:

*Therefore,*

$$h_{He} \sim 1.8 \text{ times of } h_{air}$$

&

$$Nu_{He} \sim 1/3 \text{ of } Nu_{air}$$

\* \* \*

### Publications based on the thesis

a. Published

**P. Selvaraj**, K. Natesan, K. Velusamy and T. Sundararajan, "Conceptual design of helium cooling circuit for irradiation target cooling", *Progress in Nuclear Energy* **92** (2016) 54 – 61.

**P. Selvaraj**, K. Natesan, K. Velusamy and T. Sundararajan, "Cooling of small size irradiation specimens using impinging jets", *International communications in heat and mass transfer*, **84** (2017), 20-26.

b. Under Review:

**P. Selvaraj**, K. Natesan, K. Velusamy and T. Sundararajan, "Irradiated target cooling using circular /slot air jet", International Journal of Heat Transfer Engineering.

c. Other Publications:

**P. Selvaraj**, K. Natesan, V. Baskaran, K. Velusamy and T. Sundararajan, "Experimental simulation of slot air jet cooling for irradiation targets", Proceedings of the Forty Second National Conference on Fluid Mechanics and Fluid Power, FMFP 2015 – Paper No. 314, NITK Surathkal, Karnataka, India, December 14-16, 2015.

**P. Selvaraj**, K. Natesan, V. Baskaran, K. Velusamy and T. Sundararajan, "Irradiated target cooling using circular air jet", Proceedings of the 23rd National Heat and Mass Transfer Conference and 1st International ISHMT-ASTFE Heat and Mass Transfer Conference, IHMTTC2015, Paper No.111, Thiruvananthapuram, India, 17-20 December, 2015.

\* \* \*